Title of Thesis

A Study of PREMIER Combustion Characteristics in a Pilot Ignited Dual-Fuel Biogas Engine

September 2019

Alireza Valipour Berenjestanaki

Graduate School of Natural Science and Technology,
Division of Industrial Innovation Sciences
(Doctoral Course)

Okayama University, Japan

A Study of PREMIER Combustion Characteristics in a Pilot Ignited Dual-Fuel Biogas Engine

A dissertation submitted in partial fulfillment of the requirements
for the degree of Doctor of Philosophy
(Major: Mechanical Engineering)

By

Alireza Valipour Berenjestanaki

(B.Sc. in Mechanical Engineering, Thermo & Fluid Science
Islamic Azad University, Sari branch, IRAN, 2011)
(M.Sc. in Mechanical Engineering, Thermal Science
Aligarh Muslim University (AMU), INDIA, 2014)

Under the supervision of

Professor Dr. Eiji TOMITA

Co-supervised by

Professor Dr. Kazuhito OHASHI

Professor Dr. Akihiko HORIBE

Associate Professor Dr. Nobuyuki KAWAHARA

Graduate School of Natural Science and Technology

Okayama University, Japan

TO WHOM IT MAY CONCERN

This is to certify that thesis entitled

"**A Study of PREMIER Combustion Characteristics in a Pilot Ignited Dual-Fuel Biogas Engine**" is carried out by Alireza Valipour Berenjestanaki at Heat Power Engineering Lab, Division of Industrial Innovation Sciences, Okayama University.

Signature & seal of supervisor

Professor Dr. Eiji TOMITA

Official Seal

Professor Dr. Eiji TOMITA
Dean of Graduate School of Natural Science and Technology
Okayama University, Japan

Abstract

The excessive global carbon dioxide (CO_2) emissions and other greenhouse gas (GHG) emissions from the burning of fossil fuels causes the search for climate-friendly alternative fuels. Worldwide energy demand is increasing and therefore, fossil fuel consumption as a current main source of energy increases as a result. On the other hand, limitation and depletion of petroleum resources are of concern in the near future. Internal combustion (IC) engines are widely used for transportation, power generation and industrial application and therefore, the aforementioned problems are more critical for them. Therefore, high-efficiency low-emission engines using more advanced combustion strategies, and new fuels that do not exploit conventional resources, are required. Extensive research is underway to identify alternative fuels and develop new combustion technologies.

Gas engines and in particular gas engines driven generators play an important role nowadays as an environmental friendly power generation (electricity and heat supply) technology. They can be used in various sectors such as power plants, automobile industry and also ship industry. Due to their flexibility of operating with various types of gaseous fuels and being more climate-friendly technology compared to those of diesel and gasoline engines, the more attention to this type of engine is needed.

In this study lean-burn dual-fuel combustion gas engines is used due to its ability to operate in conjunction with various environmentally friendly and renewable gaseous fuels. The main goal of a dual-fuel engine is to minimize fossil fuel dependency while improving performance and maintaining exhaust emissions as low as possible. However, knocking is an issue for operation at higher load. In order to improve the thermal efficiency of internal combustion engines at high loads, PREMIER (PREmixed Mixture

Ignition in the End-gas Region) combustion is proposed as a precursor to knocking. Engine performance, exhaust emissions, and end-gas autoignition characteristics of PREMIER combustion are investigated.

In the first part of this study, a pilot fuel-ignited dual-fuel gas engine was operated at constant speed under different intake pressures (101, 150, and 200 kPa) and various injection timings. A simulated biogas was served as the primary fuel and diesel as the pilot fuel. The biogas consisted of CH_4, CO_2, and N_2 at 58, 35, and 7% by volume, respectively. Both the maximum pressure and maximum ROHR increased when the pilot fuel injection timing was advanced. The end-gas autoignition phenomenon is observed in the ROHR traces for P_{in}=150 and 200 kPa. The ROHR peaks were evident after TDC, attributable to autoignition of end-gas unburned mixture that had attained the required conditions after the injection timing is advanced. This is defined as PREMIER combustion. The maximum mean effective pressure and thermal efficiency are evident during PREMIER operation because of autoignition in the end-gas region. Both a higher intake pressure and advanced injection timing promoted PREMIER combustion. 77 cycles attained end-gas autoignition at P_{in} = 200 kPa, and that 60 cycles attained autoignition when P_{in} = 150 kPa and end-gas autoignition attained at advanced injection timing for both cases. NOx emissions are increased with advancing injection timing at all intake pressure conditions. Maximum NO_x emission are observed under PREMIER operation at higher intake pressure cases. However, minimum CO and HC emissions are observed under PREMIER operation. As the injection timing is advanced and the pressure boosted, more cycles underwent end-gas autoignition; the associated heat release increased and, consequently, the PREMEIR intensity, PI, (indicator of degree of PREMIER combustion) value rose.

The second part of this study aimed to investigate the effect of CO_2 ratio to CH_4 in dual-fuel gas engine at high load. Typically, gaseous fuel combustion at higher load is accompanied by knocking if the proper combustion controlling strategy did not apply. Therefore, PREMIER combustion is proposed as a precursor to knocking at high load condition. Experiments are carried out using dual-fuel gas engine at supercharged condition with the intake pressure of 200kPa. The simulated biogas consisted of CH_4 and CO_2 is used as a primary fuel and diesel is used as a pilot fuel. Pilot fuel injection timing is varied during experiments. Maximum in-cylinder pressure and ROHR (during flame propagation as well as end-gas autoignition) are increased when injection timing is advanced. Within the most beneficial injection timings of all fueling cases, maximum in-cylinder pressure is observed for mixture with larger CO_2. Addition of CO_2 to CH_4 could make it possible to advance the injection timing in wider range. Thermal efficiency is slightly increased by addition of CO_2 under PREMIER combustion owing to knock-free end-gas autoignition of unburned mixture. When injection timing is advanced and PREMIER combustion achieved, IMEP increased as a result. Addition of CO_2 could suppress knocking and more knock-free end-gas autoignition cycles (PREMIER combustion) achieved. When the ratio of CO_2 to CH_4 increases, ratio of PREMIER combustion increases as well. End-gas autoignition commencements are observed earlier when CO_2 is increased in the mixture. When injection timing of pilot fuel is advanced, PI value increased because number of cycles with end-gas autoignition is larger and larger amount of heat from end-gas region is released. Finally, the relationship between PREMIER intensity (PI) and thermal efficiency and the relationship between PI and IMEP are investigated for all cycles. It is observed that thermal efficiency and IMEP are increased when PI is increased.

Acknowledgements

*In the name of **God**, the Most Gracious and the Most Merciful*

*First and foremost, all Glory and Praise be to **ALLAH**, the Almighty, the Creator, the Cherisher and Sustainer of the heavens and universe.*

*I would like to appreciate Ministry of Education, Culture, Sports, Science and Technology (**MEXT**), Japan in providing me the scholarship (MONBUKAGAKUSHOU) which it wouldn't have been possible without the generous support that I have been provided.*

*I am deeply grateful to my supervisor Professor Dr. **Eiji TOMITA,** whose expertise was invaluable, for his guidance, support and valuable advice during my studies. I can never forget his support and understanding during my Ph.D. course at Okayama University. I'll be forever grateful.*

*I would also like to thank Associate Professor Dr. **Nobuyuki KAWAHARA** and Assistant Professor Dr. **Kazuya TSUBOI** for their scientific supports and comments at different stages of my research.*

*I like to thank the members of my Ph.D. defense, Professor Dr. **Kazuhito OHASHI** and Professor Dr. **Akihiko HORIBE**, for their valuable time and willingness in accepting the task.*

Lots of appreciation and *gratefulness goes to Mrs. **Hanako OZAWA** for her continuous support and cooperation regardless of the matter whether it's personal or official. Words cannot express how grateful I am for your kindness and generosity. I'll be forever grateful.*

*I would like to thank the members of the Heat Power Engineering Laboratory specially my co-workers Mr. **Taiga HIDA**, for his help during experimental and numerical works. I would also like to thank **SAKASHITA**, **TOMOMATSU**, **HENRI** and other members of Heat Power Engineering Laboratory for their support during the course of my doctoral program.*

I am indebted to my past colleagues at *Heat Power Engineering Laboratory, Dr. **Yungjin Kim** (Post-doctoral fellow from Korea), Dr. **Kazi Mostafijur Rahman** (doctor student from Bangladesh), Dr. **Cagdas Aksu** (doctor student from Turkey). I have learnt a lot from them and I wish them all the very best.*

*I would wish to extend my appreciation to my **parents**, **my in-laws**, **brothers** and **sisters** for their pray and support during my educational life as well as personal life.*

*My heartfelt appreciation goes to my beloved wife, **Hannaneh Ahmadi**, for her support, help and encouragement. You inspired me during a difficult time when I needed words of encouragement. Words are not enough to express to you how grateful I am for the help you gave me. Thank you; I only hope I'll be able to return the favor to you sometime. I am incredibly fortunate to have someone like you in my life.*

Table of contents

List of Figures

List of Tables

1. Introduction

1.1 Internal combustion engine

Energy sources have always played a very important role in the development of human society. Energy is generally defined as the potential to do work or produce heat. A heat engine typically uses energy provided in the form of heat to do work and then exhausts the heat which cannot be used to do work. The first law and second law of thermodynamics constrain the operation of a heat engine. The internal combustion (IC) engine is a heat engine that the combustion of a fuel occurs with an oxidizer within the engine. Internal combustion engines have been used extensively to fulfill society's needs for power and transportation [1]. The exothermic reaction of a fuel with an oxidizer creates high temperature and pressure gases and engine partially converts the energy from the combustion to work by expansion of hot and high pressure gases. IC engines are widely used as power generating devices. IC engines are generally divided in two major categories: rotary (continuous-combustion) engines such as jet engines, gas turbines and most rockets, and reciprocating (intermittent-combustion) engines such as gasoline engines and diesel engines. Reciprocating engines, also known as piston engines, are the most commonly used IC engines. In this kind of engine, rotating motion is generated from combustion energy by means of reciprocating pistons and other components such as connecting rod and crankshaft. IC engines are further classified in two kinds: the spark ignition (SI) engine and the compression ignition (CI) engine. These engines can have one or more than one pistons which each piston moves inside a cylinder. They can operate on either four-stroke or two-stroke cycle. In four-stroke, four piston movements (piston stroke) are needed to complete one operating cycle, it means piston should complete four strokes to turning the crankshaft twice but in two-stroke cycle, two piston movements are needed over one revolution for each cycle. The most common IC engine is the four-

stroke. The four-stroke cycle includes intake, compression, power and exhaust and are shown in Figure 1.1.

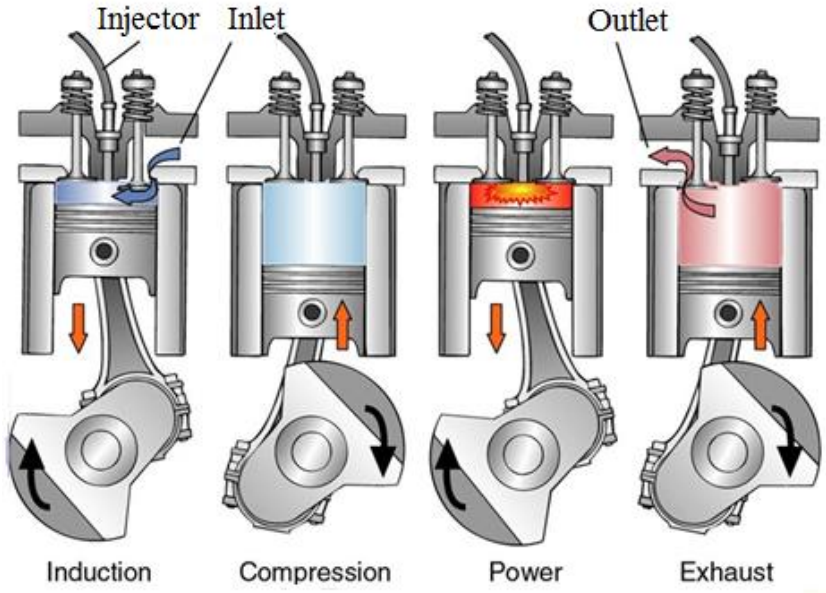

Figure 1.1. The four-stroke cycle (CI engine) (Source: Google)

In SI engines, fuel supply and fuel ignition are different from CI engines which air and fuel are mixed and then this mixture introduces into the cylinder and then compresses during compression stroke, pressure and temperature rises, and then in a pre-set ignition timing, the mixture is by means of spark plug. In CI engines, only air is introduced into cylinder and then compressed and shortly before end of compression, liquid fuel is sprayed to hot compressed air into the cylinder via injector and hence, combustion is initiated by autoignition of sprayed furl. The most outstanding advantage of CI engine such as diesel engine compare to SI engine is its efficiency. In diesel engine, compression ratio is higher than that of SI engine because unlike SI engine, only air is compressed and therefore, it is not limited by the pre-ignition problem. The original diesel engine was invented by Rudolf Diesel, a German engineer, in 1890 which was large in size and operated at low speed but later, in 1920s, high speed diesel engines were introduced for commercial

vehicle and in the 1930s for passenger cars. Since then, diesel engine has attracted much attention owing to high efficiency, better fuel economy as well as reliability. His engines were used to power pipelines, electric, water plants, automobiles, trucks, mine, oil fields, factories and marine craft.

1.2 Improvement of compression ignition engine

Diesel engines have been in constant evolution since the very beginning of motoring. Diesel engines are either two-stroke or four-stroke. From many years ago, researchers have been trying to develop the diesel engines in different fields such as engine geometry, after-treatment system, injection system, engine body material and etc. Thus, more advanced combustion strategies are being investigated, such as Homogeneous Charge Compression Ignition (HCCI) and Premixed Controlled Compression Ignition (PCCI). HCCI is an alternative combustion technology which has been emerged in order to improve engine efficiency and decrease fuel consumption as well as emissions [2-3]. HCCI combustion strategy depends on autoignition of in-cylinder mixture [4-7] similar to CI engines and is similar to SI engines as well, owing to using homogeneous charge for combustion. Thus, HCCI combustion can be regarded as the hybrid combustion processes [8]. In this type of combustion, fuel and oxidizer are well mixed and then compressed to the point of autoignition. The drawback of HCCI combustion is mainly combustion timing control and preparation of homogeneous mixture. In view point of emissions, HCCI engines have higher hydrocarbon (HC) and carbon monoxide (CO) emissions but lower oxides of nitrogen (NO_x) and particulate matter (PM) compare to diesel engines [9-11]. Although HCCI engines show higher thermal efficiency than diesel engines, there is still risk of knocking because the uncontrolled autoignition often yields knocking, therefore, an adequate combustion controlling strategy is required for this type of combustion [12,

13]. As commonly used engines are SI and diesel engines nowadays, therefore, HCCI engines require to reduce emissions of HC and CO in order to meet automobile emissions control regulations. However, practical operation range of HCCI combustion is extended but still the application of this type of combustion in practical engines is very less. Therefore, combining HCCI combustion with either SI or diesel engines are considered in order to control the combustion timing by means of spark plug or pilot fuel injection [14,15]. The PCCI combustion strategy is then applied in order to get the benefits of HCCI

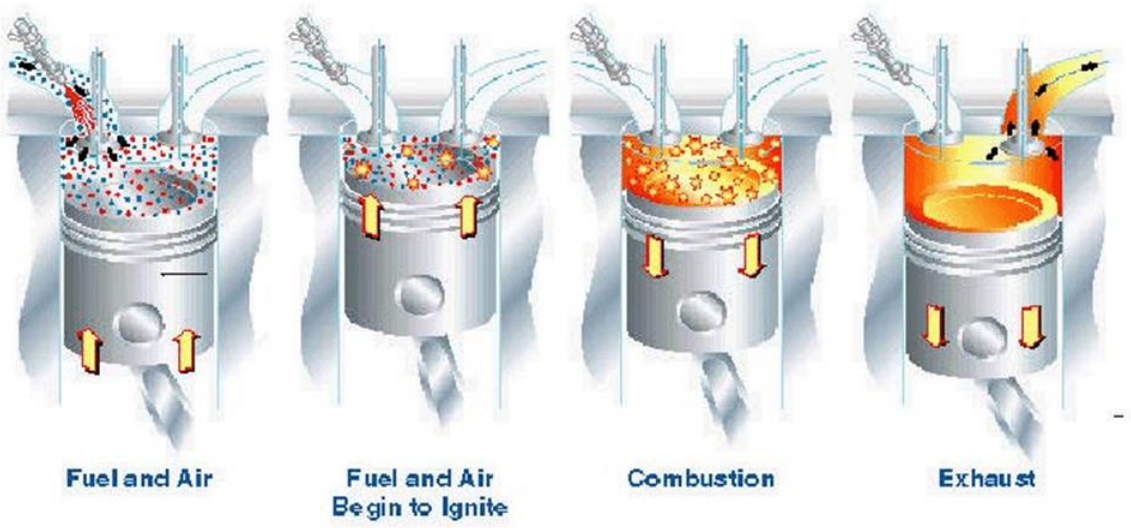

Figure 1.2. Concept of HCCI combustion [16]

combustion while retaining control over combustion phasing. Unlike HCCI combustion, in PCCI combustion air and fuel are not fully premixed (homogeneous) at the moment of ignition. In this type of combustion, air is compressed and fuel is injected prior to influence of compression begins and then air-fuel mixture is completely compressed similar to HCCI combustion and then combustion is occurred due to autoignition. The PCCI combustion can be considered as hybrid of direct injection CI and HCCI combustion. Experimental and numerical researches on four-stroke single cylinder HCCI combustion have done at the Lund University in Sweden [17-20]. Several fuels such as ethanol,

isooctane and natural gas have been used. They reported that NO_x was low for all fuels used but high emissions of HC and CO were observed. Later, by applying variable exhaust gas recirculation (EGR), they reduced HC, CO. Results of natural gas experiment [20] showed that HCCI combustion was sensitive to composition of natural gas. Advancement of HCCI combustion timing by increasing the intake temperature was reported in [21]. They also observed adverse trends of NO_x and those of CO and HC. When intake charge temperature increased, CO and HC emissions decreased but NO_x emission increased.

1.3 Dual-fuel engine

1.3.1 Dual fuel combustion process

The combustion process of dual fuel engine is a combination of combustion process of SI and CI engines. A pressure-volume (p-v) diagram of ideal SI (Otto cycle), ideal CI (Diesel cycle) and dual fuel combustion are shown in Figure 1.3. As shown in Figure 1.3 (a), the Otto cycle consists of: 1-2 isentropic compression process 2-3 constant volume heat addition 3-4 isentropic expansion process 4-1 constant volume heat rejection. In Figure 1.3(b), it can be seen that only heat addition process in diesel engine is different that occurs at constant pressure. However, dual-fuel cycle is considered as a hybrid of Otto cycle and Diesel cycle. Figure 1.3(c) shows the dual-fuel cycle process. All processes are same as Diesel cycle and Otto cycle except heat addition process, 2-4. The heat addition process in dual-fuel cycle consists of constant volume heat addition (2-3) similar to Otto cycle and constant pressure heat addition (3-4) similar to Diesel cycle. However, combustion occurs partly at constant volume and partly at constant pressure in dual-fuel combustion mode and therefore, thermal efficiency typically lies between Otto and Diesel cycle.

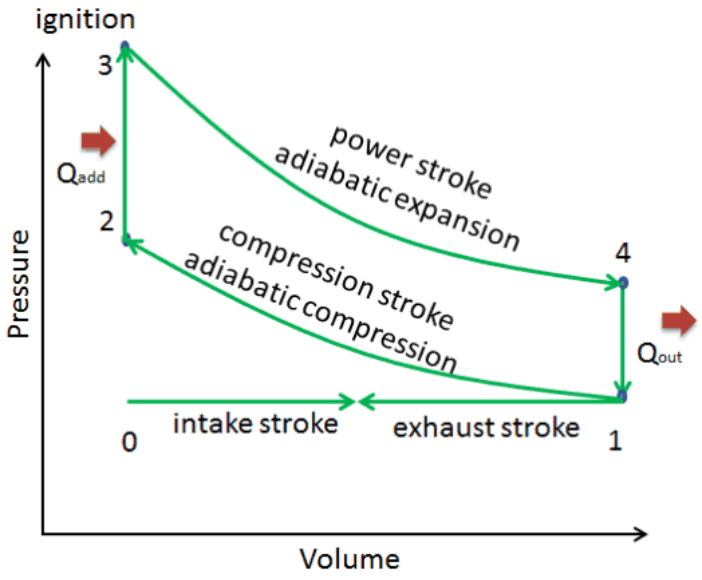
ignition
3
Qadd
2
power stroke
adiabatic expansion
compression stroke
adiabatic compression
4
Qout
Pressure
0
intake stroke
exhaust stroke
1
Volume

(a)

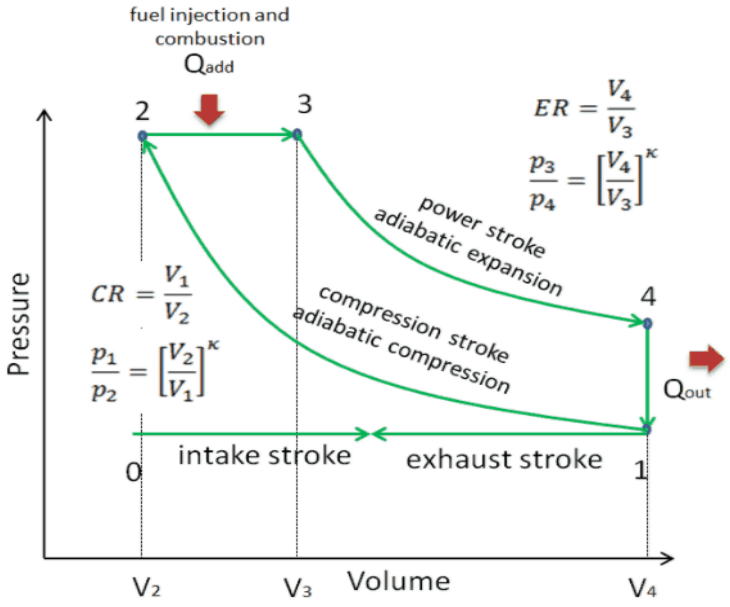
fuel injection and
combustion
Qadd
2
3
$ER = \frac{V_4}{V_3}$
$\frac{p_3}{p_4} = \left[\frac{V_4}{V_3}\right]^{\kappa}$
power stroke
adiabatic expansion
4
$CR = \frac{V_1}{V_2}$
$\frac{p_1}{p_2} = \left[\frac{V_2}{V_1}\right]^{\kappa}$
compression stroke
adiabatic compression
Qout
Pressure
0
intake stroke
exhaust stroke
1
V2
V3
Volume
V4

(b)

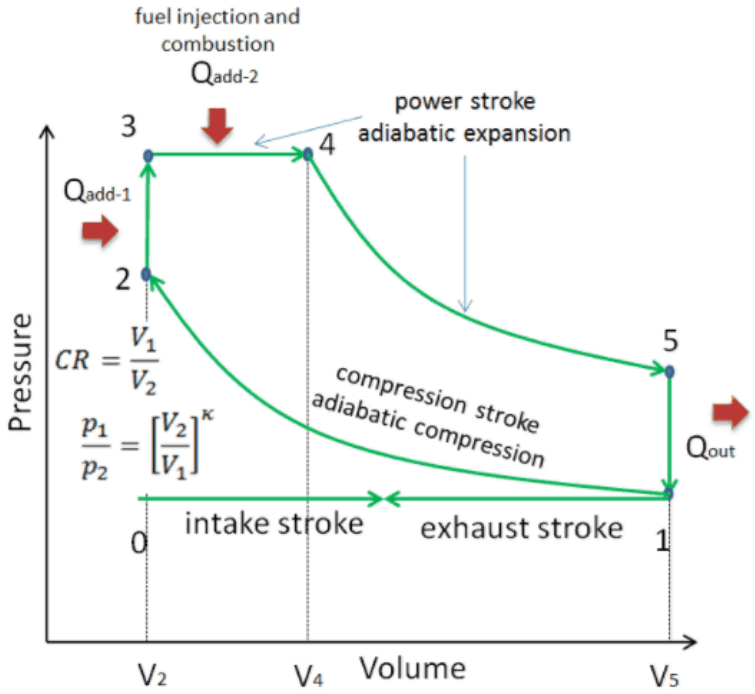

(c)

Figure 1.3. The combustion process of (a) Otto cycle (b) Diesel cycle (c) dual- cycle (www.nuclear-power.net/nuclear-engineering/thermodynamics/thermodynamic-cycles)

1.3.2 Dual fuel operation

A dual-fuel engine is a type of internal combustion engine that uses two types of fuel to generate power. Typically, one fuel is gaseous fuel and another is liquid fuel. In a dual-fuel engine, gaseous fuel is introduced at the intake port, where it is mixed with intake air, as shown in Figure 1.4. Because it is difficult to auto ignite the mixture by compression only, liquid fuel is used to support the ignition. The autoignition of liquid fuel creates the flame kernel and the gaseous fuel and air mixture (premixed mixture) is ignited by means of propagating flame. Therefore, dual-fuel combustion can be referred as combustion method which using both CI (autoignition) and SI (flame propagation) combustion process. Gaseous fuels can be used with the combination of spark plug as an ignition source, too. A reactivity controlled compression ignition (RCCI), is introduced as a

promising dual- fuel compression engine combustion strategy owing to its simultaneous reduction of NO_x and PM [22, 23]. In RCCI combustion strategy, two fuels of low and high reactivity would be used. The low reactivity fuel is introduced into cylinder to create a mixture of air and low reactivity fuel and then, high reactivity fuel is injected prior to ignition of the premixed mixture. Lower NO_x and PM emissions, fuel efficiency improvement and increasing thermal efficiency are suggested by Researchers at the University of Wisconsin [22, 23].

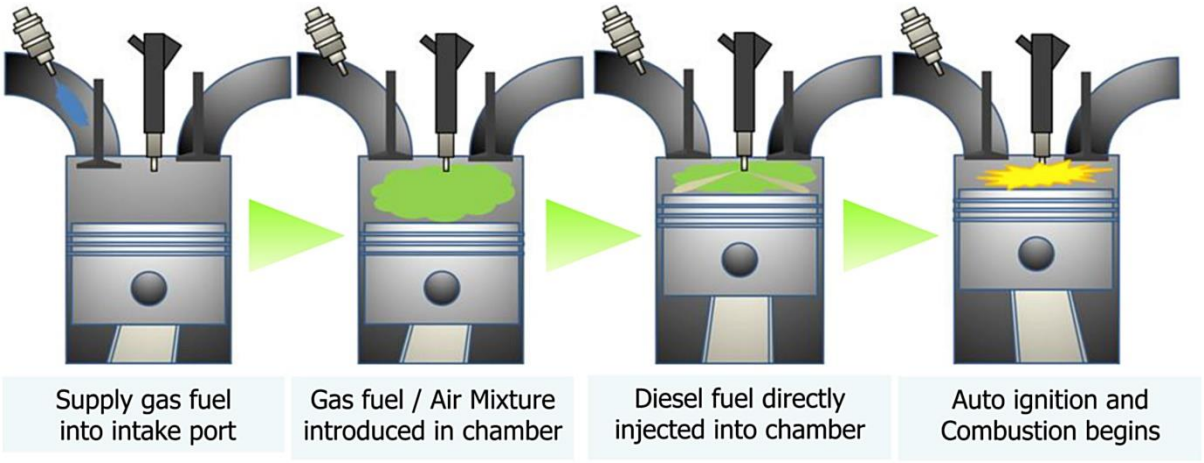

Figure 1.4. Dual fuel operation [24]

1.3.3 Gaseous fuels in dual fuel engines

As we mentioned in the previous section, one of the fuels used in dual-fuel engine is gaseous fuel. There are variety of gaseous fuels which can be used in dual-fuel engine such as natural gas or CNG, hydrogen, biogas, liquefied petroleum gas (LPG), producer gas, methane (CH_4) and etc. One of the most suitable energy resources among alternative fuels for internal combustion engines is biomass gas, because it is renewable, clean and readily available [25, 26]. Biomass is organic material obtained from animals or plants. Burning biomass releases stored energy. It can be burned directly or converted into liquid and gaseous biofuels, such as bioethanol, biodiesel and biogas, which can then be used as

fuels for transportation and electricity generation. Gaseous biofuels generated through CH_4 fermentation are called digester gas. They are produced from anaerobic fermentation of organic matter or feedstock (through biological processes) such as sewage sludge, agricultural and forest residues, manure and garbage. Anaerobic biogas is mainly composed of CH_4 and CO_2, but it also contains hydrogen (H_2), hydrogen sulfide (H_2S) and nitrogen (N_2). Its composition can vary due to differences in digestion conditions, humidity, temperature and other factors [27]. Another method to convert biomass into gaseous biofuel is gasification through thermochemical processes. The gaseous fuels obtained in this manner are called producer gases. They derive mainly from wood chips and sawdust and are mixtures of varying amounts of flammable gases (mainly carbon monoxide (CO) and H_2) and nonflammable gases of N_2 and CO_2 resulting from thermochemical conversion. Producer gas has a lower heating value and energy density compared with natural gas [28]. Use of producer gas in spark ignition (SI) engines has been studied extensively [29–33]. Among the gaseous fuels, biogas produced by CH_4 fermentation is regarded as a particularly promising alternative fuel for internal combustion engines. Biogas mainly comprises CH_4 (about 50–60%) and CO_2, and may be a good candidate fuel for power generation units in rural areas.

1.3.4 Exhaust emissions of dual-fuel engines

The combustion process of dual- fuel engine is a hybrid of SI and CI engines combustion, therefore, exhaust emissions are typically a trade-off between CI and SI engines. It is well known that if combustion is complete, exhaust products are water vapor and carbon dioxide but in actual combustion process, it is not happening. However, the major exhaust pollutants from exhaust are HC, CO, NO_x and PM or soot. Greenhouse gas (GHG) emissions are also a serious environmental concern. Carbon dioxide (CO_2), methane (CH_4), nitrous

oxide (N_2O) and fluorinated gases are considered as GHGs; they trap heat in the atmosphere. Carbon dioxide is typically produced by the burning of fossil fuels, and thus is of particular concern as a GHG. Of the GHGs, CO_2 contributes the most to climate change because of the enormous quantity that is emitted. Although it is produced naturally, human activities can greatly affect the amount of CO_2 in the atmosphere. The combustion of fossil fuels for transportation, power generation and other industrial purposes represents the main human activity responsible for increasing the amount of CO_2 in the atmosphere. CO emission is produced as a result of incomplete combustion. Generally, CO emissions are affected by the fuel type, injection timing, injection pressure, engine load and speed [34]. Hydrocarbon emission is an indicator of combustion efficiency and it is produced from unburnt fuel. Nitrogen oxides are typically produced because of higher combustion temperature which promotes the oxidation of the nitrogen contained in the air and soot is generally produced from incomplete combustion of hydrocarbons. CI engines are generally producing lower amount of HC and CO emissions compared to SI engines due to their instantaneous combustion process but on the other hand, NO_x and PM emissions are higher because of high in-cylinder temperature (local temperature) and improper fuel-air mixing, respectively. However, dual-fuel combustion strategy is a promising technique for controlling both NO_x and soot emissions that are the main concern in existing diesel engines. But still the high emissions of HC and CO (especially at part load) are the concerns of dual fuel combustion.

1.3.5 Dual-fuel compression ignition gas engine

Dual- fuel gas engine is a variety of dual-fuel engine which gaseous fuel is the main fuel. Gas engine has a long history when coal gas is used instead of steam in piston engine. After Second World War, IC engines spread quickly and they used petroleum oil as a fuel.

Later, natural gas is used in CI engine together with another fuel. Natural gas consists mainly Methane and therefore, it is considered as a clean burning fuel. As it is discussed in section 1.3.3, there are different types of gaseous fuels that can be used under dual-fuel operation. The high self-ignition temperature (autoignition temperature) of gaseous fuel prevents it from being used directly in compression ignition (CI) engines. An ignition source is required, and consequently gaseous fuel is used in a dual-fuel mode to initiate combustion. In gas engine, a homogeneous mixture of gaseous fuel and air is introduced into the cylinder and the mixture is ignited by means of pilot fuel injection. Pilot fuel autoignition creates flame kernel and further, rest of the mixture is burned by propagated flame. If the unburned mixture ignites spontaneously prior to being consumed by the propagating flame, the knocking combustion occurs. The knocking combustion should be avoided owing to its negative influence on engine. One of the main reason to increase the risk of knocking combustion is compression ratio. Extensive research has been conducted on the use of different gaseous fuels in the dual-fuel operation mode. However, the amounts of such fuel that can thus be used are limited by knocking caused by rapid heat release [35–38]. Fundamental research on the application of gaseous fuels in the dual-fuel operation mode was reviewed by Karim [39, 40]. Walsh et al. conducted extensive investigations on biogas use in SI and CI engines [41]. Increased unburned hydrocarbon (UHC) emission and reduced particulate matter (PM) were reported by Mustafi et al. [42] due to use of simulated biogas. They also reported that NO_x emission was reduced in the dual-fuel mode. Bedoya et al. [43] studied diesel fuel quality and the effects of a mixing system in a dual-fuel diesel- biogas engine. They found that the thermal efficiency increased, while CH_4 and CO emissions decreased, when the supercharged mixing system and biodiesel as pilot fuel were used compared to natural aspirated system. Yoon and Lee [44] experimentally investigated the combustion characteristics of biodiesel and diesel

as pilot fuels in a biogas dual-fuel engine. They found that the peak pressure, rate of heat release (ROHR) and indicated mean effective pressure (IMEP) were lower with biogas-biodiesel at low load. A significantly lower NO_x emission was observed in the dual-fuel mode than in the diesel fuel mode, but HC and CO emissions were significantly higher in the dual-fuel mode. Also, lower thermal efficiency was observed for dual-fuel mode operation. The advantages and disadvantages of dual-fuel operation with different gaseous fuels and pilot fuels [45-59], fuel properties [50, 51], composition and quantities [52-58], EGR [57], injection timing [45, 47, 49, 51,59], load [49, 58, 60, 61,62], speed [58, 63, 64], equivalence ratio [65] and compression ratio [59, 60] have been studied extensively. The overall results revealed that dual-fuel strategy is the promising way to use gaseous fuels. Natural gas and biogas are reported as suitable alternative fuels under dual fuel operation due to their combustion and emission characteristics [45]. Addition of hydrogen, advancing injection timing and using EGR can improve the engine efficiency as well as reducing emission in biogas/diesel under dual fuel operation [57]. Increasing compression ratio decrease carbon monoxide as well as hydrocarbon emission but increase oxides of nitrogen as well thermal efficiency [59, 60]. It is also reported that thermal efficiency can be improved with increasing engine speed and amount of pilot fuel under dual fuel operation [58, 63, 64]. A Strong effect of biogas flow rate and methane concentration on thermal efficiency was reported [58]. They also reported that maximum efficiency can be achieved by increasing load and speed [58]. Improving thermal efficiency by increasing equivalence ratio was reported by F.Z. Aklouche et.al. [65].

1.3.6 Advantages and application of dual fuel gas engine

The main advantages of gas engine over other engines is the flexibility of working with the variety of gaseous fuels. Typically, gaseous fuels are more environmentally friendly

than conventional petroleum fuels. Unlike CI engines, there is no need to use high pressure injector because small amount of pilot fuel uses as an ignition source, therefore, cheaper and simple type injector can be suitable in this type of engine. Also, strong initial combustion as a result of pilot fuel autoignition is another benefit of gas engine under dual- fuel operation. Gas engines can be a good candidate to use in road vehicles, power generation units, power plants and marine industry both for on-board power generation and propulsion duties [66, 67].

Table 1.1: Types of gas engines and their applications in industries [66]

Company	Engine type	Fuel	Application	P_{me} (MPa)	η
Wärtsilä	20V34SG	NG	Power plant/ship	2.20	0.469
MAN	18V51/60DF	NG	Power plant/ship	1.90	0.496
Mitui	18MD36G	NG	Power plant	1.84	0.460
GE Jenbacher	18J920	NG	Power plant	2.20	0.487
Rolls-Royce	C26:33L9	NG	Ship	1.85	0.483
Caterpillar	G3520C	CMM	Power plant	1.89	0.469
Caterpillar	CG132-8	NG	Power plant	1.9	0.452
Weichai Power	WP7NG260E40	NG	Road vehicle	1.39	0.389
Yanmar	CP10WE1	NG	Cogeneration	10*	NA
Yanmar	CP25WE	Biogas	Cogeneration	25*	NA

p_{me} :Mean effective pressure, η :Effective thermal efficiency, CMM: Coal mine methane

* P_e : Rated power, kW (https://www.yanmar.com/media/global/2015/catalog/cp.pdf)

1.4 PREMIER combustion

In dual- fuel combustion, gaseous fuel and air mixture is ignited by means of flame kernels which are created as a result of pilot fuel autoignition. If the mixture does not consume by propagated flame completely within certain time period, unburnt mixture may undergo autoignition in the end-gas region. Typically, the end-gas autoignition is accompanied with shock waves, high peak cylinder pressure and pressure oscillation

which are not favorable conditions for engine. This phenomenon calls “Knocking” and it should be avoided. If the end-gas region undergoes autoignition but without any pressure oscillation, it would be best condition in terms of emissions and combustion efficiency. When end-gas region exhibits autoignition, CO and HC emissions are mitigated because unburnt mixture undergoes autoignition before emerging from exhaust. The improvement of thermal efficiency and engine output expected owing to end-gas region autoignition. The end-gas region autoignition without pressure oscillation is visualized in SI natural gas engine in our laboratory [68]. This phenomenon is named as “PREMIER” combustion which is the acronym for PREmixed Mixture Ignition in the End Gas Region. Later, Azimov et al. [69], published the first paper about PREMIER combustion in dual-fuel gas engine. After that, several experimental and numerical research have been conducted in dual- fuel gas engine and in particular to extend our findings of PREMIER combustion [70-77]. Different gaseous fuels as well as different engine conditions were taken into account. In consequence, our combustion strategy showed the noticeable improvement of thermal efficiency as well as engine output. HC and CO emissions were reduced but the NO_x emission is the only drawback of this type of combustion in terms of exhaust emissions. The operation range is also another concern for this type of combustion. The operation range is limited and more study is required to extend it. However, the PREMIER combustion and results of our previous works on PREMIER combustion will be explained comprehensively in next chapter.

1.5 Problem declaration and objective of the present study

It is known that CI engines are widely used in different application such as power generation, transportation, agriculture and etc. owing to their output power and efficiency. On the other hand, emission regulations and global warming issue, as well as

depletion of fossil fuels and their cost, it is not feasible to use petroleum based fuels as an energy source especially for the power generation and transportation sector. Therefore, high-efficiency, low-emission engines using more advanced combustion strategies, and substitute fuels that do not depend on conventional resources are required.

The dual- fuel strategy is introduced in order to use gaseous alternative fuels which are more environmental friendly. However, higher CO and HC emissions of dual- fuel combustion are still an important concern. HCCI, PCCI and RCCI are introduced as well, but in terms of high load condition and combustion control, they seem not to be good candidates.

The motivation of the current study is to develop our findings in dual- fuel gas engine in order to improve efficiency and reduce exhaust emissions. Gaseous fuels such as biogas, methane and CO_2 have been used in different portions as primary fuels. A simulated biogas having the composition of 58% methane, 35% carbon dioxide and 7% nitrogen was used. Diesel fuel (pilot fuel) is used as an ignition source with small quantity which is directly sprayed into cylinder with a common rail system. In the first part of our research, three intake pressures namely 101, 150 and 200 kPa were tested with simulated biogas as a fuel. In the second part, methane – carbon dioxide mixture is investigated at 200 kPa intake pressure. Carbon dioxide is added to methane from 0 to 50% by volume. Combustion, performance, emissions and end-gas autoignition characteristics of tested fuels are presented here.

1.6 Thesis outline

The present work consists of six chapters.

In the **First** chapter, the fundamental of IC engines and their classification are discussed. Then, dual- fuel combustion as a promising method to use gaseous fuels are explained. Alternative fuels and in particular gaseous fuels are described as a suitable energy resources for IC engines. Exhaust emissions, applications and advantages of dual- fuel gas engine are presented. Finally, the concept of "PREMIER" combustion and objective of the present study are discussed.

In the **Second** chapter, PREMIER combustion is discussed in details. The differences between normal, PREMIER and knocking and how to classified them are defined. After that, our laboratory previous works on PREMIER combustion are discussed. Some important research works are selected and summarized.

In the **Third** chapter, experimental set up and data evaluation method are discussed. Details of the test engine, specifications and experimental conditions are discussed. Gaseous fuels, their properties and delivery strategies are given in the third chapter. Emission measurement devices are also explained. Some mathematical calculation are also explained in this chapter.

In the **Fourth** chapter, combustion, performance, emission and end-gas autoignition characteristics of dual- fuel gas engine fueled with simulated biogas are discussed.

In the **Fifth** chapter, combustion, performance, emission and end-gas autoignition characteristics of dual- fuel gas engine fueled with methane- carbon dioxide are discussed.

In the **Sixth** chapter, conclusions of the present work are summarized and discussed.

References

[1] S Fernando, C Hall , S Jha . NOx reduction from biodiesel fuels. Energy & Fuels; 20 (2006); 376–82.

[2] F. Zhao, T. N. Asmus, D. N. Assanis, J. E. Dec, J. A. Eng, and P. M. Najt, "Homogeneous charge compression ignition (HCCI) engines, SAE paper, 2003.

[3] R. H. Stanglmaier and C. E. Roberts, "Homogeneous charge compression ignition (HCCI): benefits, compromises, and future engine applications, SAE Paper 1999-01-3682, 1999

[4] S.V. Khandal, N.R. Banapurmath, V.N. Gaitonde, S.S. Hiremath. Paradigm shift from mechanical direct injection diesel engines to advanced injection strategies of diesel homogeneous charge compression ignition (HCCI) engines- A comprehensive review. Renewable and Sustainable Energy Reviews, 70 (2017), 369-384.

[5] J. Matthews, H. Santoso, W. Cheng. Load Control for an HCCI Engine. SAE Technical Paper 2005-01-0150, 2005,

[6] S. Jafarmadar, P. Nemati, R. Khodaie. Multidimensional modeling of the effect of Exhaust Gas Recirculation (EGR) on exergy terms in an HCCI engine fueled with a mixture of natural gas and diesel. Energy Conversion and Management, 105 (2015), 498-508.

[7] J. Kang, C. Chang, J. Chen, M. Chang. Concept and Implementation of a Robust HCCI Engine Controller. SAE Technical Paper 2009-01-1131, 2009.

[8] S Saxena, S Schneider, S Aceves, R Dibble. Wet ethanol in HCCI engines with exhaust heat recovery to improve the energy balance of ethanol fuels. Applied Energy. 98 (2012); 448-457.

[9] D. S. Kim and C. S. Lee, Improved emission characteristics of HCCI engine by various premixed fuels and cooled EGR, Fuel, 85 (2006), 695–704.

[10] D Ganesh, G Nagarajan. Homogeneous charge compression ignition (HCCI) combustion of diesel fuel with external mixture formation. Energy; 35 (2010); 148-157.

[11] AP Singh, AK Agarwal. Combustion characteristics of diesel HCCI engine: An experimental investigation using external mixture formation technique. Applied Energy; 99 (2012): 116-125.

[12] M. Andreae, W. Cheng, T. Kenney, J. Yang. On HCCI Engine Knock. SAE Technical Paper 2007-01-1858, 2007.

[13] H. Ma, H Xu, J. Wang, C Tan. Investigation on the Self-Stabilization Feature of HCCI Combustion. SAE Technical Paper 2014-01-2663, 2014.

[14] L.K. Manofsky Olesky, R.J. Middleton, G.A. Lavoie, M.S. Wooldridge, J.B. Martz. On the sensitivity of low temperature combustion to spark assist near flame limit conditions. Fuel; 158 (2015), 11-22.

[15] H. Bendu, S. Murugan. Homogeneous charge compression ignition (HCCI) combustion: Mixture preparation and control strategies in diesel engines. Renewable and Sustainable Energy Reviews, 38 (2014), 732-746.

[16] P. V. Ramana, D. Maheswar, B. Umamaheswar Gowd, An approach of experimental study on HCCI engine, International Journal of Advanced Research in Engineering and Applied Sciences, 4 (2015) | No. 5.

[17] N Iida, Alternative Fuels and Homogeneous Charge Compression Ignition Combustion Technology, SAE paper 972071, 1997.

[18] P Flynn et al., Premixed Charge Compression Ignition Engine with Optimal Combustion Control, International Patent WO9942718, World Intellectual Property Organization.

[19] M. Yao and J. Qin, Simulating the Homogenous Charge Compression Ignition Process Using a Detailed Kinetic Model for Dimethyl Ether (DME) and Methane Dual Fuel, SAE technical paper, 2004-01-2951.

[20] DL Flowers, SM Aceves, CK Westbrook, JR Smith, RW Dibble, Sensitivity of Natural Gas HCCI Combustion to Fuel and Operating Parameters Using Detailed Kinetic Modeling, In AES-Vol. 39,"Proceedings of the ASME Advanced Energy Systems Division -1999.

[21] M. Izadi Najafabadi, A. A. Nuraini, A. Nor Mariah, and L. Abdul Mutalib, Effects of intake temperature and equivalence ratio on HCCI ignition timing and emissions of a 2-stroke engine, Applied Mechanics and Materials Journal, 315 (2013), 498–502.

[22] D Splitter, R Hanson, R Reitz. High Efficiency, Low Emissions RCCI Combustion by Use of a Fuel Additive; SAE paper, 2010-01-2167.

[23] S Curran, V Prikhodko, R Wagner, K Cho, Ch Sluder, S Kokjohn, R Reitz. In-Cylinder Fuel Blending of Gasoline/Diesel for Improved Efficiency and Lowest Possible Emissions on a Multi-Cylinder Engine , SAE paper; 2010-01-2206.

[24] T Tsujimura, Y Suzuki, The utilization of hydrogen in hydrogen/diesel dual fuel engine, International Journal of Hydrogen Energy, 42 (2017), 14019-14029.

[25] S. S. Nathan, J. M. Mallikarjuna and A. Ramesh, An experimental study of the biogas–diesel HCCI mode of engine operation, Energy Conversion and Management; 51(2010); 1347–1353.

[26] A. Henham and M. K. Makkar. Combustion of simulated biogas in a dual-fuel diesel engine. Energy Conversion and Management; 39(1998); 2001–2009.

[27] S. Yadvika, T. R. Sreekrishnam, S. Kohli and V. Rana, "Enhancement of biogas production from solid substrates using different techniques––a review", Bioresource Technology, 95 (2004) –; 1-10.

[28] T. B. Reed, Encyclopedia of biomass thermal conversion–The principles and technology of pyrolysis, gasification and combustion; The Biomass Energy Foundation Press, 2002.

[29] N. Homdoung, N. Tippayawong, N. Dussadee, Performance and emissions of a modified small engine operated on producer gas. Energy Conversion and Management, 94 (2015); 286–292.

[30] S. Tsiakmakis, D. Mertzis, A. Dimaratos, Z. Toumasatos and Z. Samaras, Experimental study of combustion in a spark ignition engine operating with producer gas from various biomass feedstocks, Fuel; 122 (2014); 126–139.

[31] J. Ulfvik, M. Achilles, M. Tuner and B. Johansson, SI Gas Engine: Evaluation of Engine Performance, Efficiency and Emissions Comparing Producer Gas and Natural Gas. SAE International Journal of Engines; 4 (2011); 1202–1209.

[32] J. Ahrenfeldt, U. Henriksen, J. Schramm and T. Jensen, Combustion chamber deposits and PAH formation in SI engines fueled by producer gas from biomass gasification. SAE Technical Paper 2003-01-1770, 2003.

[33] B. Zhang, C. Ji, S. Wang, X. Liu. Combustion and emissions characteristics of a spark-ignition engine fueled with hydrogen–methanol blends under lean and various loads conditions. Energy; 74 (2014), 829-835.

[34] Ozener O, Yuksek L, Ergenc A.T, Ozkan M, Effects of soyabean biodiesel on a DI diesel engine performance, emission and combustion characteristics, Fuel. 115 (2014); 875-8.

[35] G. A. Karim. An examination of some measures for improving the performance of gas fueled diesel engines at light load. SAE Technical Paper 912366, 1991.

[36] Z. Wang. Z. Zhao, D. Wang, M. Tan, Y. Han, Z. Liu and H. Dou. Impact of pilot diesel ignition mode on combustion and emissions characteristics of a diesel/natural gas dual fuel heavy-duty engine. Fuel, 167(2016); 248–256.

[37] J. Liu, X. Zhang, T. Wang, J. Zhang and H. Wang. Experimental and numerical study of the pollution formation in a diesel/CNG dual-fuel engine. Fuel, 159 (2015); 418–429.

[38] L. Tarabet, K. Loubar, M. S. Lounici, K. Khiari, T. Belmrabet and M. Tazerout. Experimental investigation of DI diesel engine operating with eucalyptus biodiesel/natural gas under dual fuel mode. Fuel, 133 (2014); 129–139.83.

[39] G. A. Karim. A review of combustion processes in the dual-fuel engine – the gas diesel engine. Progress in Energy and Combustion Science, 6 (1980); 277–285.

[40] G. A. Karim. The dual-fuel engine of the compression ignition type - prospects, problems and solutions - a review. SAE Technical Paper 831073, 1983, https://doi.org/10.4271/831073.

[41] J. L. Walsh, C. C. Ross, M. S. Smith and S. R. Harper, Utilization of biogas, Biomass, 20 (1989); 277–290.

[42] N.N. Mustafi, R.R. Rain and S.Verhelst, Combustion and emissions characteristics of a dual-fuel engine operated on alternative gaseous fuels, Fuel, 109 (2013); 669-678.

[43] I. D. Bedoya, A. A Arrieta and F. J. Cadavid, Effects of mixing system and pilot fuel quality on diesel–biogas dual-fuel engine performance, Bioresource Technology; 100 (2009), 6624–6629.

[44] S. H Yoon and C. S. Lee, Experimental investigation on the combustion and exhaust emission characteristics of biogas–biodiesel dual-fuel combustion in a CI engine, Fuel, Fuel and Energy Abstracts; 92(2011), 992–1000.

[45] B. B. Sahoo, N. Sahoo, U. K. Saha, Effect of engine parameters and type of gaseous fuel on the performance of dual-fuel gas diesel engines—A critical review, Renewable and Sustainable Energy Reviews, 13(2009); 1151–1184.

[46] C. C. M. Luijten, E. Kerkhof, Jatropha oil and biogas in a dual fuel CI engine for rural electrification, Energy Conversion and Management 52 (2011); 1426–1438.

[47] R. Chandra, V. K. Vijay, P. M. V. Subbarao, T. K. Khura, Performance evaluation of a constant speed IC engine on CNG, methane enriched biogas and biogas, Applied Energy, 88 (2011); 3969–3977.

[48] N. H. S. Ray, M. K. Mohanty, R. C. Mohanty, Biogas as alternate fuel in diesel engines: A literature review, IOSR Journal of Mechanical and Civil Engineering (IOSR-JMCE), 9(2013), 23–28.

[49] E. Tomita, N. Kawahara, M. Kondo and Y. Sunada, Combustion and exhaust emissions characteristics of pilot-ignited engine fueled with digester gas; CIMAC congress, (2013), Shanghai, Paper No. 145.

[50] K. Cacua, A. Amell, F. Cadavid, Effects of oxygen enriched air on the operation and performance of a diesel-biogas dual-fuel engine, Biomass and Bioenergy, 45(2012); 159–167.

[51] V. Makareviciene, E. Sendzikiene, S. Pukalskas, A. Rimkusb and R. Vegneris. Performance and emission characteristics of biogas used in diesel engine operation. Energy Conversion and Management, 75 (2013); 224–233.

[52] S. Bari, Effect of carbon dioxide on the performance of biogas/diesel dual-fuel engine, Renewable Energy; 9 (1996), 1007–1010.

[53] M. Feroskhan and S. Ismail, Investigation of the effects of biogas composition on the performance of a biogas–diesel dual fuel CI engine, Biofuels, 7(2016); 593–601.

[54] S. Swami Nathan, J. M. Mallikarjuna, A. Ramesh, An experimental study of the biogas–diesel HCCI mode of engine operation, Energy Conversion and Management 51 (2010); 1347–1353.

[55] D. Barik, S. Murugan, Investigation on combustion performance and emission characteristics of a DI (direct injection) diesel engine fueled with biogas- diesel in dual fuel mode, Energy, 72 (2014); 760–771.

[56] D. Barik, A. K. Satapathy and S. Murugan, Combustion analysis of the diesel–biogas dual fuel direct injection diesel engine– the gas diesel engine, International Journal of Ambient Energy, 38(2015), 259–266.

[57] X. Shan, Y. Qian, L. Zhu, X. Lu, Effects of EGR rate and hydrogen/carbon monoxide ratio on combustion and emission characteristics of biogas/diesel dual fuel combustion engine, Fuel, 181 (2016); 1050–1057.

[58] H. Ambarita, Performance and emission characteristics of a small diesel engine run in dual-fuel (diesel-biogas) mode, Case Studies in Thermal Engineering, 10 (2017); 179–191.

[59] B. J. Bora and U. K. Saha. Optimization of injection timing and compression ratio of a raw biogas powered dual fuel diesel engine. Applied Thermal Engineering, 92 (2016); 111–121.

[60] B. J. Bora, UK Saha, S. Chatterjee and V. Veer. Effect of compression ratio on performance, combustion and emission characteristics of a dual fuel diesel engine run on raw biogas. Energy Conversion and Management, 87 (2014); 1000–1009.

[61] D. K. Ramesha, A. S. Bangari, C. P. Rathod and S. Chaitanya, Combustion, performance and emissions characteristics of a biogas fuelled diesel engine with fish biodiesel as pilot fuel, Biofuels, 6(2015); 9–19.

[62] R. Uma, T. C. Kandpal and V. V. N. Kishore, Emission characteristics of an electricity generation system in diesel alone and dual fuel modes, Biomass & Bioenergy; 27(2004), 195–203.

[63] N. Tippayawong, A. Promwungkwa and P. Rerkkriangkrai. Long-term operation of a small biogas/diesel dual-fuel engine for on-farm electricity generation, Biosystems Engineering. 98 (2007); 26–32.

[64] P. M. Duc, K. Wattanavichien, Study on biogas premixed charge diesel dual fuelled engine, Energy Conversion and Management 48 (2007); 2286–2308.

[65] F. Z. Aklouche, K. Loubar, A. Bentebbiche, S. Awad, M. Tazerout, Experimental investigation of the equivalence ratio influence on combustion, performance and exhaust emissions of a dual fuel diesel engine operating on synthetic biogas fuel, Energy Conversion and Management 152 (2017) 291–299.

[66] L Feng, J Zhai, L Chen, W Long, J Tian, B Tang. Increasing the application of gas engines to decrease China's GHG emissions, Mitigation and Adaptation Strategies for Global Change, 22 (2017), 839–861.

[67] Information concerning the application of Gas Engines in the Marine industry, From the CIMAC Working Group 17 "Gas Engines", 2013.

[68] E. Tomita, N. Kawahara and J. Zheng, Visualization of auto-ignition of end gas region without knock in a spark-ignition natural gas engine, Journal of KONES. Powertrain and Transport; 17(2010), 521–527.

[69] U. Azimov , E. Tomita , N. Kawahara and Y. Harada, Premixed mixture ignition in the end-gas region (PREMIER) combustion in a natural gas dual-fuel engine: operating range and exhaust emissions, International Journal of Engine Research; 12 (2011), 484–497.

[70] E. Tomita, N. Kawahara, M. Kondo and Y. Sunada, Combustion and exhaust emissions characteristics of pilot-ignited engine fueled with digester gas; CIMAC congress, (2013), Shanghai, Paper No. 145.

[71] E. Tomita, Y. Harada, N. Kawahara and A. Sakane, Effect of EGR on combustion and exhaust emissions in supercharged dual-fuel natural gas engine ignited with diesel fuel, SAE Technical Paper 2009-01-1832, (2009).

[72] M. M. Roy , E. Tomita , N. Kawahara , Y. Harada and A. Sakane, Comparison of performance and emissions of a supercharged dual-fuel engine fueled by hydrogen and hydrogen-containing gaseous fuels, International Journal of Hydrogen Energy; 36(2011), 7339–7352.

[73] U. Azimov , E. Tomita, N. Kawahara and Y. Harada, Effect of syngas composition on combustion and exhaust emission characteristics in a pilot-ignited dual-fuel engine

operated in PREMIER combustion mode, International Journal of Hydrogen Energy; 36(2011), 11985–11996.

[74] U. Azimov, E. Tomita and N. Kawahara, Ignition, combustion and exhaust emission characteristics of micro-pilot ignited dual-fuel engine operated under PREMIER combustion mode, SAE Technical Paper; 2011-01-1764, (2011).

[75] C. Aksu, N. Kawahara, K. Tsuboi, S. Nanba, E. Tomita and M. Kondo, Effect of hydrogen concentration on engine performance, exhaust emissions and operation range of PREMIER combustion in a dual fuel gas engine using methane-hydrogen mixtures. SAE Technical Paper; 2015-01-1792, (2015).

[76] C. Aksu, N. Kawahara, K. Tsuboi, M. Kondo and E. Tomita, Extension of PREMIER combustion operation range using split micro pilot fuel injection in a dual fuel natural gas compression ignition engine: A performance-based and visual investigation, Fuel; 185 (2016), 243–253.

[77] N. Kawahara, Y. Kim, H. Wadahama, K. Tsuboi, E. Tomita, Differences between PREMIER combustion in a natural gas spark-ignition engine and knocking with pressure oscillations, Proceedings of the Combustion Institute; 37(2018), 4983-4991. https://doi.org/10.1016/j.proci.2018.08.055.

2.1 PREMIER combustion

In normal combustion, pilot fuel autoignition creates flame kernel and then flame propagation moves toward the combustion chamber uniformly with normal speed. Knocking combustion is a phenomenon that part of air- fuel mixture may be autoignited in the end- gas region when they reach to autoignition condition [1- 6]. The PREMIER combustion strategy has been proposed to improve the performance and exhaust emission of internal combustion engines and in particular dual- fuel combustion engines [7- 18]. PREMIER combustion differs significantly from normal combustion and knocking combustion in its end-gas autoignition characteristics. Typically, end- gas autoignition occurs at very high rate and yields the sudden pressure and temperature rise. After compression of the gaseous fuel, some flame kernels are created due to autoignition of pilot fuel. The autoignition triggers flame propagation of gaseous fuel and air mixture. Combustion heat is released and the in-cylinder pressure and temperature increase further. From this point onward, the characteristics of the unburned gas have an important role in determining the mode of combustion. At this stage, the autoignition timing of the end-gas region and heat release characteristics determine the occurrence of knock or PREMIER combustion. If the end-gas region has reached the autoignition state, which takes place typically after top dead center (TDC), a second combustion occurs, which results in either PREMIER or knocking combustion. PREMIER combustion lacks the properties of knocking combustion, such as pressure oscillation. Consequently, higher thermal efficiency and engine output, as well as lower CO and HC emissions, can be achieved when the engine works in the PREMIER mode due to occurrence of knock-free end-gas autoignition. In PREMIER combustion, rises in pressure and ROHR is not as steep as knocking combustion. However, due to longer sustainability of in-cylinder pressure

and temperature, NO_x emission is increasing. Prior to the present research work, several experimental researches have been done on SI engine and dual-fuel engines and in particular PREMIER combustion. Some of them are summarized in this chapter.

2.2 Nobuyuki Kawahara and Eiji Tomita (2009) [6]

The visualization of end-gas autoignition and pressure wave in a hydrogen SI engine has been performed by means of high speed camera [6]. Relationship between amount of unburned mixture and knocking intensities, end-gas autoignition location, timing and pressure wave were investigated using high-speed visualization images. A compression–expansion engine with a bore and stroke of 78 and 85 mm, compression ratio of 9.0:1 and 600 RPM operation speed was used. The cylinder was charged with homogeneous H_2+ 0.5 O_2+ 1.9 Ar mixture. The spark timing varied from 330° to 370° in order to obtain several combustion modes from normal to severe knocking combustion. Also, a spectrometer equipped with an intensified CCD was used to investigate the effects of knocking and pressure wave on combustion inside engine cylinder.

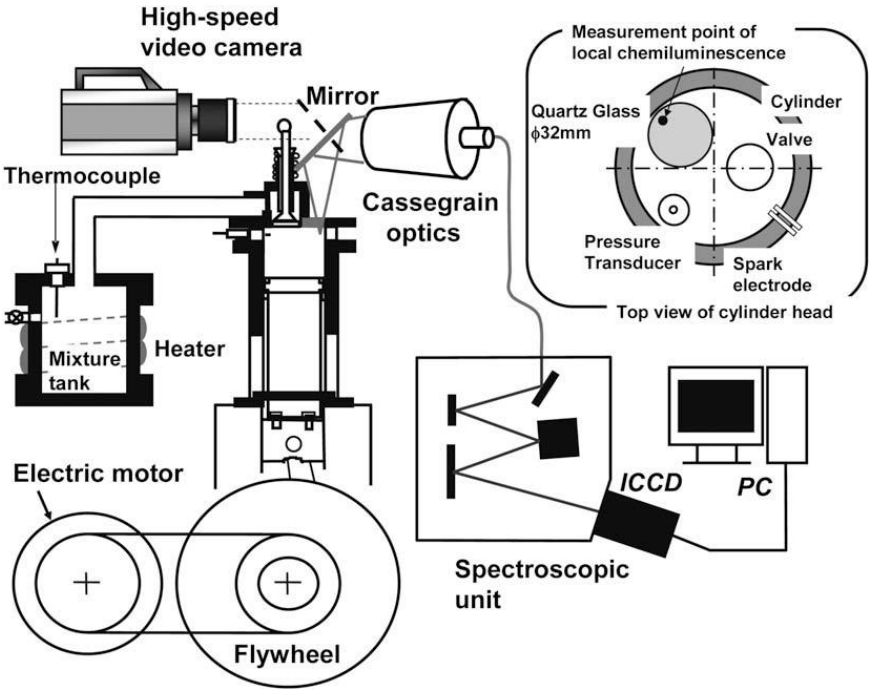

Figure 2.1: Schematic diagram of experimental setup

Figure 2.2 shows the in-cylinder pressure histories along with the knocking intensities (K_{INT}) for three spark timing conditions namely θ_{IT} = 340°, 350° and 360°. The in-cylinder pressure increased sharply right after the spark timing (θ_{IT}). When θ_{IT} are advanced from 340° to 360°, K_{INT} increased from 0.32 MPa to 1.40 MPa. Time series images for both normal and knocking cycles with the in-cylinder pressure histories are shown in Figure 2.3. The upper images show normal combustion cycles and lower images correspond to the knocking cycles. In case of normal combustion, nitrogen was used instead of argon gas. On the other hand, for visualizing knocking combustion, argon was used to increase unburned gas temperature at spark timing. In both cases, equivalence ratio was ϕ-1.0 and spark timing set at 360°. It can be seen from Figure 2.3 that after spark timing, flame propagation started from lower right side to the upper left side of the engine (images a–g) for the normal combustion and there is no any sign of autoignition or pressure oscillation. In knocking combustion, autoignition is observed in the end-gas region (image D) which is occurred at the upper left corner of the engine. As it is shown in images D and E, pressure wave moved after autoignition to the lower right of the engine. The knocking intensity of 1.53 MPa was obtained in knocking cycle. Finally, relationships among knocking intensity, unburned gas temperature, and mass of the unburned mixture are shown in Figure 2.4. The lower flame propagation speed was observed at larger end-gas region (unburned gas mass) as well as higher unburned gas temperature. It is also shown in figure that stronger knocking intensity obtained when unburned gas mass was larger. Larger mass autoignition causes stronger pressure wave. **Main Conclusion:**

- According to visualization result, knocking intensity was strongly influenced by mass of unburned mixture in the end-gas region.
- Autoignition of large amount of unburned mixture generates the strong pressure wave.

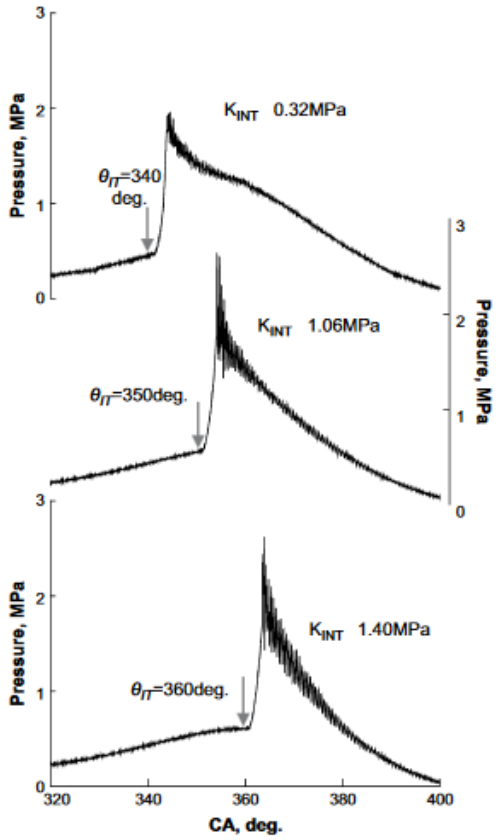

Figure 2.2: In-cylinder pressure during knocking cycle

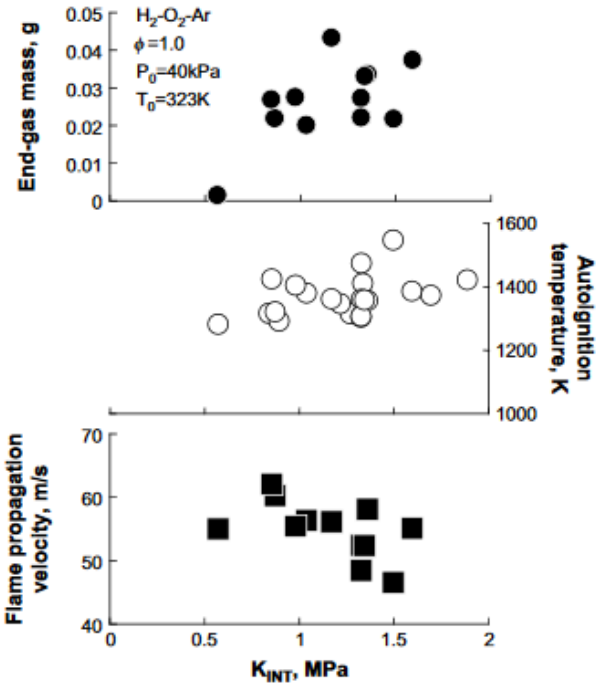

Figure 2.4: Relationships among knocking intensity, unburned gas temperature, and unburned gas mass.

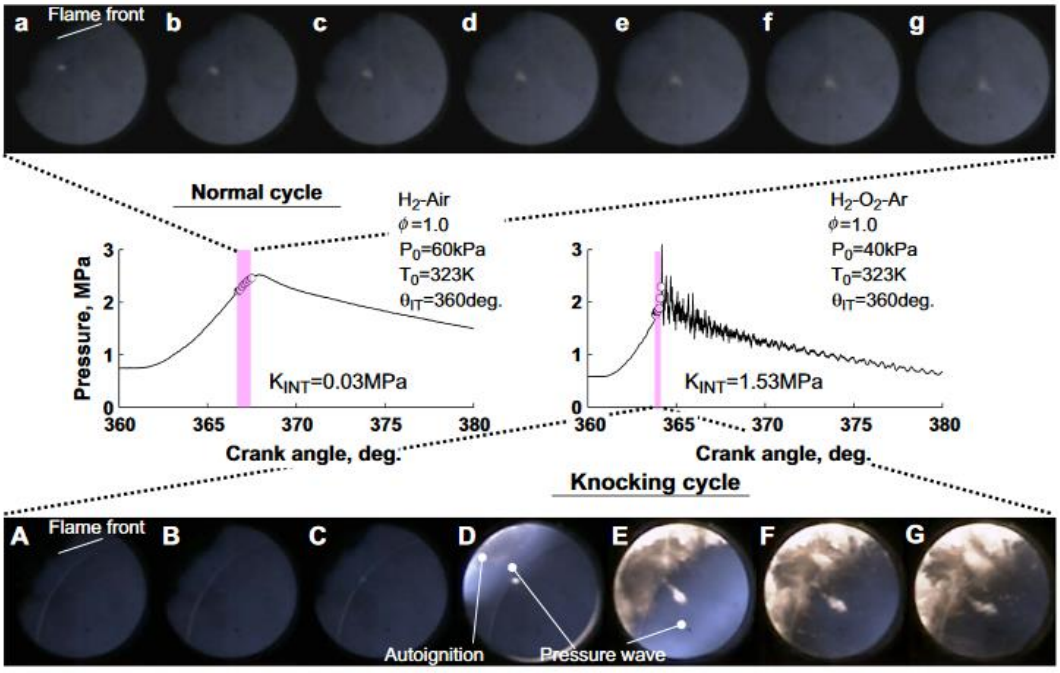

Figure 2.3: Time series images for normal and knocking cycles with related in-cylinder pressure histories

2.3 Eiji Tomita and co-workers (2010) [9]

Visualization of end gas autoignition without knock in a SI natural gas engine has been investigated by Tomita et. al. [9]. The behavior of autoignition is captured with a high-speed camera. The experimental setup used in this study was the same shown in section 2.2. The phenomena of one cycle without residual gas can be achieved in this type of engine. The cylinder was charged with homogeneous natural gas, oxygen and argon mixture with the equivalence ratio of 1.0. The spark timing set to 15° before top dead center (TDC). A small quartz window is installed in the cylinder head for visualization purpose. The visualization setup is shown in Figure 2.5.

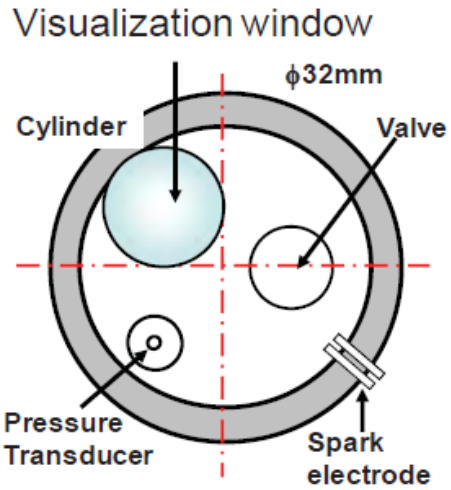

Figure 2.5: Visualization setup and optical window

Figure 2.6 (a) and (b) show pressure histories and rates of heat release (ROHRs). It can be seen that in Figure 2.6(a), pressure oscillation is seen after TDC along with steep rise in ROHR. This is considered as knocking combustion. Interestingly, the end-gas autoignition is occurred in Figure 2.6(b) also but there is no any pressure oscillation or steep rise in ROHR. As shown in Figure 2.6(b), after the first peak in ROHR which is due to flame propagation, another peak is seen owing to autoignition of end-gas region. This

phenomenon is called “Mild autoignition” which is different from either knocking or normal combustion. In this type of the combustion, thermal efficiency is expected to be increase because of increase in degree of constant-volume.

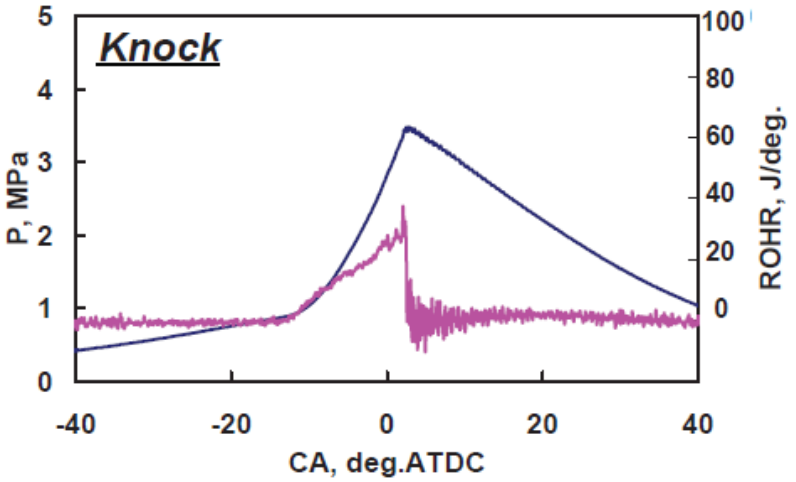

(a) Knocking combustion

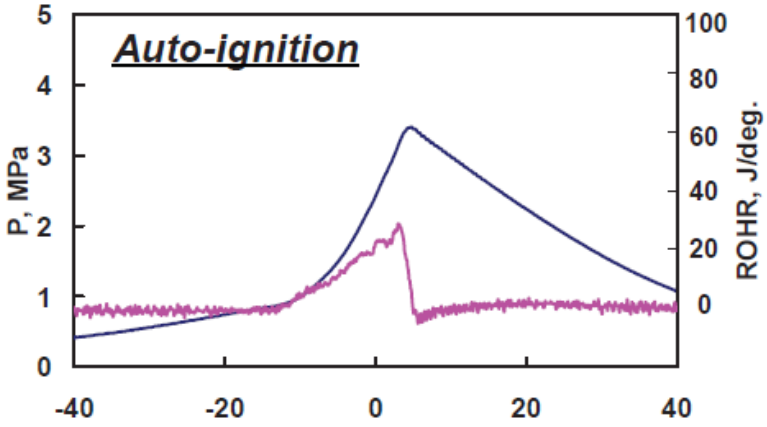

(b) Mild autoignition

Figure 2.6: Pressure history and ROHR (a) Knocking combustion (b) Mild autoignition

Main Conclusion:

- According to the result, end-gas autoignition can occur without pressure oscillation. Second peak which typically occurs after TDC is due to end-gas autoignition.

2.4 Murari Mohon Roy and co-workers (2011) [11]

In this study, performance and emissions of a supercharged dual-fuel engine fueled by hydrogen and hydrogen-containing gaseous fuels were investigated by Roy et. al. [11]. The hydrogen-containing fuels tested in this study were 13.7% H_2-content producer gas, 20% H_2-content producer gas and 56.8% H_2-content coke oven gas (COG). The gas compositions of fuels used in this study are shown in Table 2.1. Experiments were carried out on dual- fuel gas engine at supercharged condition (P_{in}= 200 kPa). A small quantity of diesel fuel (3 mg/cycle) was used as an ignition source. The injection timing and equivalence ratio varied during the experiments.

Table 2.1: Gas compositions of fuels

	H_2 (%)	CO (%)	CH_4 (%)	CO_2 (%)	N_2 (%)	LCV (MJ/NM^3)
13.7%H2-content gas	13.7	22.3	1.9	16.8	45.3	5
20%H2-content gas	20	22.3	1.9	16.8	39	5.65
Coke oven gas	56.8	5.9	29.5	2.2	5.6	17.45
Neat H_2	100	0	0	0	0	10.8

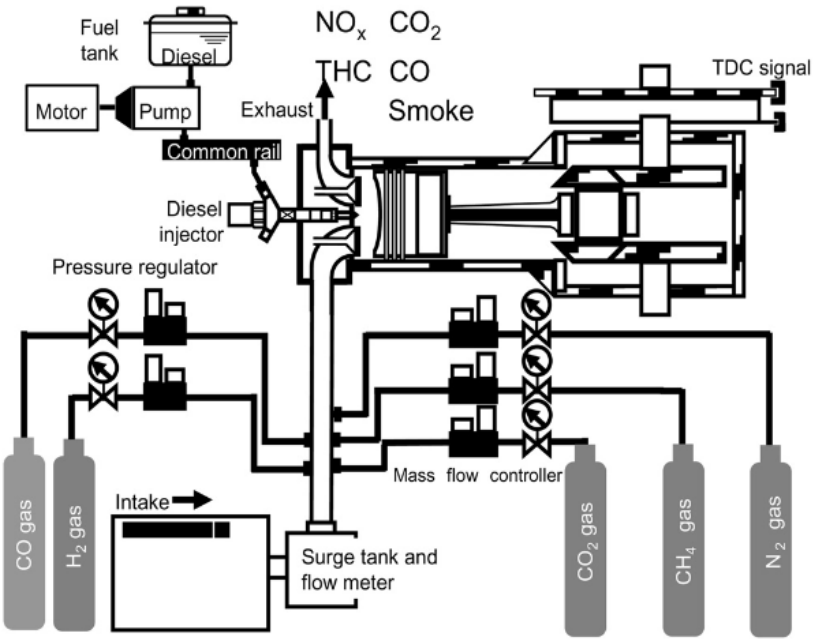

Figure 2.7: Schematic diagram of the experimental setup

Figures 2.8(a) to (d) show in- cylinder pressure histories and ROHRs of all fuels used in this study. Injection timings varied from 23 to 3º BTDC at different ranges of equivalence ratio for 13% H_2-content producer gas, 17º BTDC to 3º ATDC for 20% H_2-content producer gas, 21º BTDC to 1º ATDC for coke oven gas and 18 to 4º BTDC for neat H_2 operation. In Figure 2.8(a), with 13.7% H_2-content producer gas fuel operation at ϕ-0.4, normal combustion occurred at injection timing (θ_{inj}) of 20º BTDC and when θ_{inj} was advanced from 21-23º BTDC, second stage combustion (end- gas autoignition) occurred without any sign of knocking. At ϕ-0.63, normal combustion produced at θ_{inj}= 8º BTDC and end- gas autoignition occurred when θ_{inj} was advanced from 9-11º BTDC. At ϕ-0.85, normal combustion occurred at θ_{inj}= 5º BTDC whereas θ_{inj}= 6 and 7º BTDC produced end-gas autoignition. At ϕ-0.95, due to low cylinder pressure and temperature, only normal combustion occurred for all injection timings. Similarly, for other fuels used in this study, end-gas autoignition occurred with advancing injection timing. In case of 20% H_2-content producer gas operation, similar to 13.7% H_2-content producer gas operation, only normal combustion occurred at higher equivalence ratio (ϕ-0.88). By considering the amount of heat release as a result of end- gas autoignition, it can be found that engine power as well as thermal efficiency can be improved. Therefore, end- gas autoignition without knocking and pressure oscillation could be an important way to improve engine combustion and performance and consequently, reduce emissions.

Main conclusion:

- The two-stage combustion was found as a condition of higher engine power and a precursor of knocking combustion for all the fuels used.
- The two-stage combustion could be a promising method for improving engine performance in dual- fuel engines running with gaseous fuels.

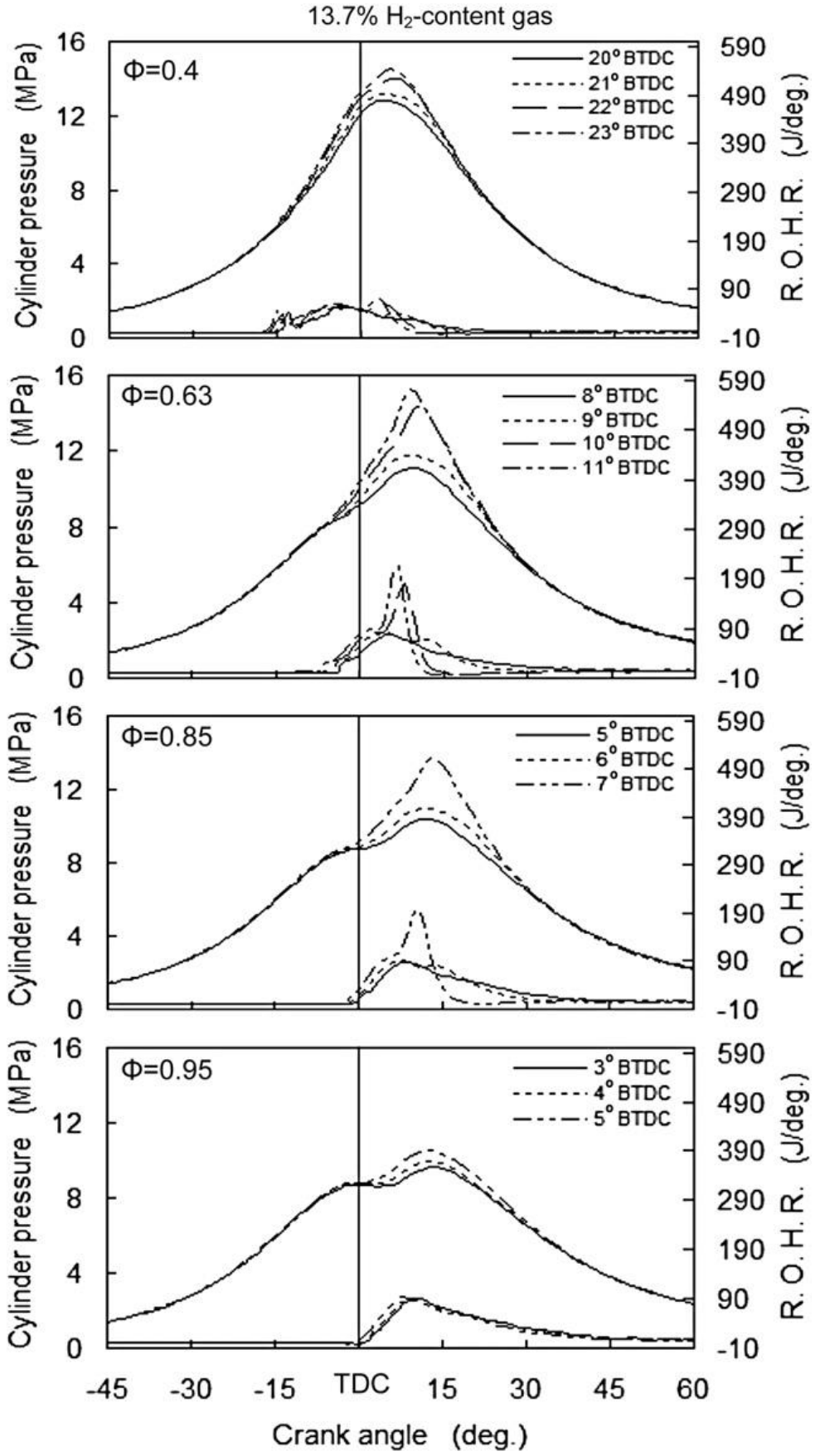
13.7% H2-content gas
Φ=0.4
20° BTDC
21° BTDC
22° BTDC
23° BTDC
Φ=0.63
8° BTDC
9° BTDC
10° BTDC
11° BTDC
Φ=0.85
5° BTDC
6° BTDC
7° BTDC
Φ=0.95
3° BTDC
4° BTDC
5° BTDC
Cylinder pressure (MPa)
R.O.H.R. (J/deg.)
0
4
8
12
16
-10
90
190
290
390
490
590
-45
-30
-15
TDC
15
30
45
60
Crank angle (deg.)

(a)

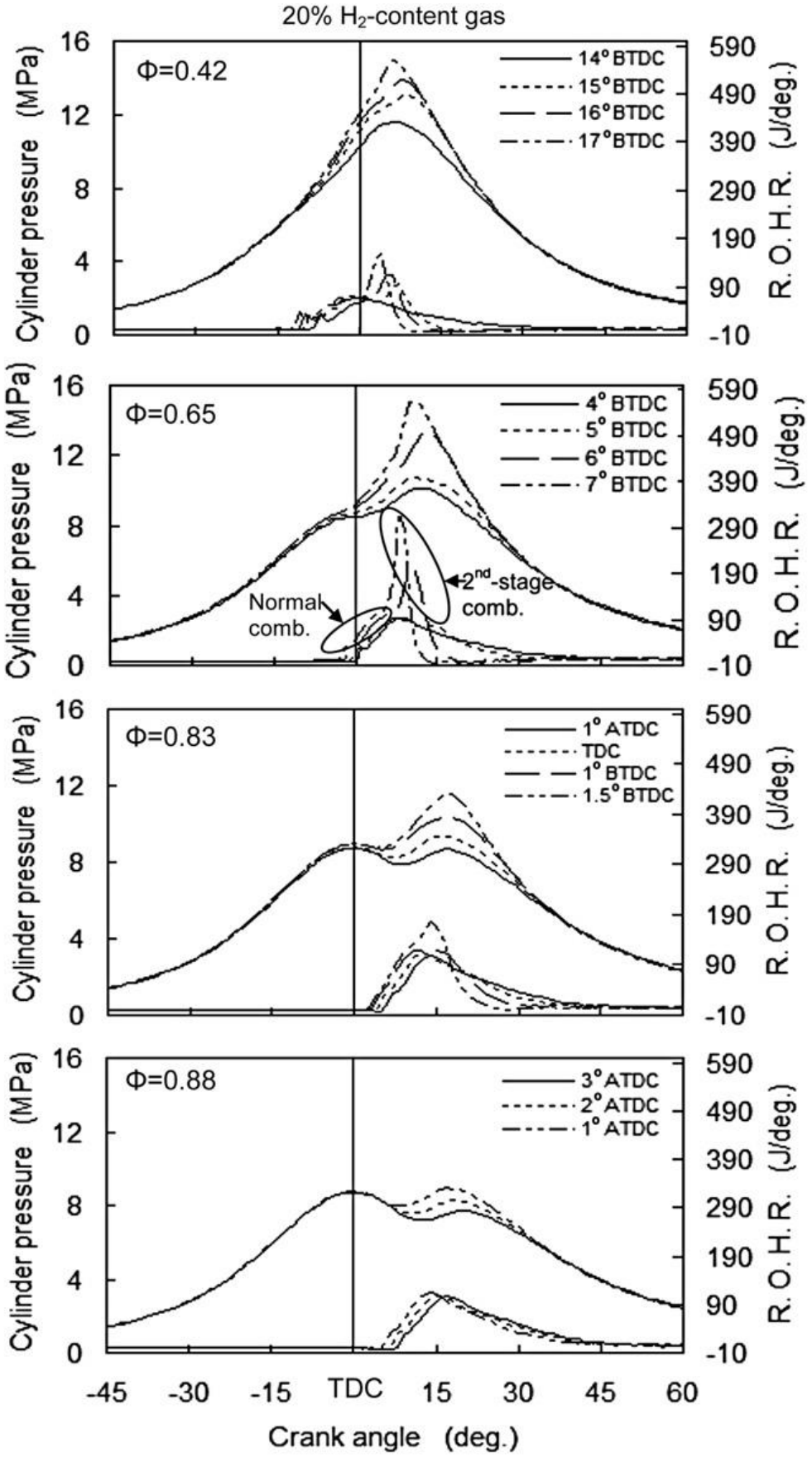
20% H2-content gas
Φ=0.42
14° BTDC
15° BTDC
16° BTDC
17° BTDC
Φ=0.65
4° BTDC
5° BTDC
6° BTDC
7° BTDC
Normal comb.
2nd-stage comb.
Φ=0.83
1° ATDC
TDC
1° BTDC
1.5° BTDC
Φ=0.88
3° ATDC
2° ATDC
1° ATDC
Cylinder pressure (MPa)
R.O.H.R. (J/deg.)
0
4
8
12
16
-10
90
190
290
390
490
590
-45
-30
-15
TDC
15
30
45
60
Crank angle (deg.)

(b)

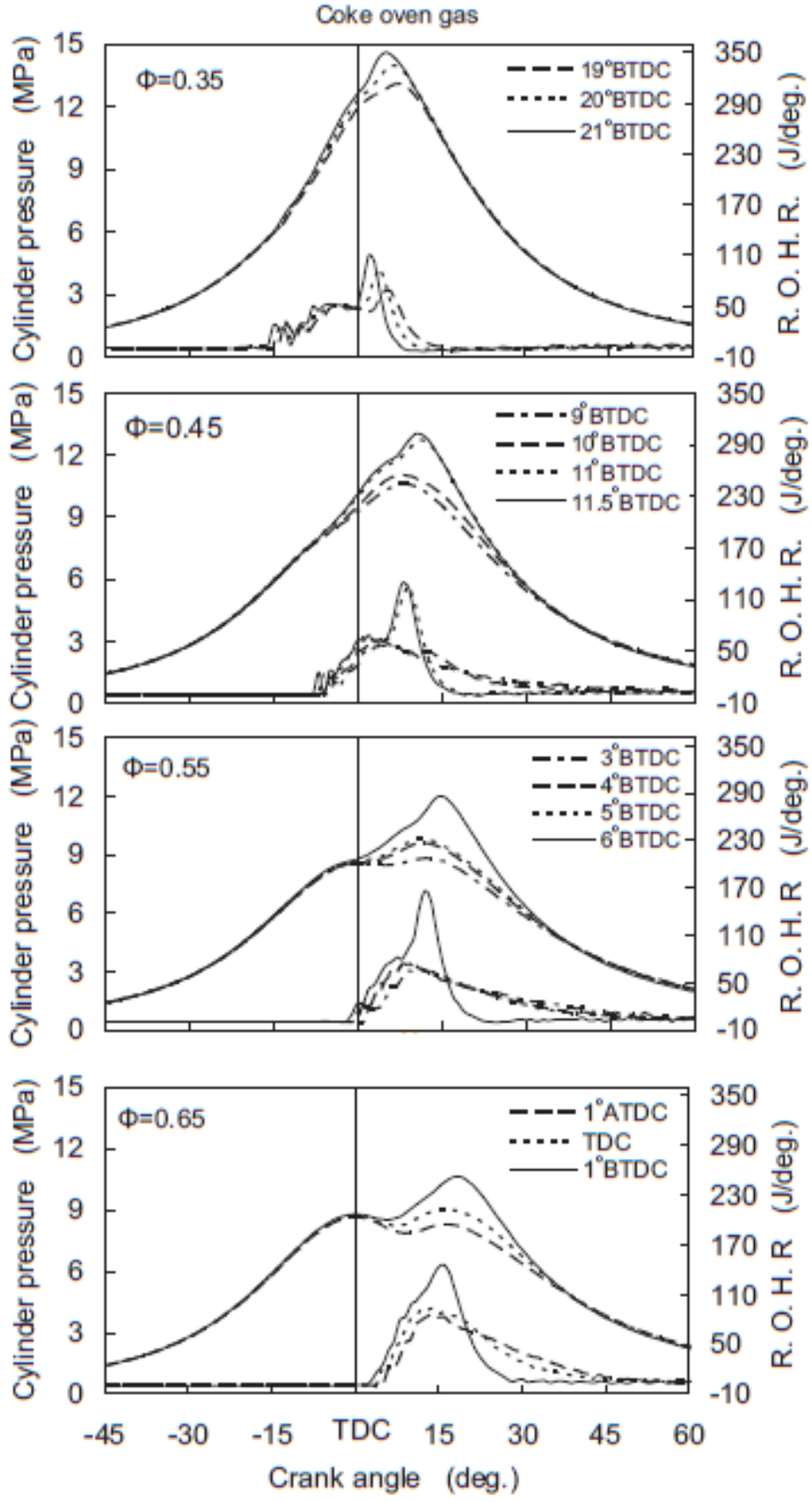
Coke oven gas
Φ=0.35
19°BTDC
20°BTDC
21°BTDC
Φ=0.45
9°BTDC
10°BTDC
11°BTDC
11.5°BTDC
Φ=0.55
3°BTDC
4°BTDC
5°BTDC
6°BTDC
Φ=0.65
1°ATDC
TDC
1°BTDC
Cylinder pressure (MPa)
R. O. H. R. (J/deg.)
0
3
6
9
12
15
-10
50
110
170
230
290
350
-45
-30
-15
TDC
15
30
45
60
Crank angle (deg.)

(c)

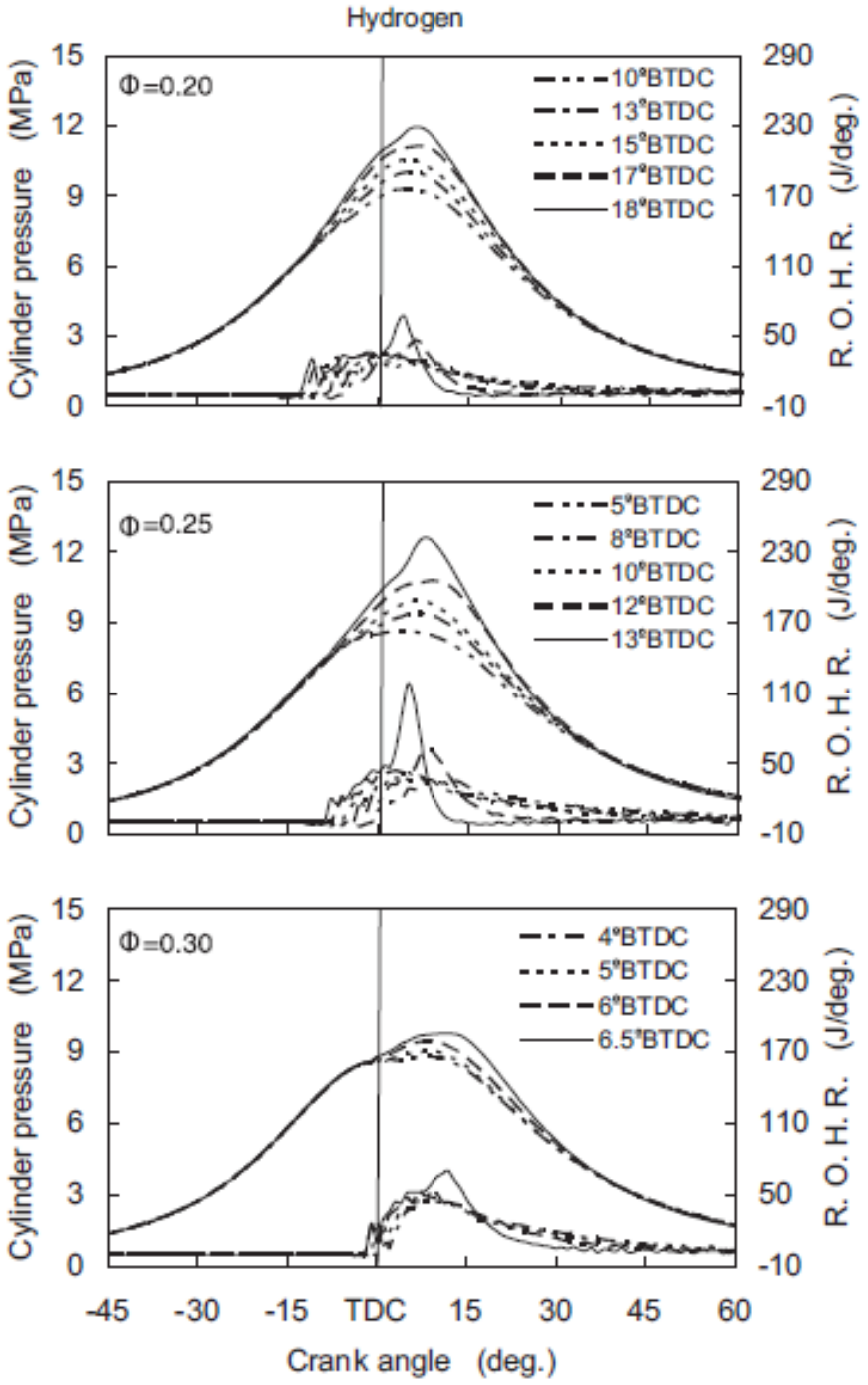

(d)

Figure 2.8: (a) In- cylinder pressure and ROHR of 13% H_2- content producer gas (b) In- cylinder pressure and ROHR of 20% H_2- content producer gas (c) In- cylinder pressure and ROHR of coke oven gas (d) In- cylinder pressure and ROHR of neat H_2- operation

2.5 Azimov and co-workers (2011) [12]

Premixed mixture ignition in the end-gas region (PREMIER) combustion in a natural gas dual-fuel engine was investigated by Azimov and co-workers [12]. It was a first paper using the name "PREMIER combustion". Combustion, performance and exhaust emission are investigated and compared in three combustion modes namely conventional combustion, PREMIER combustion and knocking combustion. Experiments were carried out on dual- fuel natural gas engine and several parameters such as effect of injection timing and EGR were examined. The natural gas used in this study consist of methane (CH_4, 88 percent), ethane (C_2H_6, 6 percent), propane (C_3H_8, 4 percent) and n-butane (C_4H_{10}, 2 percent). The diesel fuel is used as an ignition source. Simulated EGR gas, composed of 86 percent N_2, 10 percent O_2, and 4 percent CO_2, was added to the intake air in order to test the effect of EGR. In addition, the spectroscopic analysis of PREMIER combustion is done. The schematic diagram of experimental setup is shown in Figure 2.9.

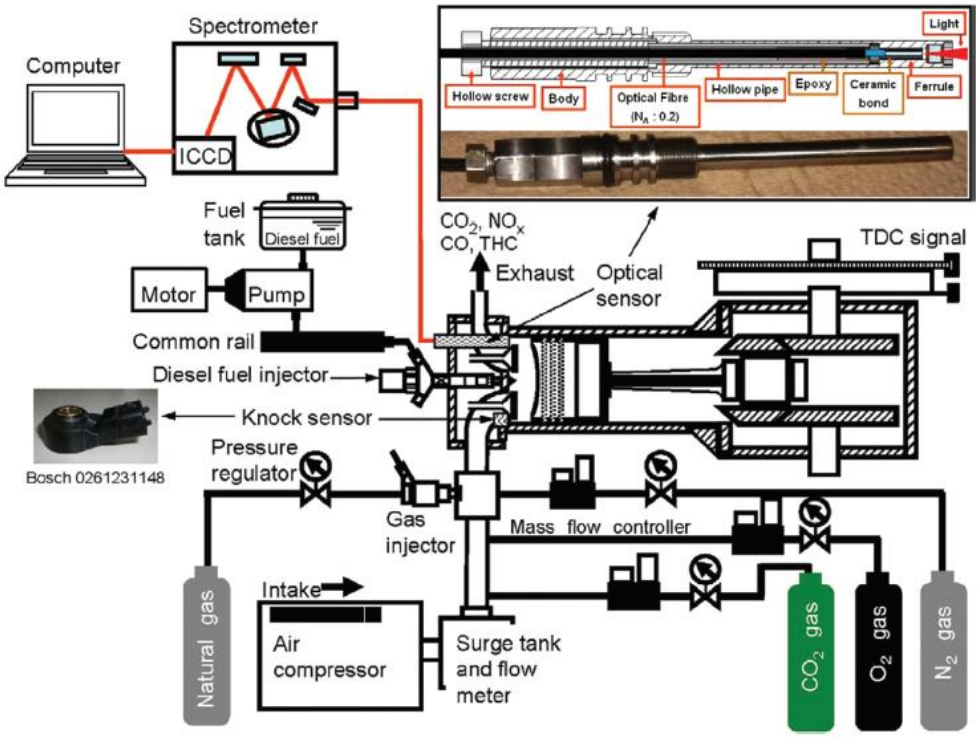

Figure 2.9: Schematic diagram of experimental setup

2.5.1 Cyclic variation of the in- cylinder pressure

Figure 2.10 shows the cycle- to- cycle variation of in- cylinder pressure in three combustion modes namely conventional. PREMIER and knocking. As shown in Figure 2.10, in- cylinder peak pressure, P_{max}, is increased for all three combustion modes when injection timing is advanced. Also, when injection timing is advanced from 3.5°BTDC to 4.5°BTDC, PREMIER combustion is achieved and by further advancing the injection timing, knock is occurred. Pressure fluctuation is changing from horizontal line structure to vertical line structure for conventional and knocking combustion, respectively. PREMIER combustion fluctuation is not as large as knocking combustion. Authors considered the combustion processes as slow, fast and very fast combustion. They revealed that in case of slow combustion P_{max} fluctuation is small whereas for very fast combustion, this fluctuation is very large.

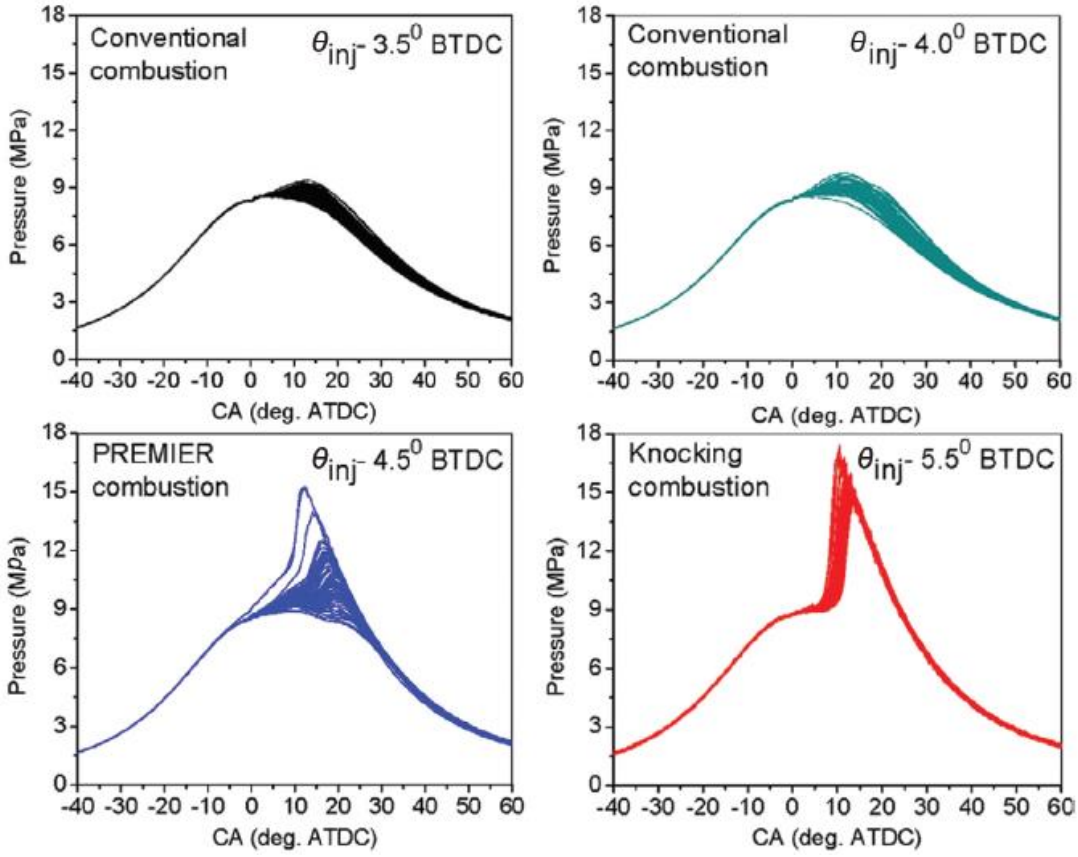

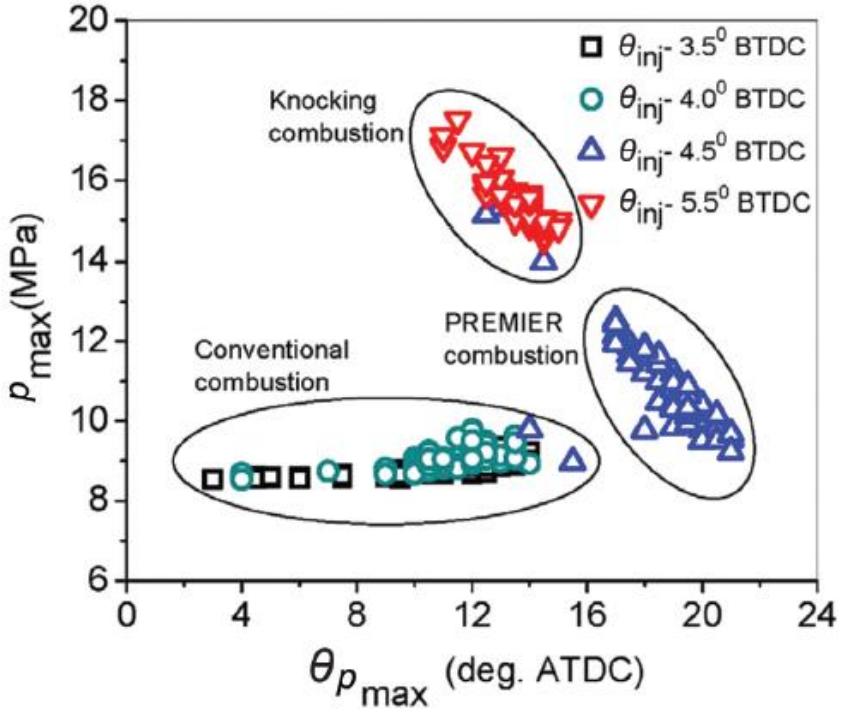

Figure 2.10: Cyclic P_{max} versus its angle (P_{max}, Θ_{Pmax}) for different injection timings. P_{inj} = 80 MPa, P_{in} = 200 kPa, D_{hole} = 0.1mm, N_{hole}=3, m_{DF} = 2 mg/cycle

2.5.2 Spectroscopy analysis

In this study, a spectrometer equipped with an intensified charge-coupled device (ICCD) is used for emission measurement in the end- gas region. Figure 2.11 shows an averaged spectra obtained between 200 and 800nm. As shown in Figure 2.11, high OH radical emission intensities are seen at wavelength 310 nm and weak intensities at 286 nm for both knocking and PREMIER combustion. The OH radical emission intensities are stronger for knocking combustion than those in PREMIER combustion. In conventional combustion, these intensities are not seen. In knocking case, OH radical emission intensity at wavelength 310 nm increased from 9 to 6° ATDC which is the result of pressure and temperature increases in the end-gas region but in case of PREMIER combustion, the OH radical emission intensity shows the same value. A similar trend was observed by Hashimoto et. al. [4].

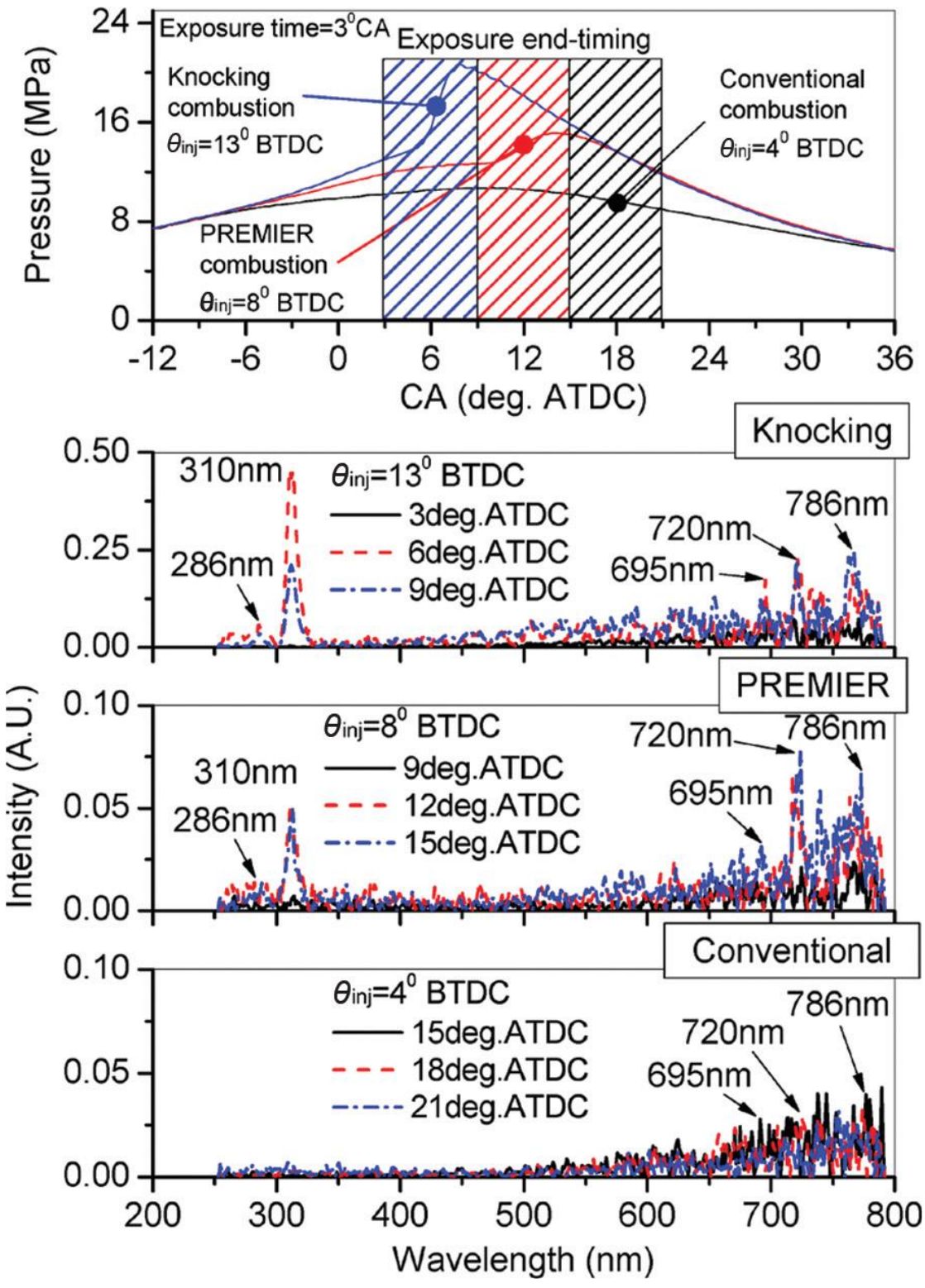

Figure 2.11: Spectra analysis in the end-gas region. P_{inj} = 40 MPa, P_{in} = 200 kPa, D_{hole} = 0.1mm, N_{hole}=3, m_{DF} = 2 mg/cycle

2.5.3 Effect of injection timing

Figure 2.12 shows pressure histories and ROHRs at different injection timings and ranges of injection pressure from 80 MPa to 150 MPa. As shown in the Figure, injection pressure influence is not remarkable and within wide range of injection pressures, PREMIER combustion is achieved. On the other hand, advancing injection timing promote PREMIER combustion. When injection timing is advanced, rapid combustion as a result of better diesel fuel evaporation and autoignition is achieved and therefore, end-gas region temperature increased further and it is the suitable condition for end-gas autoignition.

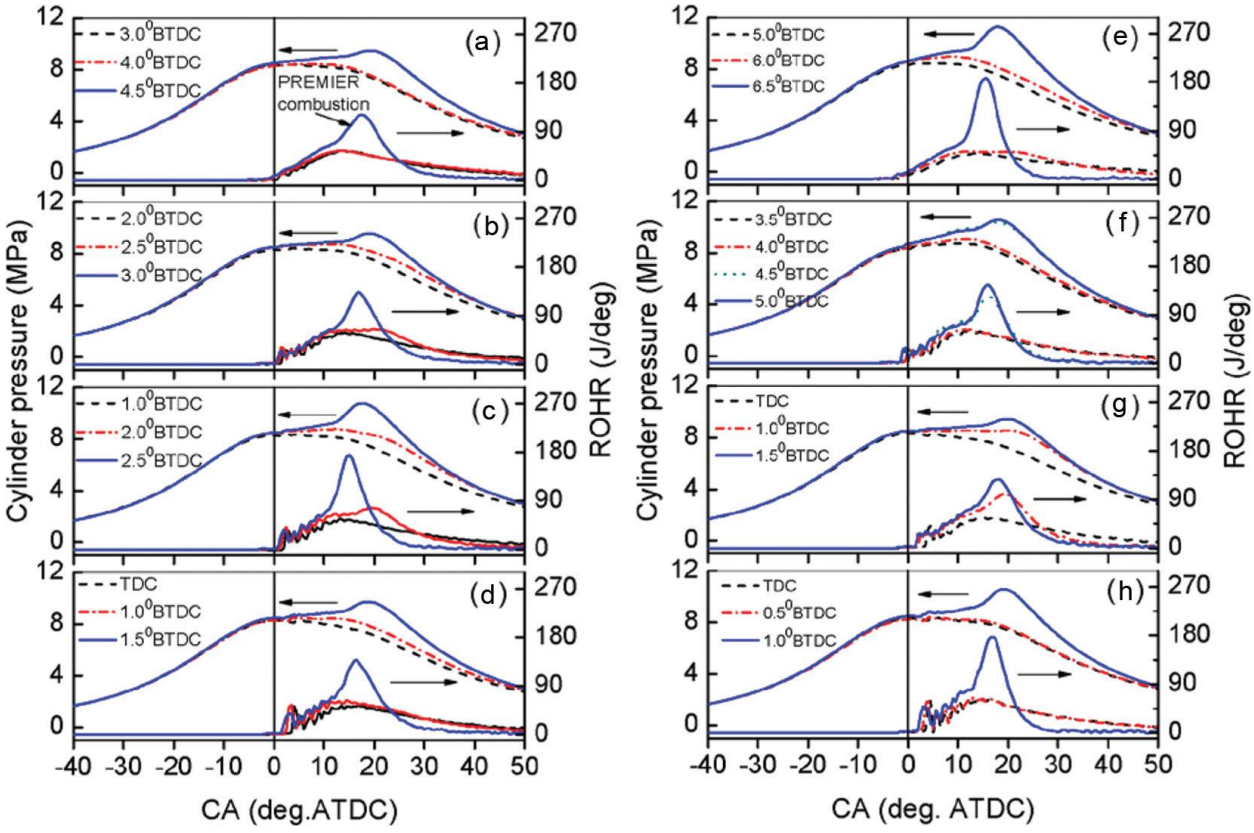

Figure 2.12: Effect of pilot fuel injection timing on cylinder pressure and the rate of heat release. (a)P_{inj} = 40 MPa, P_{in} = 200 kPa, D_{hole} = 0.1mm, N_{hole}=3, m_{DF} = 3 mg/cycle; (b) P_{inj} = 80 MPa,P_{in} = 200 kPa, D_{hole} = 0.1mm, N_{hole}=3, m_{DF} = 3 mg/cycle; (c) P_{inj} = 120 MPa, P_{in} = 200 kPa, D_{hole} = 0.1mm, N_{hole}=3, m_{DF} = 3 mg/cycle; (d) P_{inj} = 150 MPa, P_{in} = 200 kPa, D_{hole} = 0.1mm, N_{hole}=3, m_{DF} = 3 mg/cycle; (e) P_{inj} = 40 MPa, P_{in} = 200 kPa, D_{hole} = 0.1mm, N_{hole}=3, m_{DF} = 2 mg/cycle; (f) P_{inj} = 80 MPa, P_{in} = 200 kPa, D_{hole} = 0.1mm, N_{hole}=3, m_{DF} = 2 mg/cycle; (g) P_{inj} = 150 MPa, P_{in} = 200 kPa, D_{hole} = 0.08mm, N_{hole}=3, m_{DF} = 3 mg/cycle; (h) P_{inj} = 150 MPa, P_{in} = 200 kPa, D_{hole} = 0.1mm, N_{hole}=4, m_{DF} = 3 mg/cycle

2.5.4 Effect of EGR

Figure 2.13 shows pressure histories and ROHRs at different EGR rate. It is possible to achieve the PREMIER combustion if the EGR rate do not exceed a certain level. As shown in Figure 2.10, the second stage of combustion is occurred when EGR was used. The influence of EGR is not very considerable to achieve PREMIER combustion but when injection timing is advance more and the risk of knocking is getting higher, EGR would be helpful in order to suppress knocking.

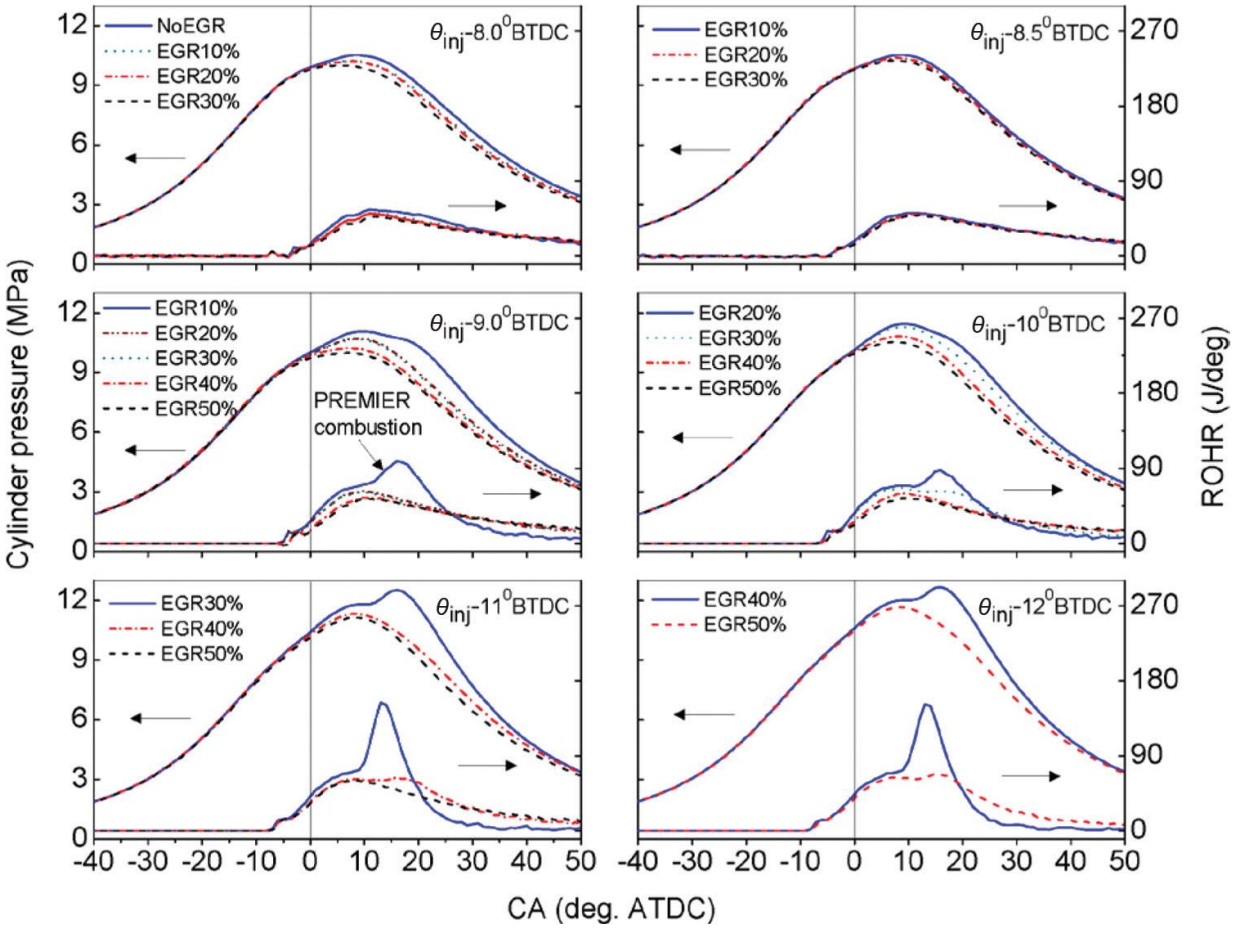

Figure 2.13: Effect of EGR on cylinder pressure and the rate of heat release. P_{inj} = 40 MPa, P_{in} = 200 kPa, D_{hole} = 0.1mm, N_{hole}=3, m_{DF} = 2 mg/cycle

2.5.5 Exhaust emissions and engine performance

Figure 2.14 shows exhaust emissions of HC, CO and NO_x and engine performances of indicated mean effective pressure (IMEP) and thermal efficiency. An encircled data in the figure correspond to PREMIER combustion. It is very clear that IMEP and thermal efficiency increased significantly when engine operate under PREMIER combustion. It is the result of sharp increase of the second heat-release peak. HC and CO emissions reduced under PREMIER combustion but NO_x is increased due to higher in- cylinder pressure and temperature owing to end- gas autoignition.

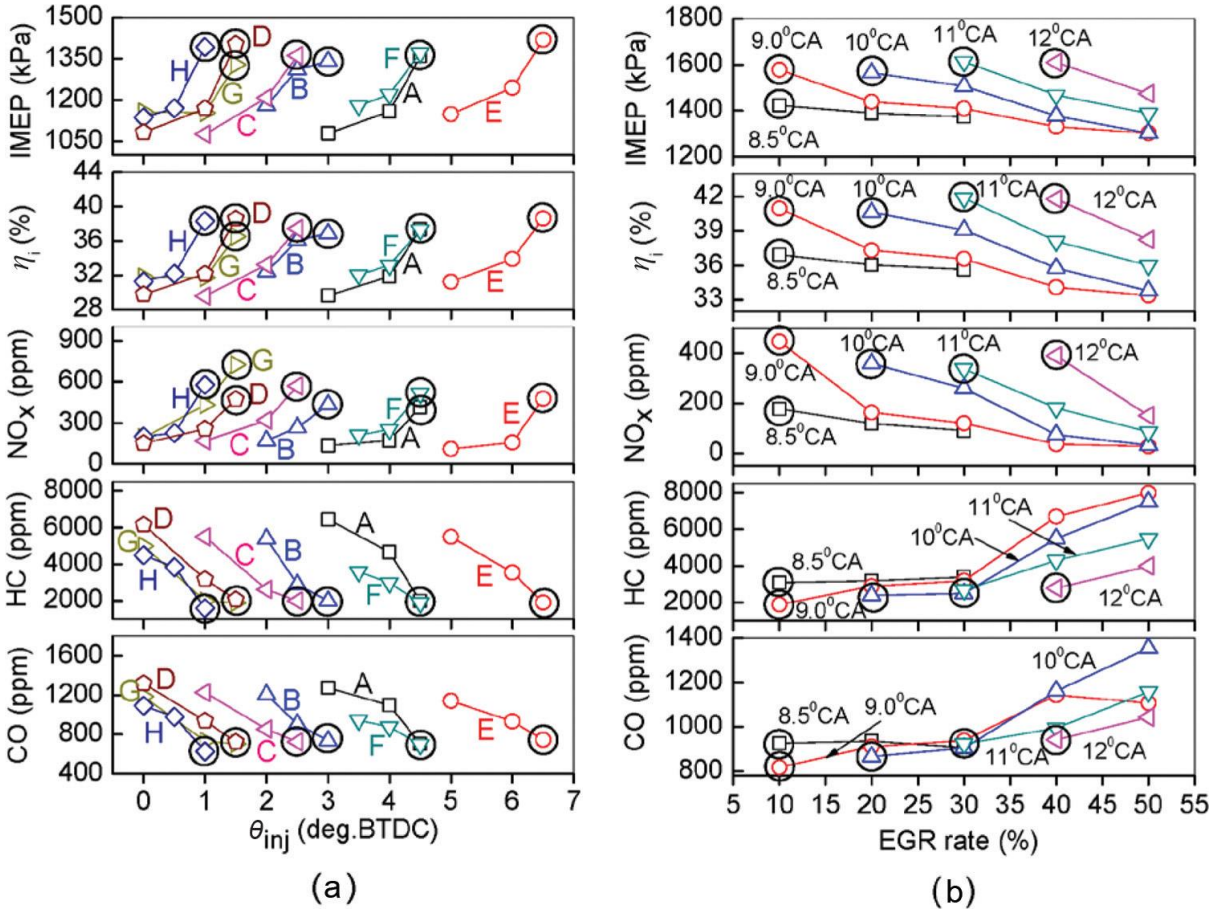

Figure 2.14: Effect of pilot fuel injection timing and EGR on engine performance and emissions. (a) Conditions correspond to those in figure 2.12 and (b) conditions correspond to those of figure 2.13.

Main conclusion:

- End- gas autoignition without pressure oscillation was achieved and the phenomena named PREMIER (Premixed mixture ignition in the end-gas region) combustion.
- OH radical emission intensities were stronger in knocking combustion than those in PREMIER combustion.
- Engine performances improved and exhaust emissions of HC and CO decreased under PREMIER combustion while NO_x is increased.

2.6 Cagdas Aksu and co-workers (2016) [17]

The aim of this study was extension of PREMIER combustion operation range by using split micro pilot fuel injection strategy in dual- fuel natural gas CI engine [17]. In- cylinder flame visualization was performed in order to explain the effect of second injection timing on combustion mode. Experiments were conducted in two setups for performance test and visualization. Intake pressure and temperature were 101 kPa and 313 K, respectively. A compression ratio and equivalence ratio were 17.0:1 and 0.6 during both performance tests and visualization experiments. Natural gas was used as a main fuel with the supply rate of 26.7 mg/cycle and diesel fuel was used as an ignition source with the rate of 0.6 mg/cycle in both single and split injection experiments. In single-injection experiments, injection timing (θ_{inj}) was varied from 6º BTDC to 3º BTDC. In split-fuel injection experiments, the first injection timing (θ_1) was varied in the range of 6º BTDC to 3º BTDC and the second injection timing (θ_2) was varied from 3.5 ºCA after the first injection to θ_2 = 15ºATDC. A 4–20 kHz band-pass filter is applied to pressure history for knock analysis. A 6.5 kHz low-pass filter is applied in order to obtain ROHR and performance characteristics. In visualization experiment, an extended piston of flat top geometry and

a sapphire window were used to perform visualization. In-cylinder images were captured using a high speed camera at 12 kfps frame rate.

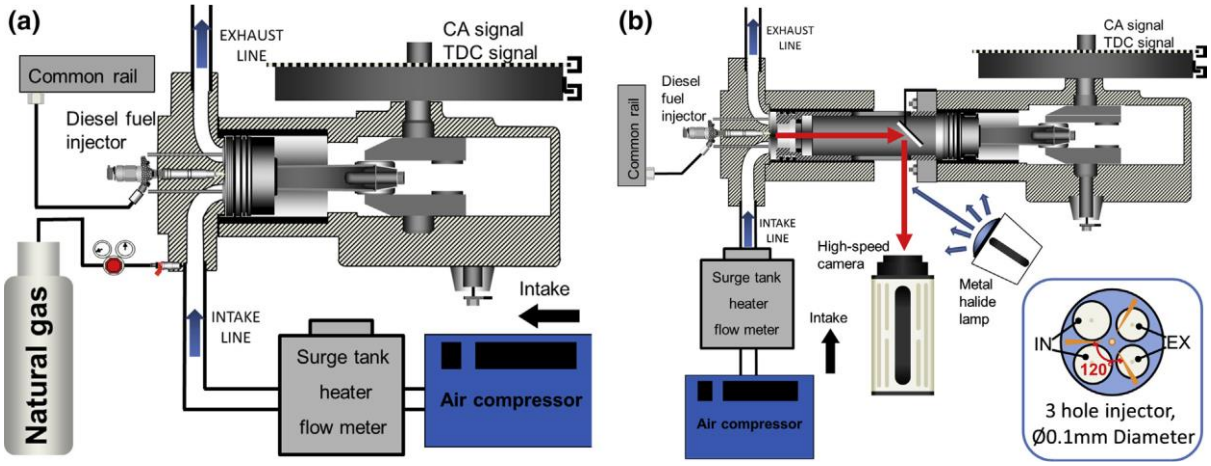

Figure 2.15: Experimental setup of (a) performance experiments and (b) visualization.

2.6.1 Pressure history, ROHR and fraction of PREMIER combustion cycles

Figures 2.16 and 2.17 show pressure histories, ROHRs and percentage of cycles with end-gas autoignition with both single and split injection, respectively. The single injection timings are θ_{inj}= 6º BTDC, θ_{inj}= 5º BTDC, θ_{inj}= 4º BTDC and θ_{inj}= 3º BTDC and second injection timings are varied. Pressure histories and ROHRs of single injection timing, θ_{inj}= 6º BTDC /2.5º BTDC split injection and θ_{inj}= 6º BTDC /1º BTDC show an oscillation and sudden rise and therefore, these are considered as knocking combustion. When second injection timing was advanced, PREMIER combustion was achieved. In case of θ_{inj}= 5º BTDC, both single and split injection timing resulted PREMIER combustion. When second injection timing was delayed, the number of cycles with end- gas autoignition gradually decreased. In case of θ_{inj}= 4º BTDC, single injection timing exhibited normal combustion but with the second injection timing until θ_{inj}= 3º ATDC, PREMIER combustion was achieved and further advancement of second injection timing resulted normal

combustion. In case of θ_{inj}= 3º BTDC, both single and split injection showed normal combustion. In this study, pressure histories and ROHRs are presented as averages of 80 consecutive cycles unless indicated as ‘‘one cycle” in relevant figures. If 50% of cycles showed end- gas autoignition with knocking intensity below threshold, the overall cycle considered as PREMIER cycle.

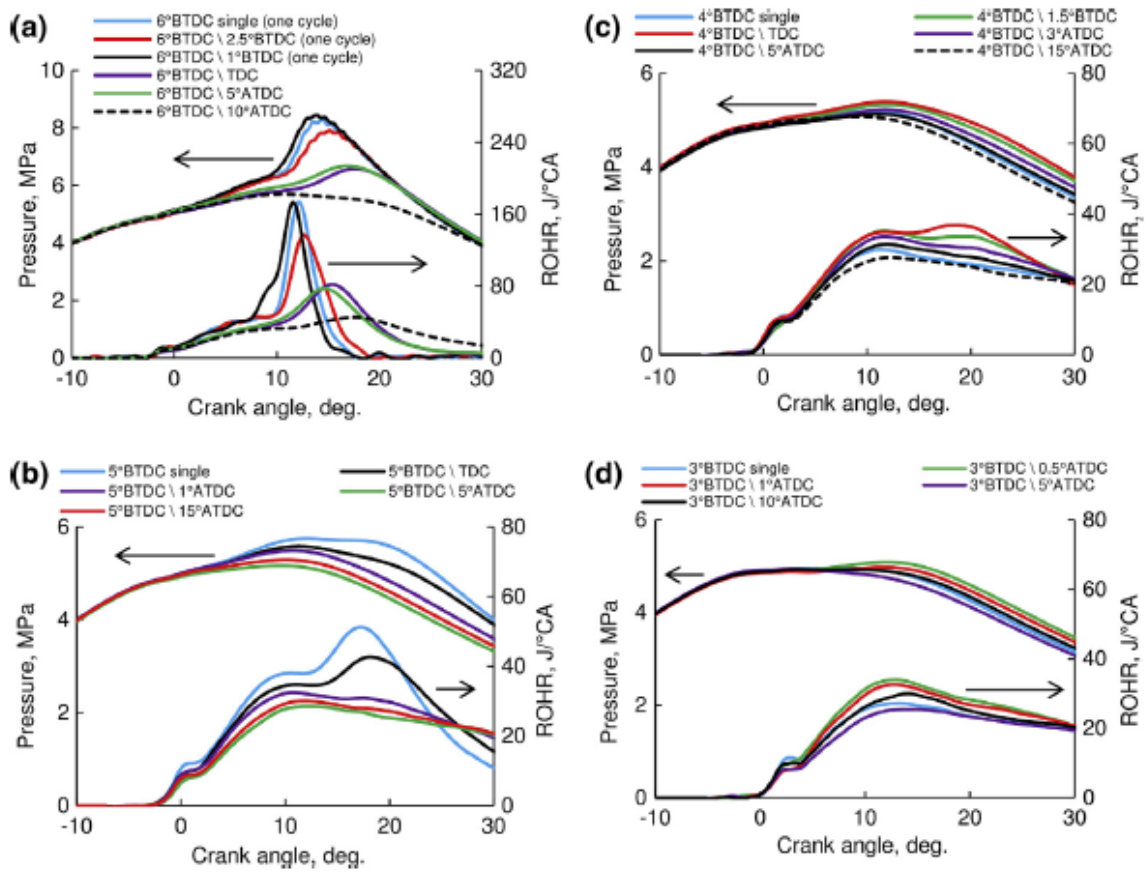

Figure 2.16: Pressure histories and ROHRs with single and split injections

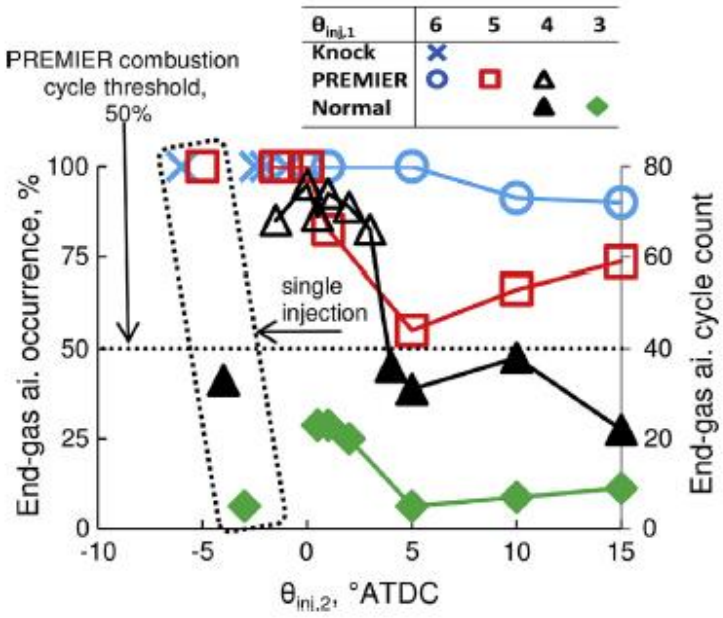

Figure 2.17: Percentage of cycles with end-gas autoignition

2.6.2 Indicated mean effective pressure (P_{mi}), thermal efficiency and coefficient of variation of indicated mean effective pressure ($COV_{(Pmi)}$)

Engine performances and operation stability are shown in Figures 2.18 (a) to (c). It can be seen that both P_{mi} and thermal efficiency were improved when engine operated under PREMIER combustion mode. Also, it is clear that using split injection strategy could improve P_{mi} and thermal efficiency compared to those of single injection. In case of θ_{inj}= 6º BTDC, knocking suppressed with split injection strategy and in case of θ_{inj}= 4º BTDC, split injection promoted normal combustion to PREMIER combustion. Regarding operation stability, $COV_{(Pmi)}$ of θ_{inj}= 6º BTDC was less than 1% in both knocking and PREMIER combustion until the second injection timing was θ_2 = 5º ATDC.

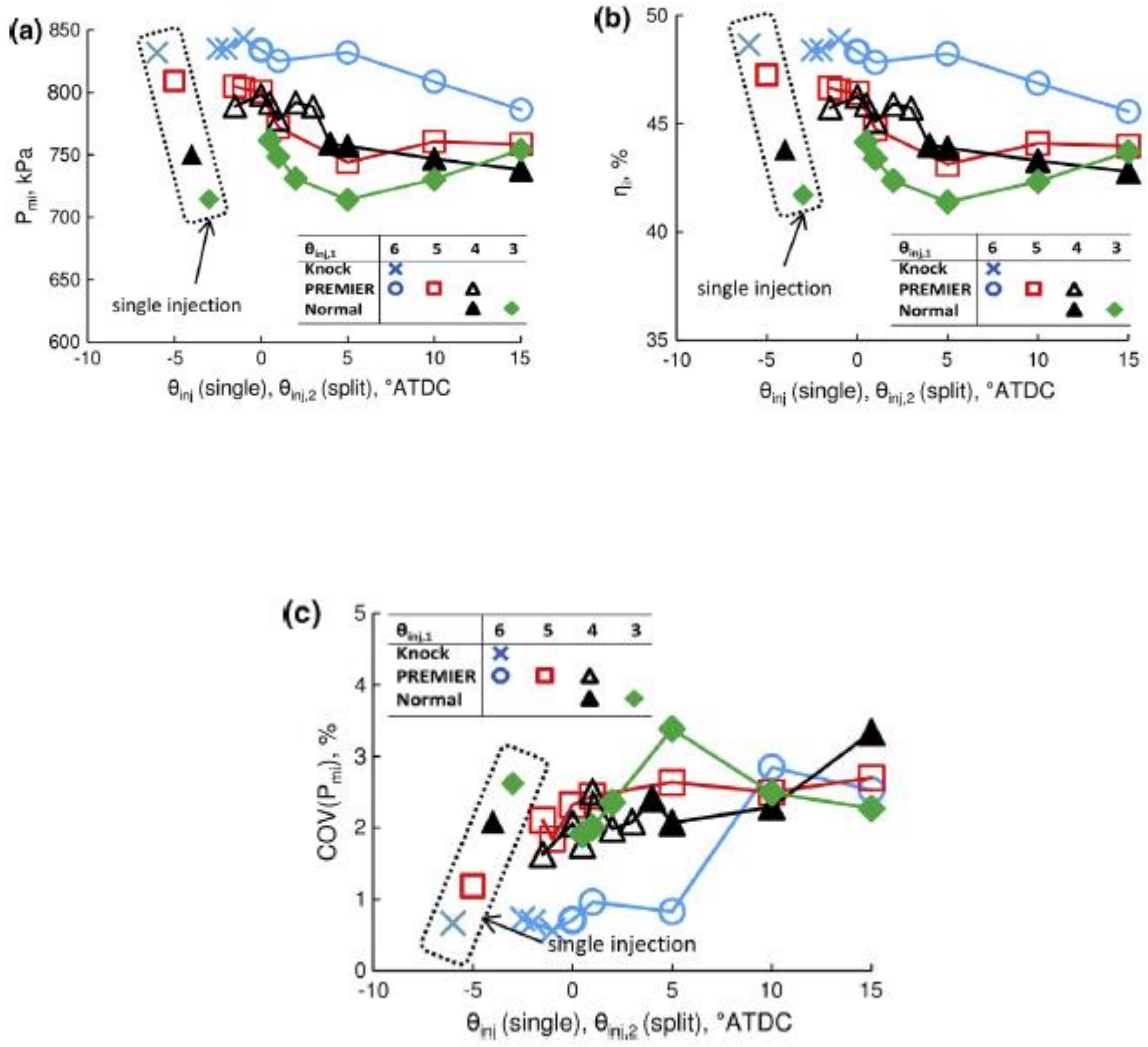

Figure 2.18: (a) Indicated mean effective pressure (b) thermal efficiency (c) coefficient of variation of indicated mean effective pressure

2.6.3 Promotion of normal combustion to PREMIER combustion with split injection

As shown in Figures 2.19 and 2.20, normal combustion can be converted to PREMIER combustion by split injection strategy. In split injection cases, ROHR is faster than single injection case due to second injection and therefore, peak of ROHR shows higher value. As a result, this process increases in-cylinder pressure and temperature and this is the suitable condition for end- gas autoignition.

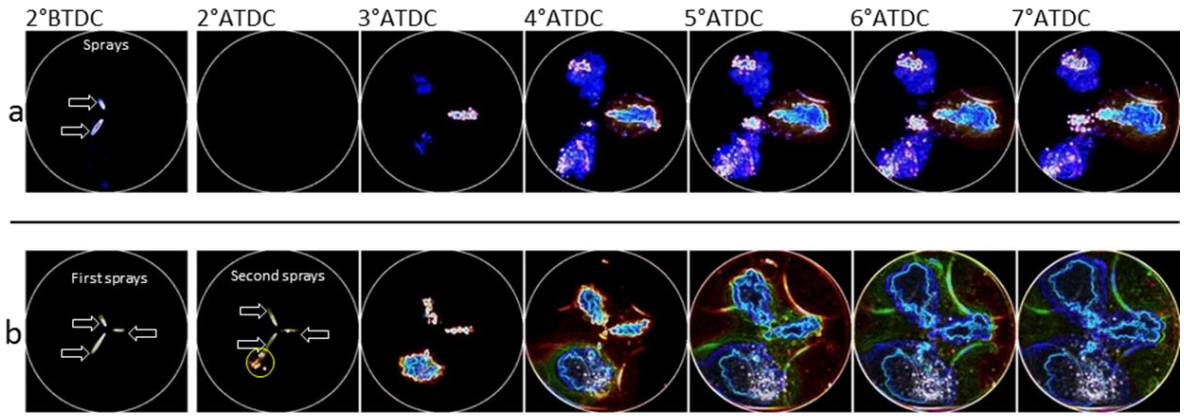

Figure 2.19: Visual investigation of promotion of normal combustion to PREMIER combustion: (a) θ_{inj}=4°BTDC single injection, (b) θ_{inj}=4°BTDC/0.5°BTDC.

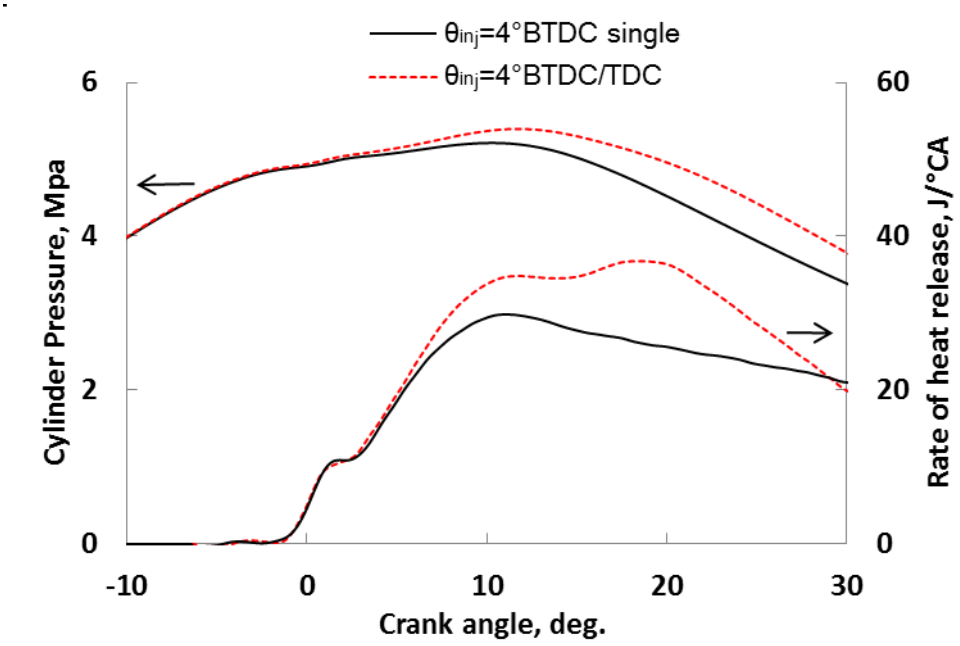

Figure 2.20: Comparison of pressure histories and ROHR of single- and split-injection strategies at θ_{inj} = 4°BTDC and θ_{inj} = 4°BTDC/TDC.

Main conclusion:

- Split injection strategy was used to promote normal combustion to PREMIER combustion.
- Split injection strategy accelerated the rate of growth of flame kernels.
- Engine output, stability and thermal efficiency increased under PREMIER combustion.

2.7 Nobuyuki Kawahara and co- workers (2018) [18]

In the latest publication of our laboratory, differences between PREMIER combustion in a natural gas spark-ignition engine and knocking with pressure oscillations was studied by Kawahara et. al. [18]. They performed experiments in a compression–expansion machine (CEM) with bore and stroke of 92mm and 96mm and compression ratio of 9.14. In this study, CEM is equipped with combustion visualization systems. High-speed camera with a frame speed of 20,000 fps was used for visualization purpose. The combustion images were captured from the spark onwards. The air–fuel mixture gas was composed of natural gas, argon and oxygen, with an equivalence ratio of 0.8. Argon was used to increase the gas temperature at the spark timing. The experimental setup and conditions are shown in Figure 2.21 and Table 2.2, respectively.

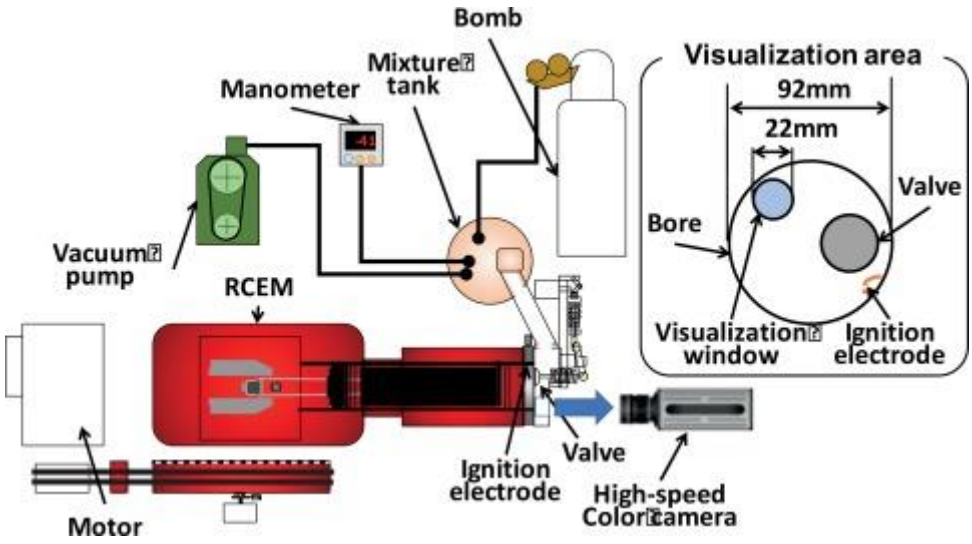

Figure 2.21: Schematic diagram of experimental setup

Table 2.2: Experimental conditions

Compression–expansion machine,CEM	
Initial mixture pressure	90 kPa
Initial mixture & cylinder temperature	343 K
Spark timing	9º-5º BTDC
Equivalence ratio	0.8

2.7.1 Flame images, in- cylinder pressure and ROHR

Figure 2.22 shows a flame images of normal, PREMIER and knocking combustion. The initial mixture pressure and temperature were 90 kPa and 343 K, respectively. The spark timing set to 6° BTDC for normal combustion, 7° BTDC for PREMIER combustion and 8° BTDC for knocking combustion. In these images, dark regions are the unburned mixture and bright regions are the flame. Images of normal combustions show only flame propagation but in case of PREMIER combustion and knocking combustion, end- gas autoignition occurred near the cylinder wall just before the combustion flame reached the cylinder wall, as indicated in the Figure 2.22.

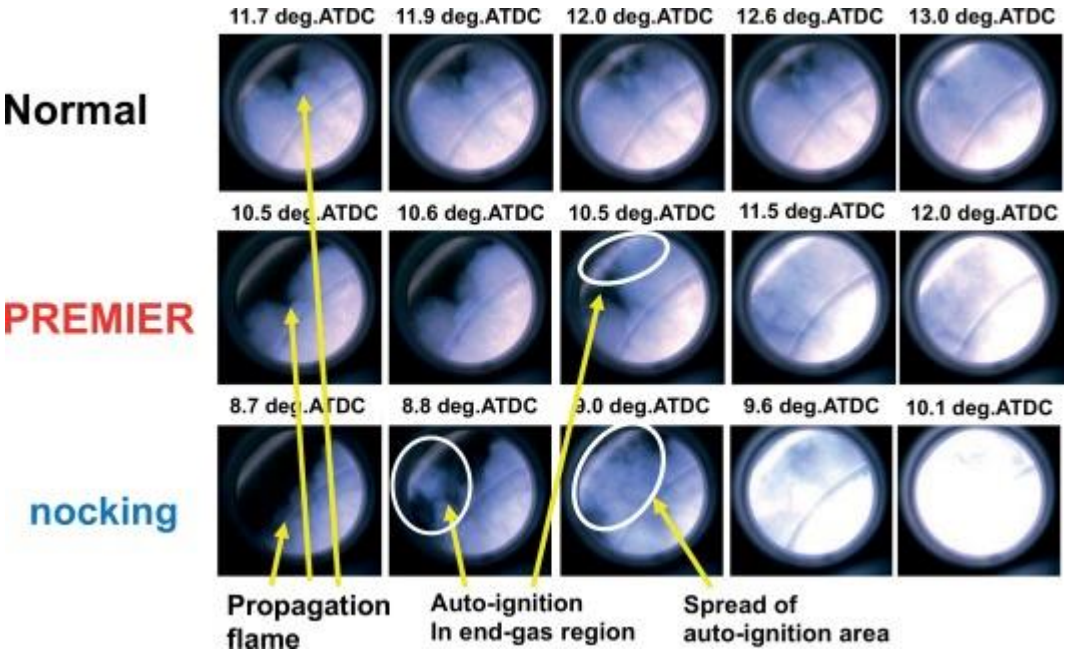

Figure 2.22: Time-series visualization of normal, PREMIER and knocking combustion

Figure 2.23 shows a pressure histories and ROHRs of normal, PREMIER and knocking combustion observed in the experiments shown in Figure 2.22. As shown in Figure 2.23, second peak in ROHR appeared in PREMIER and knocking cases which is due to end- gas autoignition. However, in knocking combustion, high-frequency pressure oscillations

occurred after peak pressure which no such pressure oscillation occurred in PREMIER combustion.

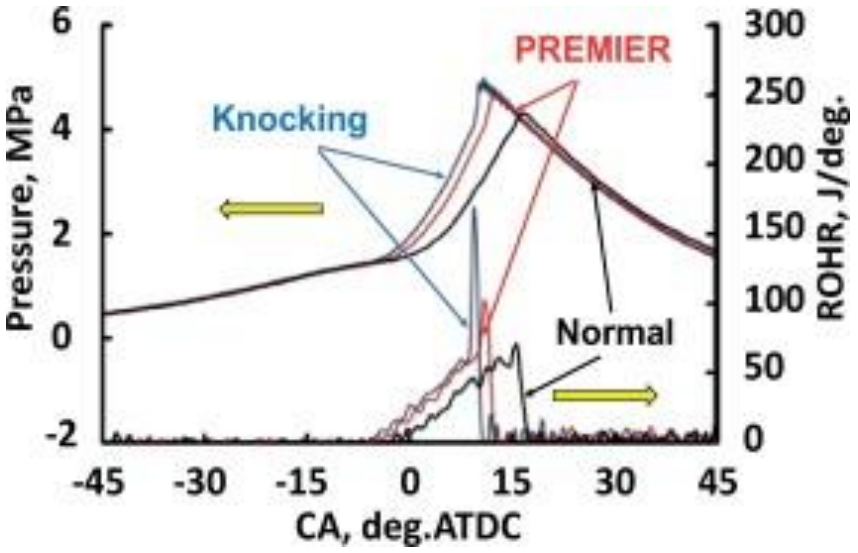

Figure 2.23: Pressure history and ROHR of normal, PREMIER and knocking combustion

2.7.2 Relationship between the end-gas area and autoignition timing

Figure 2.24 **s**ho**ws** relationship between the end-gas area and crank angle just before auto-ignition. The spark timing varied between 9° and 5° BTDC. As shown in the figure, end- gas area of PREMIER combustion was smaller than knocking combustion. It is clearly shows in the figure that the onset of autoignition is later during PREMIER combustion compared to knocking combustion. Therefore, it can be concluding that larger end- gas volume as a result of earlier autoignition causes knocking. In PREMIER combustion, end-gas area was smaller and therefore, pressure increase as a result of autoignition is smoother and no pressure oscillation can be observed.

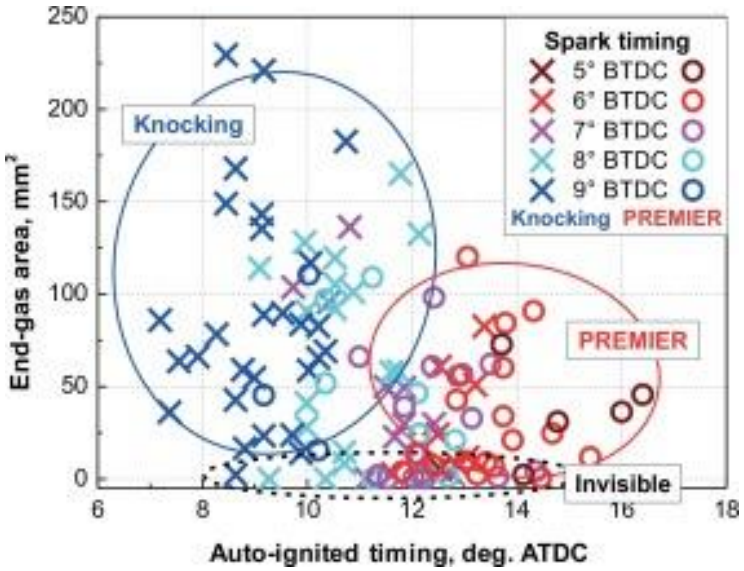

Figure 2.24: Relationship between the end-gas area and autoignition timing

Main conclusion:

- No pressure oscillation was observed during normal and PREMIER combustion but pressure oscillation was observed during knocking combustion when spark timing was advanced.
- As the autoignition in PREMIER combustion was later than in knocking, the area and volume of the end-gas region were smaller**.**

2.8 Summary

PREMIER combustion was observed under various experimental conditions, different fuels and mixtures, injection timing, EGR, split injection strategy and etc. Overall results show that engine performance and combustion characteristics of dual- fuel mode operation can improve by autoignition of unburned mixture in the end- gas region without knocking. PREMIER combustion can be achieved either in spark ignition engines or compression ignition engines. Advancing injection timing is an important factor in order to achieve PREMIER combustion in compression ignition engines and advancing spark timing is an important factor in spark ignition engines. In addition, in comparison to normal combustion, PREMIER combustion is more thermally efficient and emits less hydrocarbon and carbon monoxide. However, its nitrogen oxides emissions are slightly larger.

Moreover, it was possible to suppress knocking which is the unflavored condition for engine and achieve PREMIER combustion with split injection strategy. Engine output and thermal efficiency were improved with split injection compared to those in single injection. Finally, pressure oscillation during knocking combustion and pressure without oscillation during normal and PREMIER combustion were observed by using high speed camera in CEM equipped with visualization system.

However, in this study, simulated biogas and methane-CO_2 with different ratio were investigated in dual-fuel gas engine. Effect of injection timing and intake pressure in simulated biogas experiment and effect of injection timing and ratio of CO_2 to methane in methane-CO_2 experiment were studied and results are presented in chapters 4 and 5.

References

[1] Y Nakagawa, Y Takagi, T Itoh, and T Iijima. Laser shadowgraphic analysis of knocking in SI engine. SAE technical paper 845001, 1984.

[2] J Pan and C.G.W Sheppard. A theoretical and experimental study of the modes of end gas autoignition leading to knock in SI engines. SAE technical paper 942060, 1994.

[3] B Stiebels, M Schreiber, and S Sadat. Development of a new measurement technique for the investigation of end-gas autoignition and engine knock. SAE technical paper 960827, 1996.

[4] S. Hashimoto, Y. Amino, K. Yoshida, H. Shoji, and A. Saima. Analysis of OH radical emission intensity during autoignition in a 2-stroke SI engine. In Proceedings of the 4th COMODIA, 1998, pp. 405–410.

[5] N Kawahara, E Tomita, and Y Sakata. Autoignited kernels during knocking combustion in a spark-ignition engine. Proc. Combust. Inst., 31 (2007), 2999–3006.

[6] Kawahara, N., Tomita, E., Visualization of Auto-ignition and Pressure Wave during Knocking in a Hydrogen Spark-Ignition Engine, Int. J. of Hydrogen Energy, 34 (2009), pp. 3156-3163.

[7] N. Kawahara, E. Tomita, Y. Sakata, Auto-ignited kernels during knocking combustion in a spark-ignition engine, Proceedings of the Combustion Institute, 31(2007), pp. 2999-3006.

[8] E. Tomita, Y. Harada, N. Kawahara and A. Sakane, Effect of EGR on combustion and exhaust emissions in supercharged dual-fuel natural gas engine ignited with diesel fuel, SAE Technical Paper 2009-01-1832, (2009).

[9] E. Tomita, N. Kawahara and J. Zheng, Visualization of auto-ignition of end gas region without knock in a spark-ignition natural gas engine, Journal of KONES. Powertrain and Transport; 17(2010), 521–527.

[10] M. M. RoY, E. Tomita, N. Kawahara, Y. Harada, A. Sakane. An experimental investigation on engine performance and emissions of a supercharged H_2-diesel dual-fuel engine, International Journal of Hydrogen Energy; 35(2010), 844–853.

[11] M. M. Roy , E. Tomita , N. Kawahara , Y. Harada and A. Sakane, Comparison of performance and emissions of a supercharged dual-fuel engine fueled by hydrogen and hydrogen-containing gaseous fuels, International Journal of Hydrogen Energy; 36(2011), 7339–7352.

[12] U. Azimov , E. Tomita , N. Kawahara and Y. Harada, Premixed mixture ignition in the end-gas region (PREMIER) combustion in a natural gas dual-fuel engine: operating range and exhaust emissions, International Journal of Engine Research; 12 (2011), 484–497.

[13] U. Azimov , E. Tomita, N. Kawahara and Y. Harada, Effect of syngas composition on combustion and exhaust emission characteristics in a pilot-ignited dual-fuel engine operated in PREMIER combustion mode, International Journal of Hydrogen Energy; 36(2011), 11985–11996.

[14] U. Azimov, E. Tomita and N. Kawahara, Ignition, combustion and exhaust emission characteristics of micro-pilot ignited dual-fuel engine operated under PREMIER combustion mode, SAE Technical Paper; 2011-01-1764, (2011).

[15] E. Tomita, N. Kawahara, M. Kondo and Y. Sunada, Combustion and exhaust emissions characteristics of pilot-ignited engine fueled with digester gas; CIMAC congress, (2013), Shanghai, Paper No. 145.

[16] C. Aksu, N. Kawahara, K. Tsuboi, S. Nanba, E. Tomita and M. Kondo, Effect of hydrogen concentration on engine performance, exhaust emissions and operation range of PREMIER combustion in a dual fuel gas engine using methane-hydrogen mixtures. SAE Technical Paper; 2015-01-1792, (2015).

[17] C. Aksu, N. Kawahara, K. Tsuboi, M. Kondo and E. Tomita, Extension of PREMIER combustion operation range using split micro pilot fuel injection in a dual fuel natural gas compression ignition engine: A performance-based and visual investigation, Fuel; 185 (2016), 243–253.

[18] N. Kawahara, Y. Kim, H. Wadahama, K. Tsuboi, E. Tomita, Differences between PREMIER combustion in a natural gas spark-ignition engine and knocking with pressure oscillations, Proceedings of the Combustion Institute; 37(2019), 4983-4991. https://doi.org/10.1016/j.proci.2018.08.055.

3.1 Experimental setup

3.1.1 Test engine

The experiments are carried out using a single-cylinder, four-stroke, water-cooled, direct-injection, dual-fuel gas engine. A schematic diagram of the experimental setup is shown in Figure 3.1. The engine had a bore and stroke of 96 and 108 mm, respectively, with a displacement volume of 781 cm^3 and the connecting rod length of 168mm. A diesel fuel injector with a three-hole nozzle (ϕ 0.1 mm) is used with a common rail system to spray the pilot fuel. Fuel is pressurized by a high-pressure oil pump. The purpose of this nozzle was to inject as little diesel fuel as possible.

Table 3.1 Test engine specification and experimental conditions

Engine type	Four stroke, single cylinder
Bore * stroke	96 mm * 108 mm
Displacement volume	781 cm^3
Equivalence ratio, ϕ_t	0.6 (biogas), 0.56 (CH_4-CO_2)
Compression ratio	17:1 (biogas), 16:4 (CH_4-CO_2)
Combustion system	Pilot ignited dual fuel combustion
Intake pressure, P_{in}	101, 150, 200 kPa
Injection system	Common rail direct injection
Injection pressure	40 MPa
Injection quantity	0.8 mg/cycle (biogas), 1.6 mg/cycle(CH_4-CO_2)
Injection timing	Varying
Fuel delivery	3 hole, ϕ 0.1mm (biogas), ϕ 0.11mm (CH_4-CO_2)
Engine speed	1000 rpm
Gaseous fuel supply	Premixed charged through intake port
Air intake	Supercharged condition
Intake valve open/close	340°ATDC/135°BTDC
Exhaust valve open/close	130°ATDC/345°BTDC

The gaseous fuel is introduced from intake port and gas flow rate is controlled with mass flow controllers. In-cylinder pressure is measured with a Kistler type 6052C pressure transducer. A Kistler type 5011 charge amplifier is used to amplify the in-cylinder pressure signal. A compression ratio is changeable by choosing cylinder head gasket with

suitable thickness. In this study, compression ratio of 17:1 is used for biogas experiment and 16.4:1 is used for methane- carbon dioxide experiment. A shallow dish piston is used during experiments. This piston type is more suitable for premixed fuel combustion.

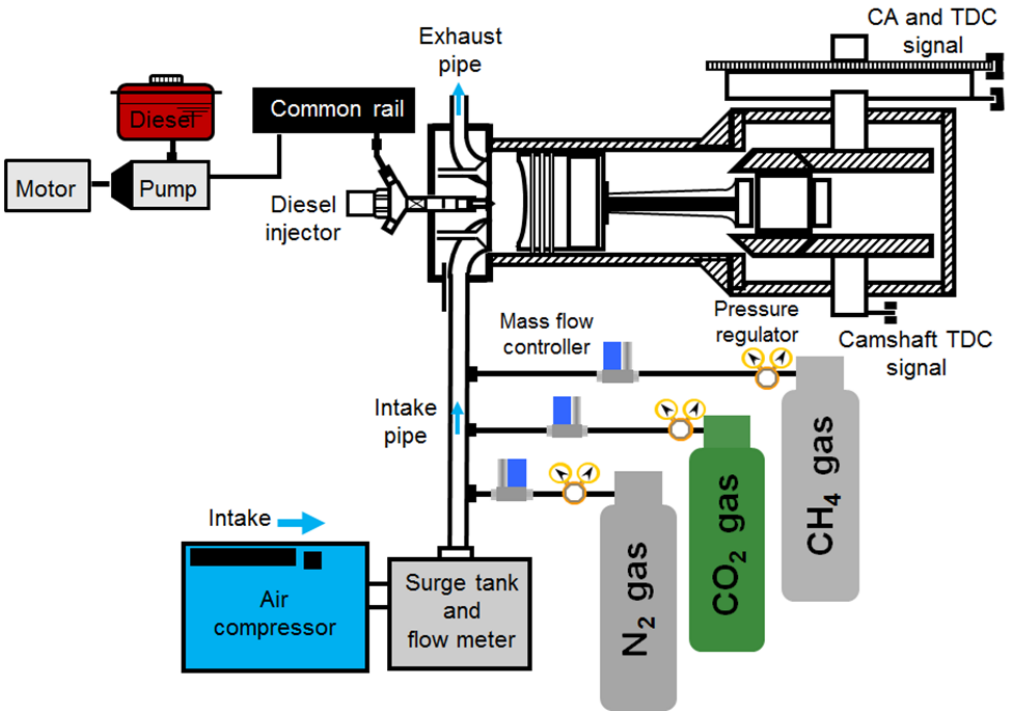

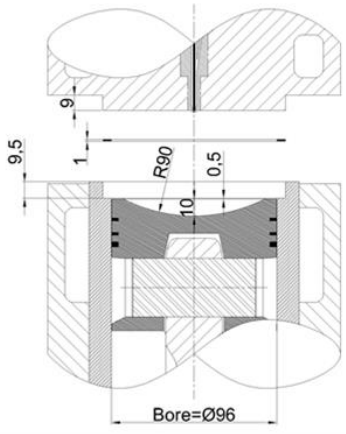

Compression ratio: 17.0:1
Piston type: Shallow dish
Head gasket thickness: 1.0mm
Piston dish diameter: 90mm
Piston top dish depth: 10 mm

(a)

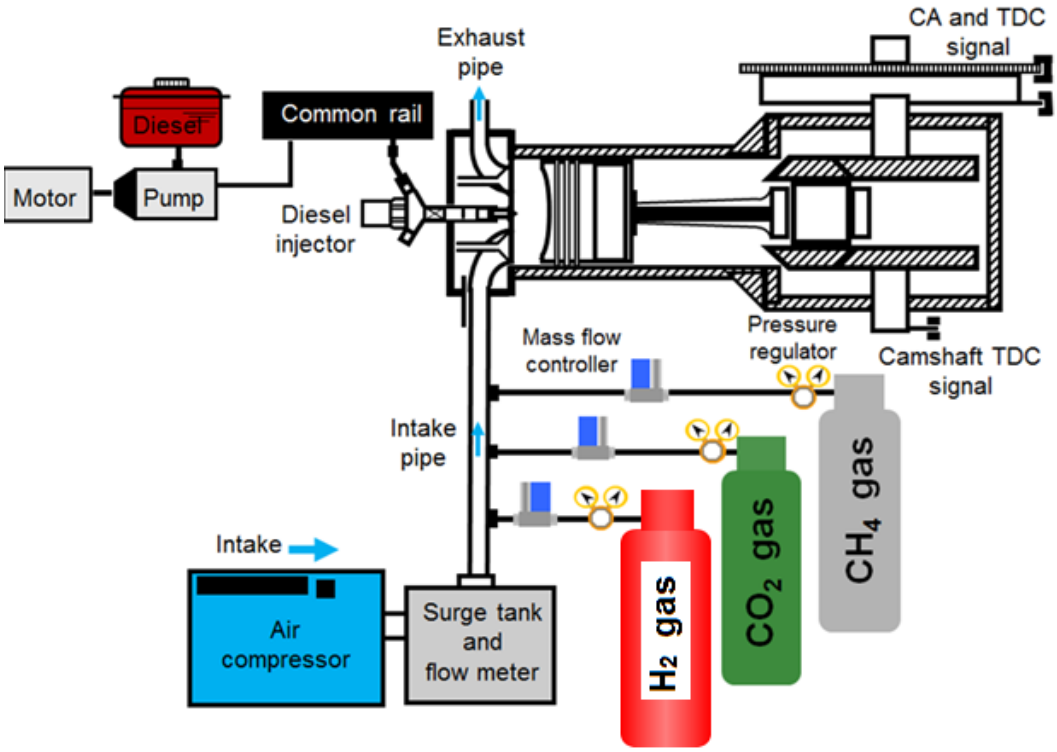

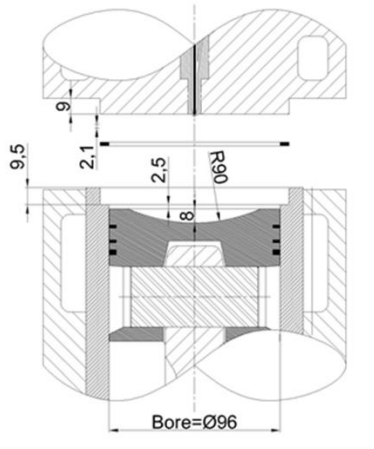

C.R.:16.4:1
Piston type: Shallow dish
Head gasket thickness: 2.1mm
Piston dish diameter: 90mm
Piston top dish depth: 8 mm

(b)

Figure 3.1: Schematic diagram of experimental setup and simplified sketches of combustion chamber geometries for (a) biogas experiment (b) methane- carbon dioxide experiment

3.1.2 Crank angle, cam angle and top dead center sensors

In order to detect crank angle position, camshaft top dead center position and cam full rotation signals, an optical sensor (photo interrupter) is used. A crank angle signal of every 0.5 °CA is detected with a photo interrupter (SG 206, KODENSHI CO., LTD.) With 720 teeth of a rotary blade directly connected to the crankshaft, and this signal is used as a reference clock. 720 teeth mean the crank angle sensor will be triggered on and off 720 times in each rotation. In addition, the TDC signal is detected by a signal rising once per revolution attached to the crankshaft and a cam TDC signal rising once in two revolutions attached to the output shaft. The outputs of the sensors are connected to both the timer circuits and the data acquisition system. A timing generator (Ascom corp., TIME 98 - 50 MHz), is used for synchronizing the engine position and output signals. However, two input signals of a clock signal and trigger signal (cam position and the top dead center sensors) are required for synchronization process. In this study, the value of 720 is the top dead center position. Figure 3.2 shows the overall circuit diagram outline used in the experiment, and Figure 3.3 shows the circuit diagram used to detect the TDC signal and crank angle signal.

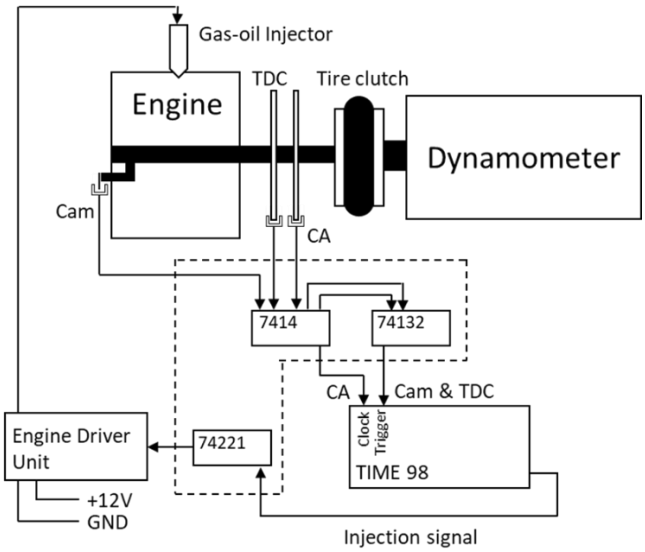

Figure 3.2: Schematic diagram of overall circuit

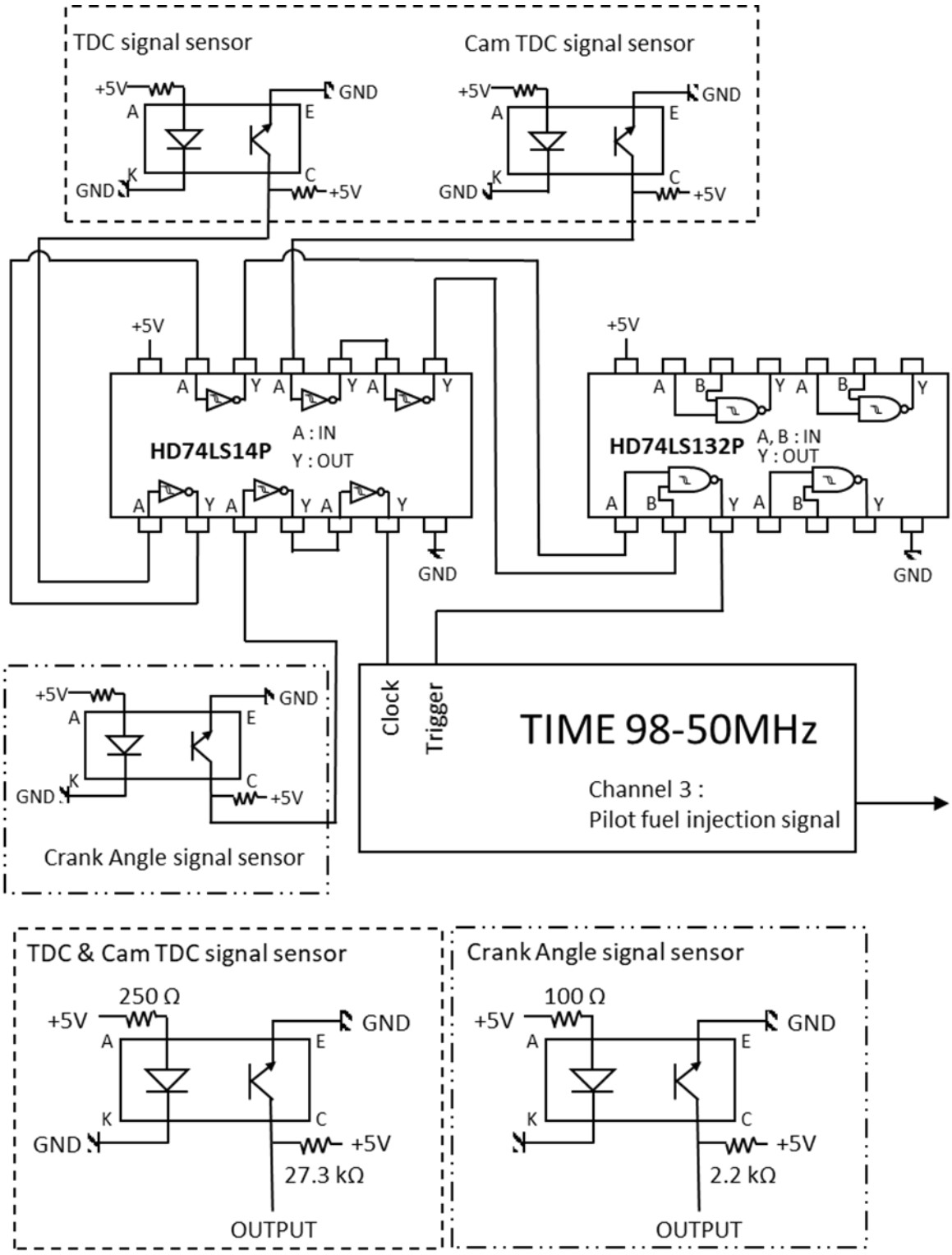

Figure 3.3: Circuit diagram of TDC signal and crank angle signal detector

3.1.3 Pilot fuel injection timing control

As mentioned in chapter 2, injection timing is one of the most important parameter in order to achieve PREMIER combustion. Therefore, the injection timing control is an important issue which must be controlled precisely. Thus, in order to improve the reading of the crank angle, it is necessary to sufficiently ensure the responsiveness of the photo interrupter. Figure 3.4 shows the diesel fuel injection command generation circuit used in this study. The diesel fuel injection command pulse generator is composed of drivers and integrated circuit (IC) groups for controlling the electric drive unit (EDU) and the injector, respectively. The TIME 98 - 50 MHz which receives the trigger signal of TDC, reads the program saved in the personal computer. Then, the number of rise of the reference clock from the crank angle is counted, and the diesel fuel injection signal is sent to the monostable multivibrator, SN 7421, at the time written in the program. A monostable multivibrator outputs a signal of a pulse width determined by the value of a capacitor and a resistance with respect to a certain signal input. The calculation formula of the pulse width τ is:

$$\tau\,[\mathrm{s}] = 0.7 * \mathrm{C} * \mathrm{R}$$

By using this resistance as a variable resistor, the pulse width can be changed during the experiment. Then, the signal outputted from the monostable multivibrator is sent to the EDU, so that injection is getting possible. Regardless of whether the engine is motored or halted, the timing generator does not send signals unless the process is started manually over the user interface on the computer.

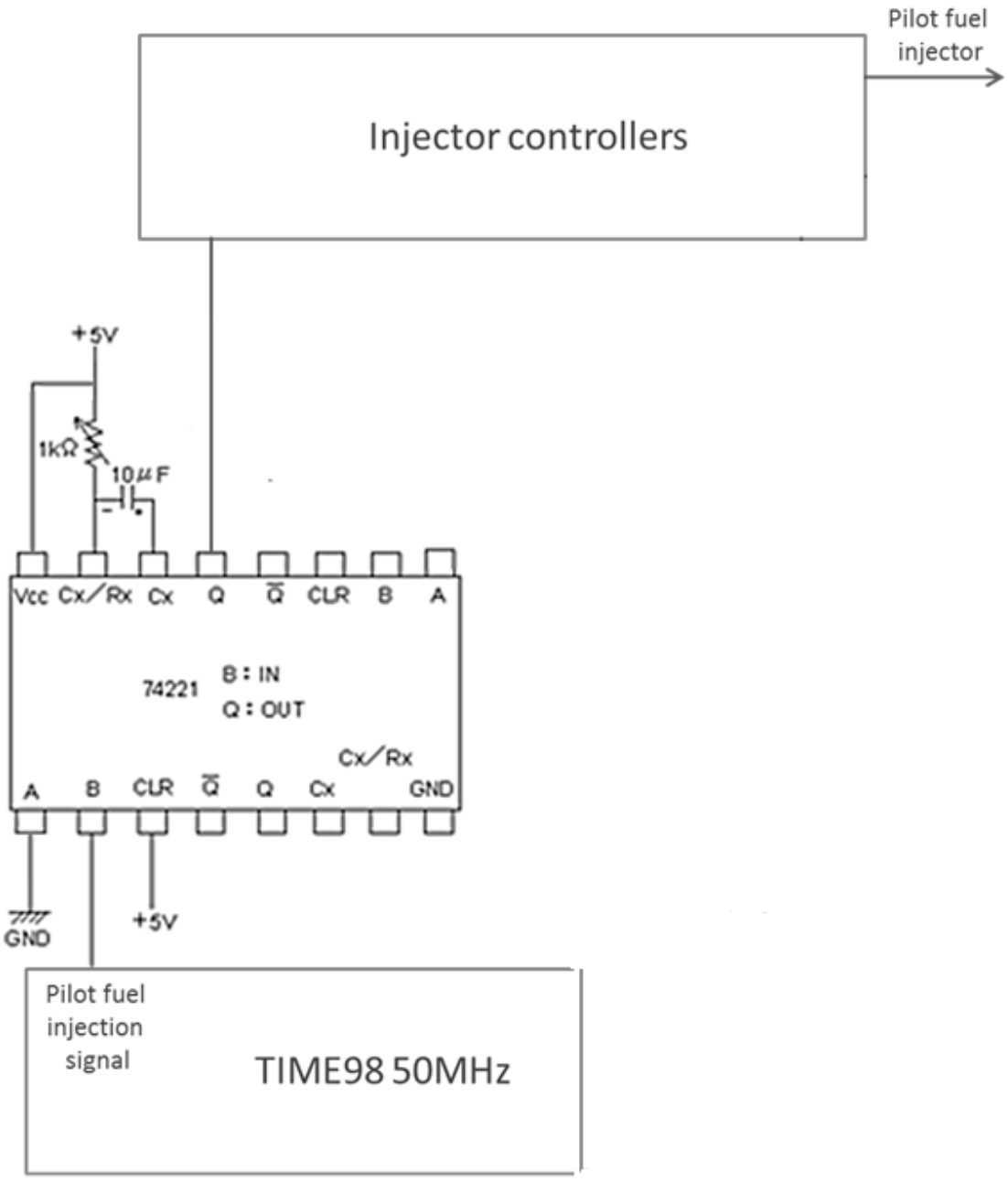

Figure 3.4: Diesel fuel injector circuit diagram

3.1.4 Pilot fuel injection system

Figure 3.5 shows a schematic diagram of the pilot fuel injection system. As shown in the figure, diesel fuel circulates in the low and high pressure lines. The pump is operated by the motor with the maximum speed. The pump used in this study is capable to pressurize diesel fuel up to 200 MPa. The pressurized diesel fuel exit from pump and enter to the common rail system. The common rail connects the high pressure line to the injector. In addition, in this system, by changing the spring of the pressure relief valve, it is possible to change the diesel oil injection pressure to desired point. The pressure relief valve is a detachable component.

In this study, a solenoid valve controlled injector manufactured by DENSO is used. This injector uses in commercial diesel engine vehicles. The injection signal determines the opening and the closing timing of the nozzle. When the injection signal enters the injector, the solenoid opens the needle valve and the diesel fuel is injected into the combustion chamber.

The spray orientation is shown in Figure 3.6. The sprays are oriented 120 degrees from each other on the plane normal to the central axis of the injector.

By using a measuring pipette (3 milliliters capacity) in parallel to the fuel tank, fuel supply from the fuel tank is measured. The method for measuring the injection quantity is the stopwatch measuring. The fuel supply is closed when injection rate is measuring. The time it takes to consume a 1 milliliter is measured. When engine is running at constant speed of 1000 rpm, by knowing the density of diesel fuel (0.832 g/ml) and number of injection times per minute, the amount of injected fuel can be measured.

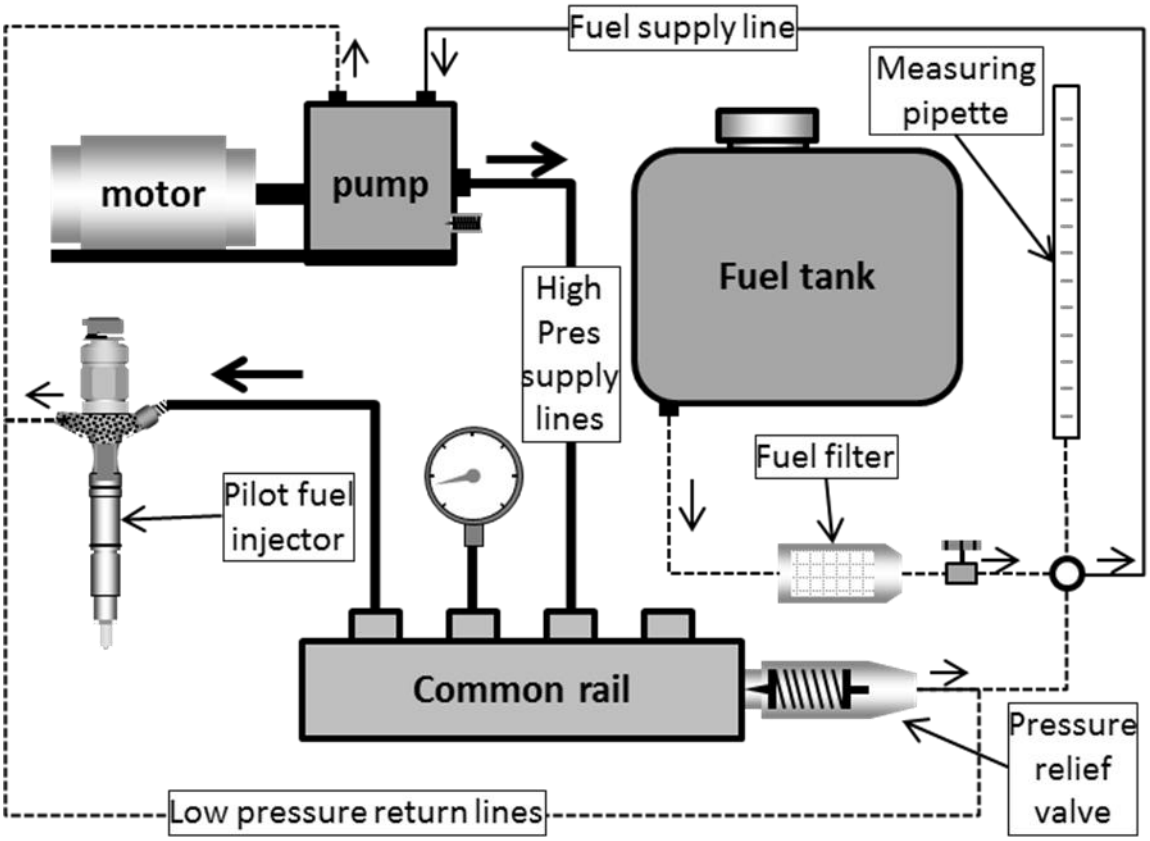

Figure 3.5: Schematic diagram of the pilot fuel injection system

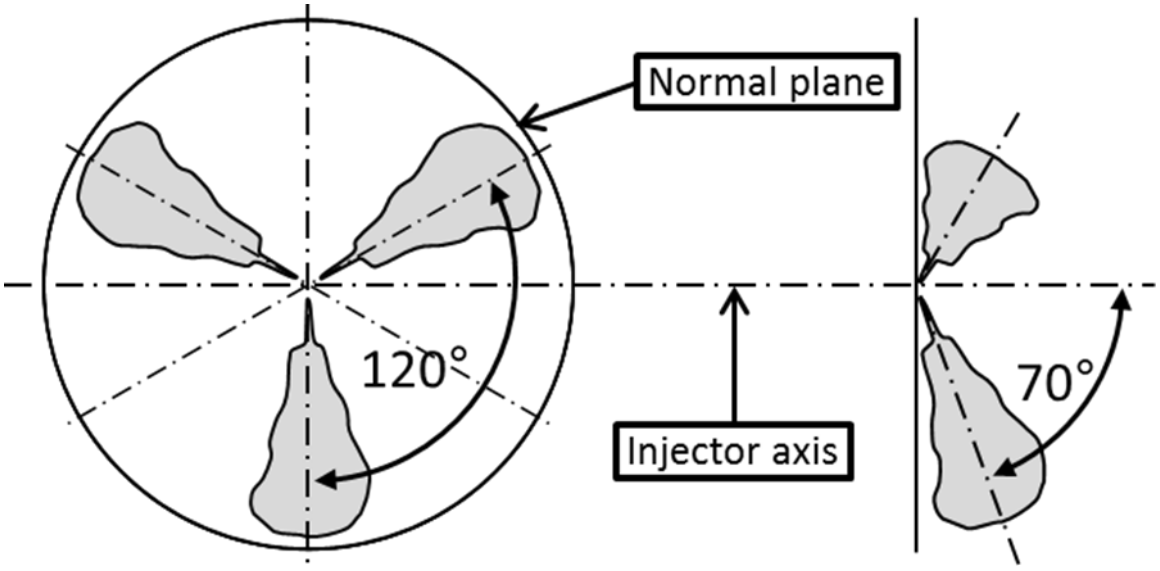

Figure 3.6: Pilot fuel spray orientation

3.1.5 Supercharging system

Figure 3.7 shows the outline of supercharging system. The supercharging system consists of a screw type air compressor, two surge tanks, a solenoid valve for flow control, an absolute pressure sensor, an air flowmeter and the air pressure and temperature PIV controller. Ambient air (outside air) is supplied by an air compressor and stored in the first surge tank at 7 atm pressure. The pressure sensor is installed in the second surge tank. When the air is sent to the second surge tank, the PIV controller and the solenoid valve are activated in order to maintain the pressure at the required level in the second surge tank. Therefore, second surge tank serves as an air accumulator. A solenoid valve is activated after the PIV controller read the pressure value received from pressure sensor. As shown in the figure, there is an air flowmeter which installed to the exit of second surge tank. This is used in order to measure the air flow rate during experiments. To maintain the intake air temperature at the desired level, an air heater is installed downstream from the air flowmeter. The temperature of intake air is measured by a k-type thermocouple and controlled by another PIV controller. Both cooling and heating can be set in the control panel manually, but in order to keep it constant, it is necessary to always check the supply air temperature before and after operating the engine.

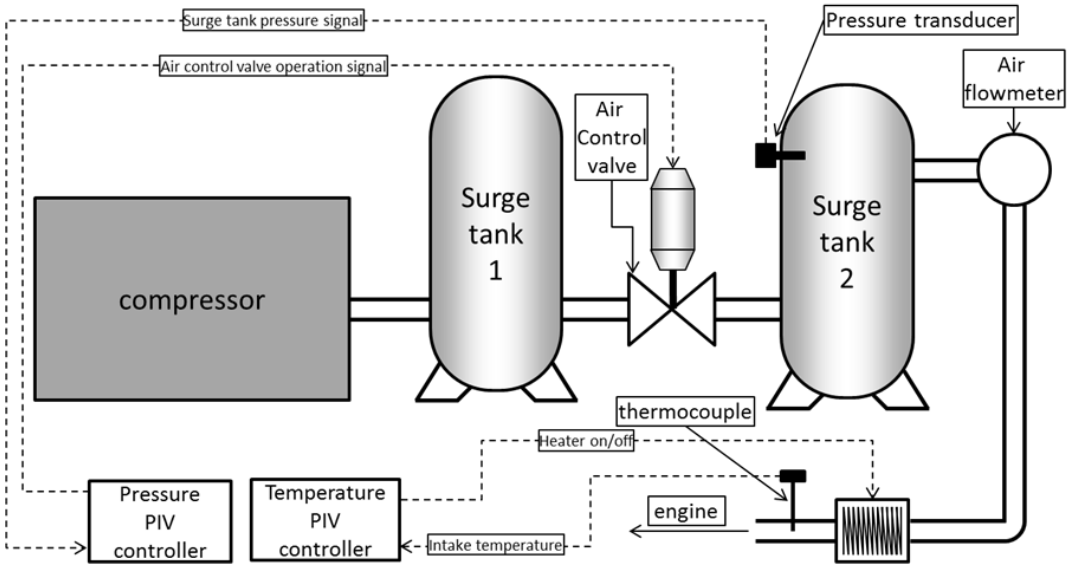

Figure 3.7: Supercharging and intake air heater systems

3.1.6 Gaseous fuel supply system

The gas flow rates of gaseous fuels (CH_4 and CO_2) are automatically calculated by using a programmable logic controller (PLC) in order to obtain an accurate gas composition and equivalence ratio. The main components in the gaseous fuel supply system are mass flow controllers. The air flow rate is obtained from flowmeter and PLC reads this flow rate and then calculate the CH_4 and CO_2 ratios as well as equivalence ratio based on the mathematical definitions.

Then required gas flow rate is converted to the analog signal in the range of 1-5 V. The mass flow controller receives this signal and sends the corresponding amount to the intake pipe. The gas entries to the intake port are installed approximately 3 meters upstream from the intake valves to perform more homogeneous premixing with air. Figure 3.8 shows the outline of the gaseous fuel supply system.

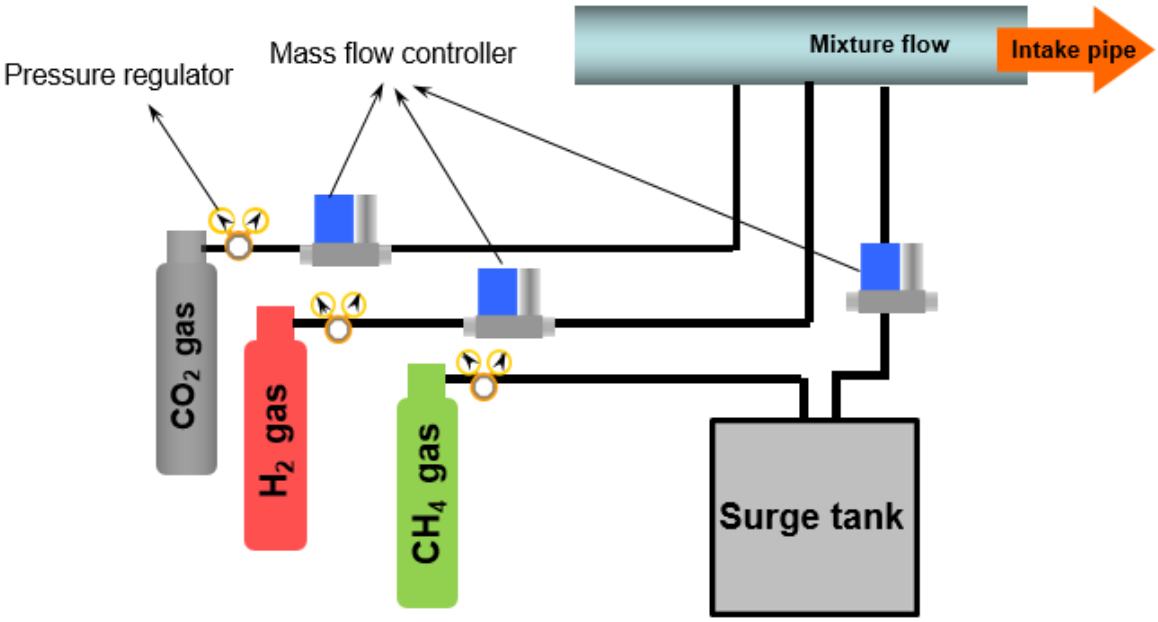

Figure 3.8: The outline of the gaseous fuel supply system

3.1.7 The main control panel

A number of parameters are measured and controlled by means of main control panel. Figure 3.9 show the components of this unit and these functions are listed below.

1) Natural gas pressure indicator: This is not used in our experiment.

2) (3) Exhaust gas temperature indicators: Exhaust temperature is measured in two locations using k-type thermocouples. The first measurement is taken 250 millimeters downstream from the engine head and displayed on indicator (2), and the other at the exhaust gas analyzer connection barrel and displayed on indicator (3).

4) Intake pressure PIV controller and indicator: The units are in kilopascals (absolute).

5) Intake air flowrate indicator: The air flowrate in cubic meters per hour.

6) Engine oil temperature indicator:

7) Intake air temperature PIV controller:

8) Coolant/heating fluid temperature controller:

9) Supercharger on-off control

10) Recirculation water pump on-off control

11) Intake air heater on-off indicator (top) and switch (bottom)

12) Recirculation heater on-off indicator (top) and switch (bottom)

13) Diesel fuel pump motor speed governor knob (top) and on-off switch (bottom):

14) Panic button: When pressed, this button terminates the power connection into the control panel.

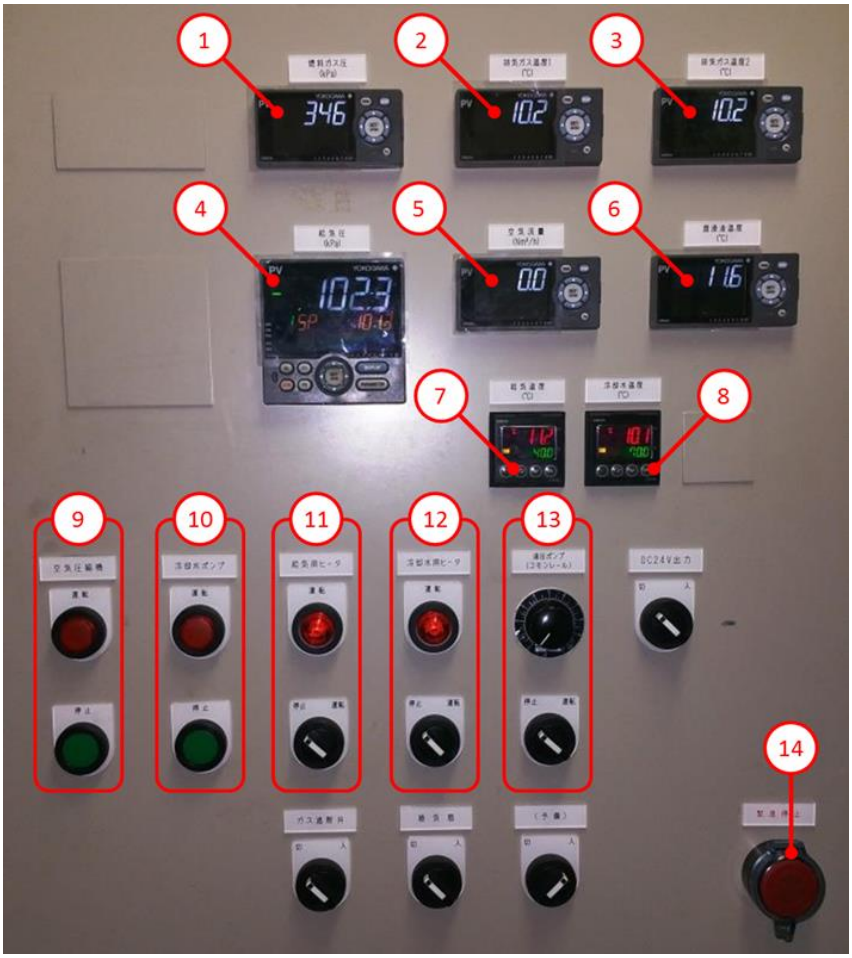

Figure 3.9: The main control panel

3.1.8 Data logger

The pressure signal and the diesel fuel injection timing signal are recorded with a digital data recorder (DL 750, manufactured by Yokogawa Electric Corporation) together with the crank angle signal and the TDC signal. This device is capable of measuring data from 16 separate channels. After recording, the data is transferred to a PC and analyzed further in a PC.

3.1.9 Exhaust gas analyzers

Regarding to exhaust emissions, the NOx, CO, CO_2 and O_2 concentrations are measured with a multi gas analyzer (Horiba, PG-240) and the HC concentration is measured with a hydrocarbon gas analyzer (Horiba, MEXA-1170 HFID). Smoke (soot) is also measured with an opacimeter (Horiba, MEXA-600S) based on the opacity of the exhaust gases.

3.2 Experiment conditions

As we mentioned earlier, all required signals are recorded by data logger (DL 750, manufactured by Yokogawa Electric Corporation). In each test, a charge amplifier is reset after the oil temperature stabilized at 80ºC. It takes time to engine oil temperature reach to desired level. After completion of the test, engine is allowed to run for few seconds in order to collect data for recording. All signals properties can be confirmed by checking the data logger screen. After confirmation, the data logger is paused and the data is recorded. The format of recorded data is .wvf format and therefore, it is needed to convert to any known format. The conversion is done by xviewer software supplied from manufacturer. The .wvf format is then converted to .csv file which is known format native to excel. A charge amplifier output voltage, crank angle, TDC and injection signals as well as outputs of other connected measurement devices are given in a single row at a

sampling point. Figure 3.10 shows a data logger and sample of data logger screen. The experiment is carried out with the supply air pressure fixed at 200 kPa under all conditions for CH_4- CO_2 mixture. The injection pressure is set to 40 MPa and the injection amount is set to 1.6 mg / cycle. This amount is chosen due to better injection stability. Injection timing is varied during experiments. In this work, pressure data is evaluated at a crank angle interval of 0.1. Table 3.2 shows the fuel mixtures and fuel supply timings.

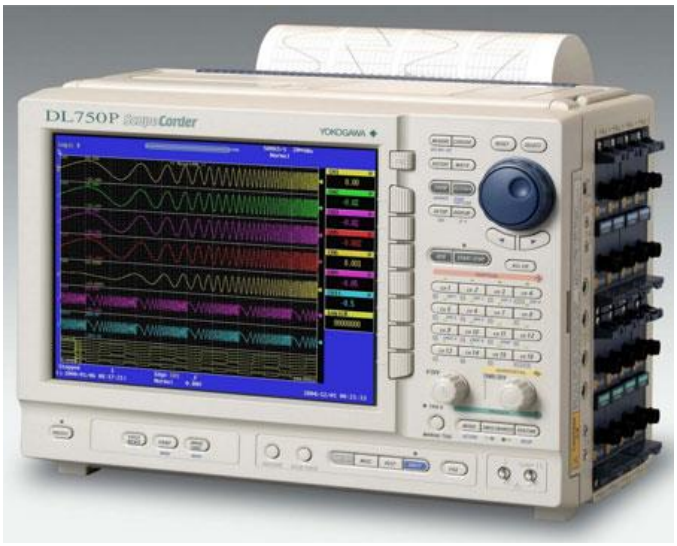

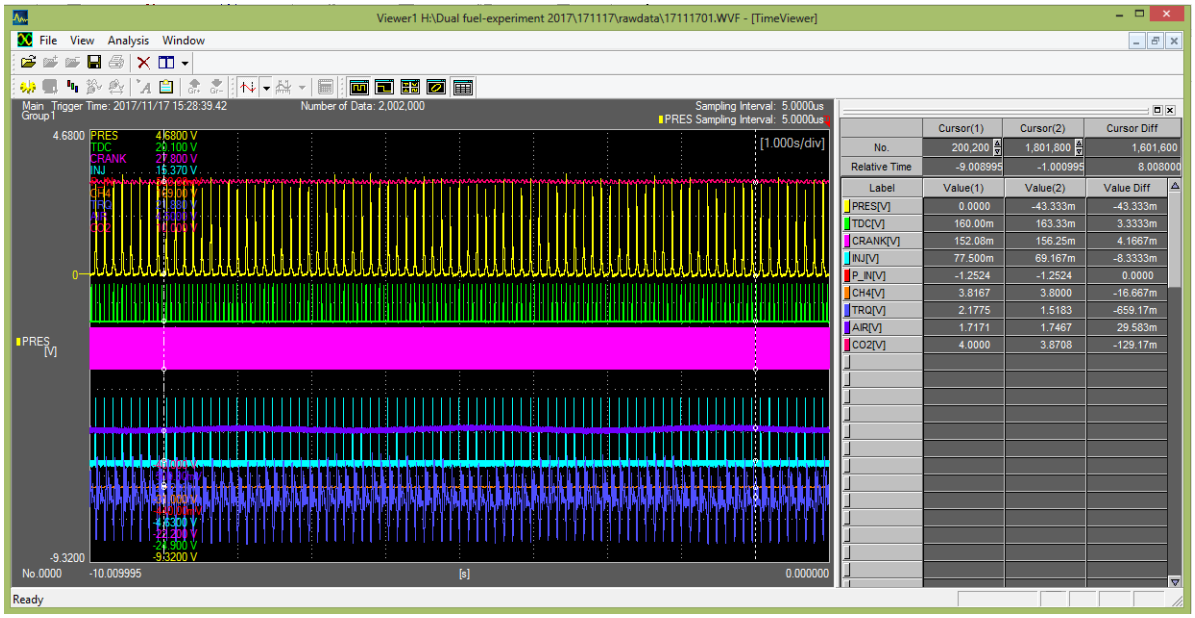

Figure 3.10: DL750 data logger and the sample screen

Table 3.2 Gas composition and diesel fuel injection timing

Fuel	CH_4(Vol.%)	CO_2(Vol.%)	N_2(Vol.%)	Injection timing (°CA)
50% CO_2	50	50	0	12, 14, 15, 16, 17, 18, **19**, **20**
40% CO_2	60	40	0	12, 14, 15, 16, **17**, 18
30% CO_2	70	30	0	10, 11, 12, 13,14, **15**, 16, 17
20% CO_2	80	20	0	10, 11, 12, **13**, 14
10% CO_2	90	10	0	10, 11, **12**, 13
100% CH_4	100	0	0	10, 11, **12**, 13
Biogas	58	35	7	15, 17, 20 (P_{in}= 101 kPa) 10, 12, **14** (P_{in}= 150 kPa) 8, 9, **10** (P_{in}= 200 kPa)

3.3 Gaseous fuels and their properties

In this work, gaseous fuels are used as a primary fuels and diesel fuel is used as a pilot fuel or ignition source. Gaseous fuels are simulated biogas which consisting 58% methane, 35% carbon dioxide and 7% nitrogen by volume, pure methane, and methane-carbon dioxide mixture. The properties of diesel and methane are listed in the Table 3.3.

Table 3.3 Properties of diesel and methane

	Methane	Diesel
Density (kg/m^3)	0.717	0.832
Specific heat ratio (0°C, 1atm)	1.32	-
Stoichiometric A/F ratio (kg/kg)	17.4	14.6
Lower heating value (MJ/kg)	50.1	43.4
Self-ignition temperature (°C)	632	255
Minimum ignition energy (mJ)	0.28	-
Theoretical air volume, (kg/kg)	17.12	-
Flame temperature (°C)	1957	-
Maximum burning velocity [0.1MPa] (m/s)	0.45	0.38
Octane number (RON)	120	15-25

3.4 Theoretical Background

3.4.1 Pressure history and rate of heat release (ROHR)

As it is mentioned in chapter one, internal combustion (IC) engines are heat engines and their working principle are based on the pressure and volume variation inside the engine. In a real internal combustion engine, characteristics of a cycle can be obtained from the pressure history. The in- cylinder pressure measures with pressure sensor. In this study, in-cylinder pressure is measured with a Kistler type 6052A pressure transducer and recorded with respect to the position of the crank angle. Rate of heat release (ROHR) is an important parameter which can be obtained from pressure history. By obtaining ROHR, it is possible to unlock some important combustion related information. Some thermodynamic background is needed in order to better understanding of ROHR.

To begin, we start with the first law of thermodynamic:

$dQ_c = dW + dQ_h + dU$ ……(3.1)

here; Q_c= heat released by combustion, W = Work done, Q_h = Heat transfer from the cylinder and U = Internal energy of the cylinder contents.

whereas the work done on the system is:

$W=\int P\, dV$ ……(3.2)

P= pressure and dV= volume change

The internal energy of a fluid in a system is typically a function of temperature and if it is assumed as ideal gases, therefore:

$dU= mc_v dT$ ……(3.3)

c_v is defined as constant volume specific heat and it is the derivative of the internal energy with respect to the temperature then;

$$c_v = \left(\frac{dU}{dT}\right) \quad \text{.....(3.4)}$$

pV= mRT (equation of state)

Equation of state in differential form and arrangement:

$$\text{mdT} = \frac{1}{\text{R}}(\text{pdV} + \text{Vdp}) \quad \text{.....(3.5)}$$

Now, substitute equation 3.5 into equation 3.3:

$$\text{dU} = \frac{\text{c}_\text{v}}{\text{R}}(\text{pdV} + \text{Vdp}) \quad \text{.....(3.6)}$$

Then substitute equations 3.2 and 3.6 into equation 3.1 in differential form with respect to crank angle:

$$\frac{dQc}{d\theta} = \frac{\text{c}_\text{v}}{R}\left(P\frac{dV}{d\theta} + V\frac{dP}{d\theta}\right) + P\frac{dV}{d\theta} + \frac{dQh}{d\theta} \quad \text{.....(3.7)}$$

Where R is a universal gas constant and it is written as: $\text{R} = c_p - c_v$

Where c_p is a specific heat capacities at constant pressure.

Heat capacity ratio is defined as: $\text{k} = \frac{\text{c}_\text{p}}{\text{c}_\text{v}}$

Equation 3.7 can be written as:

$$\frac{dQc}{d\theta} - \frac{dQh}{d\theta} = \frac{1}{\text{k}-1}\left(P\frac{dV}{d\theta} + V\frac{dP}{d\theta}\right) + P\frac{dV}{d\theta} \quad \text{.....(3.8)}$$

It is not possible to measure the heat loss in the engine; therefore, the term of heat transfer (Q_h) needed to be neglected.

$$\frac{dQc}{d\theta} = \frac{1}{\text{k}-1}\left(P\frac{dV}{d\theta} + V\frac{dP}{d\theta}\right) + P\frac{dV}{d\theta} \quad \text{.....(3.9)}$$

And the net heat release rate can be finally written as:

$$\frac{dQc}{d\theta} = \frac{\mathrm{k}}{\mathrm{k}-1} P \frac{dV}{d\theta} + \frac{1}{\mathrm{k}-1} P \frac{dV}{d\theta} \quad \text{(3.10)}$$

3.4.2 Mass fraction burned (MFB)

When the rate of heat release is integrated, the term of mass fraction burned (MFB) can be obtained. The MFB reflects the amount of fuel burned throughout the combustion process. In this study, MFB is calculated as follows:

$$MFB = \int_{-360^\circ CA}^{360^\circ CA} \frac{dQ}{d\theta} d\theta \,/\mathrm{Q}_{total} \quad \text{(3.11)}$$

The integration interval is from -360 °CA to 360 °CA. In addition, MFB is represented at a maximum of 100% because it is calculated by means of total energy input (Q_{total}), however, the calculated MFB is lower than the actual MFB because heat loss cannot be considered.

3.4.3 Specific heat ratio calculation method

In this study, the specific heat ratio κ was determined as follows:

$$\kappa = (\sum \kappa_i * v_i)/v \quad \text{(3.11)}$$

Here, κ_i: specific heat ratio of each gas component, v_i: volume of each gas component, v: volume of all gases.

3.4.4 Produced work based on pressure history and cylinder volume

As it is mentioned earlier, principle working of IC engines is based on variation of in-cylinder pressure and volume. It can be characterized by pressure-volume (p-v) diagram of typical cycles of IC engines that shows pressure variations as a function of volume for a complete engine cycle. Figure 3.11 shows the p-v diagram of a typical cycle.

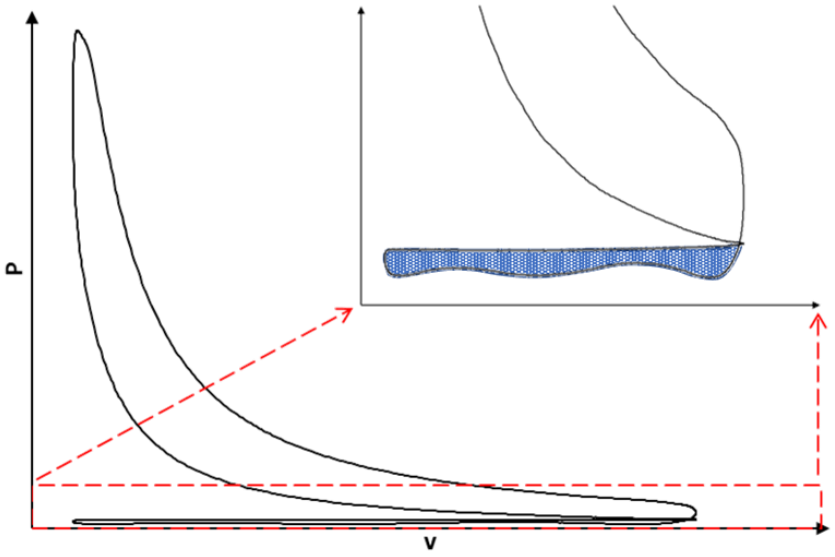

Figure 3.11: Typical P-v diagram of a four stroke cycle in a real engine.

Four strokes of engine cycle are starting by drawn the air in the cylinder and increasing the volume while pressure is lower than atmospheric pressure. Then air is compressed by moving the piston from BDC towards TDC and gradually increasing the pressure while cylinder volume is decreasing. Before piston reach the TDC, in-cylinder mixture is ignited by either spark plug or fuel injection. The in-cylinder pressure rise as a result of combustion pushing the piston from TDC towards BDC, cylinder volume again rises while pressure is gradually drops. It can be inferred that the produced work of engine is directly depends on in-cylinder pressure and volume variation. The colored area in Figure 3.11 is negative work when engine is operating under naturally aspirated condition. In this study, supercharged system was used, thus, the colored area represents pumping loop of supercharging system, however, the colored part is positive work under supercharging condition. Produced work is calculated as follows:

$W = F \times L$ ……(3.12)

Where W is work (J), F is the force which pushing the piston in power stroke, and L is the displacement or piston stroke. It is known that force is the pressure multiple area, therefore;

$F = p \times A$ ……(3.13)

Where p is the in-cylinder pressure (Pa) and A is the piston area (m^2). Replacing (3.13) in (3.12), gives:

$W = p \times A \times L$ ……(3.14)

It is known that area multiple distance will give us volume, thus;

$W = p \times V$ ……(3.15)

Equation 3.15 is the instantaneous work produced in the cylinder for a certain pressure and volume. To determine the work for the complete engine cycle we need to integrate the instantaneous work:

$$\mathbf{W = \int p.dV} \quad \text{……(3.16)}$$

Equation 3.16 is the work produced in the cylinder for a complete cycle.

W is the indicated work per cycle, p is the pressure and dV is the rate of change of the volume. To analyze the engine performances, the exact values of pressure and volume in the equation 3.16 is needed. Pressure can be measured by using pressure sensor during experiment and the value of cylinder pressure with respect to crank angle position can be obtained. Volume of cylinder can be obtained easily because the dimension of engine is known and it is not changing from cycle to cycle. In order to obtain the volume of the cylinder at given crank angle, an equation 3.17 can be used. Figure 3.12 shows the required parameters in the equation 3.17.

$$\frac{V}{V_{min}} = 1 + 0.5(CR - 1)\left[\left(\frac{l}{a}\right) + 1 + cos\theta - \sqrt{\left(\left(\frac{l}{a}\right)^2 - sin^2\theta\right)}\right] \quad \text{.....(3.17)}$$

In this equation

V: instantaneous volume

V_{min}: Volume of the cylinder at top dead center position

l: connecting rod length

a: crank arm length, equal to half of stroke

θ: the instantaneous angular position of crank arm.

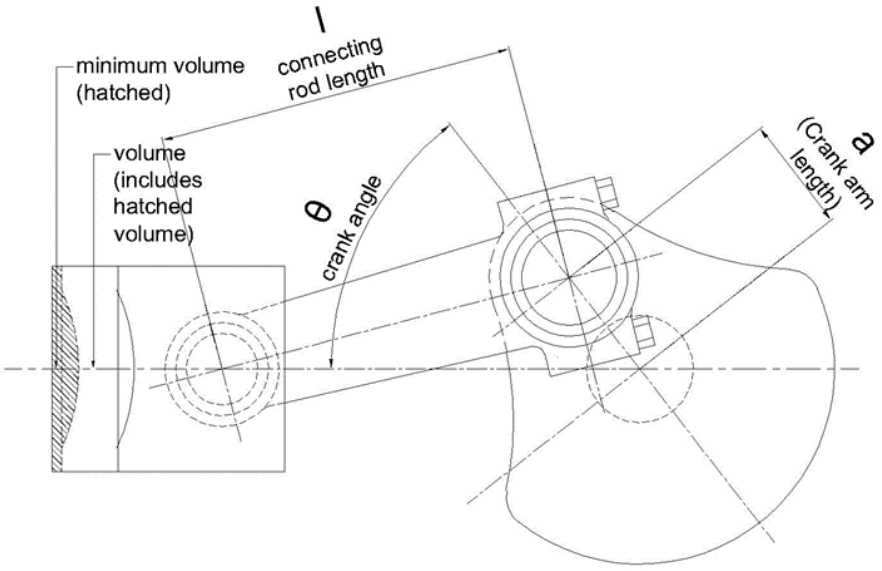

Figure 3.12: The dimensions required for obtaining instantaneous cylinder volume

3.4.5 Indicated mean effective pressure (IMEP)

IMEP is a parameter that can be used to determine the engine performance of IC engines. IMEP is defined as the work done by unit volume of the engine. In the other words, the

ratio between the produced work and cylinder displacement and it can be obtaining as follows:

$$\mathbf{IMEP} = \frac{\mathbf{W}}{\boldsymbol{V_d}} \quad \text{(3.18)}$$

Where V_d refers to the swept volume and W refers to work.

3.4.6 Indicated thermal efficiency (η_i)

Thermal efficiency of the engine describes how efficiently chemical energy released from burning of the fuel can be converted to useful work. Thermal efficiency is the ratio of the produced work per cycle to the input energy of fuel based on its lower heating value (LHV) and it can be obtained as follows:

$$\eta_{\mathbf{i}} = \frac{\mathbf{W}}{\mathbf{m_{fuel} \times Q_{HV}}} \quad \text{(3.19)}$$

Where m_{fuel} is the amount of fuel delivered to the engine per cycle and Q_{HV} is the heating value of the fuel.

4.1. Introduction

Greenhouse gas (GHG) emissions are of serious environmental concern. Carbon dioxide (CO_2), methane (CH_4), nitrous oxide (N_2O), and fluorinated gases are all considered GHGs; they trap heat in the atmosphere. Carbon dioxide is typically produced by the burning of fossil fuels, and is thus of particular concern. Of the various GHGs, CO_2 contributes the most to climate change because of the enormous quantity that is emitted. Although CO_2 is also produced naturally, human activities greatly affect the amount in the atmosphere. Transportation, power generation, and other industrial purposes involving fossil fuel combustion are the principal human activities increasing the amount of atmospheric CO_2. Electricity demand continues to rise due to worldwide population growth and economic development. In terms of future energy demands, the depletion of petroleum resources is also of concern. Long-term use of petroleum derivatives as energy sources for transportation and power generation may not be feasible, given the dwindling global reserves, increasing costs, and environmental issues. The internal combustion engine situation is particularly critical; such engines are widely used in the automobile and electricity generation industries. Therefore, high-efficiency low-emission engines using more advanced combustion strategies, and new fuels that do not exploit conventional resources, are required. Extensive research is underway to identify alternative fuels and develop new combustion technologies.

One of the most suitable energy resources among alternative fuels for internal combustion engines is biomass gas, which is renewable, clean, and readily available [1, 2]. Biomass is organic material from animals or plants. Burning of biomass releases stored energy. Biomass can be burned directly or converted into liquid and gaseous biofuels such as bioethanol, biodiesel, and biogas, which can then be used as fuels for

transportation and electricity generation. Gaseous biofuels generated via CH_4 fermentation are termed digester gases. These gases are produced by anaerobic fermentation of organic matter or feedstocks, such as sewage sludge, agricultural and forest residues, manure, and garbage. Also, biomass can be converted into gaseous biofuel via thermochemical gasification. Gaseous fuels obtained in this manner are termed producer gases. Of the various gaseous fuels, biogas produced via CH_4 fermentation is regarded as a particularly promising alternative fuel for internal combustion engines. This biogas is composed principally of CH_4 (about 50–60%) and CO_2, and may be a useful fuel for power generation in rural areas. Biogas exhibits good anti-knocking properties because it includes CH_4. Global warming can be reduced by burning biogas, which can be used without any major modification of spark ignition (SI) engines [3–5]. However, the combustion quality and thermal efficiency of engines fueled by biogas are reduced by the biogas CO_2. This gas reduces NO_x emission by decreasing the burning velocity, but increases hydrocarbon (HC) emission by reducing the combustion temperature. The high self-ignition temperature of biogas means that the fuel cannot be used alone in compression ignition (CI) engines. An ignition source is required; biogas is used in dual-fuel internal combustion engines. In a dual-fuel gas engine, gaseous fuel is introduced at the intake port, where it is mixed with air. As it is difficult to autoignite the mixture via compression only, liquid fuel is used to support ignition. The mixture is thus ignited by combustion of injected fuel. Gaseous dual-fuels have been extensively researched. Fundamental work on the use of such fuels was reviewed by Karim [6, 7]. Walsh et al. extensively explored biogases for SI and CI engines [8]. The advantages and disadvantages of dual-fuel operation using different gaseous and pilot fuels [9–13], as well as fuel properties [14, 15], fuel composition and quantities [16, 17], exhaust gas recirculation (EGR) [13], injection timing [9, 10, 15, 18, 19], loads [9, 17, 20, 21, 22], speed

[23, 24], the equivalence ratio [25], and the compression ratio [12, 20] have all been studied extensively. Overall, the dual-fuel strategy is the most promising way to exploit gaseous fuels. However, the amounts of such fuel that can thus be used are limited by knocking caused by rapid heat release [26–29].

Advanced combustion methods such as homogeneous charge compression ignition (HCCI) are more recent developments. These combustion methods were initially introduced to achieve significant reductions in NO_x and PM emissions while maintaining the thermal efficiency of CI engines. The HCCI combustion strategy features autoignition of an in-cylinder mixture [30–33]. Two drawbacks of HCCI combustion are that control of combustion timing is difficult, as is operation under high loads. HCCI engines emit more HCs and carbon monoxide (CO) than do diesel engines [34–36]. Although several improvements have been made, and modern HCCI engines are more thermally efficient, a risk of knocking caused by uncontrolled autoignition remains; therefore, a better combustion control strategy is required [37, 38]. However, although the operation range of HCCI combustion has been extended, practical applications remain difficult. Therefore, combinations of HCCI combustion with either SI or diesel engines have been considered; ignition timing is controlled using a spark plug or via autoignition on fuel injection [39, 40]. The operation of HCCI engines at high loads is compromised by knocking. Spark-assisted compression ignition (SACI) was introduced to extend the operation range of HCCI combustion while maintaining low emissions and high efficiency [41–46]. Spark timing controls autoignition and prevents accidental combustion. In [46], it was observed that the stability of gasoline HCCI combustion can be improved by spark assistance near the misfire limit. Nevertheless, combustion stability at higher loads remains problematic. Combustion control via diesel fuel injection is termed reactivity controlled compression ignition (RCCI) combustion [47–49]; this is a variant of HCCI combustion developed at

the University of Wisconsin-Madison. The RCCI combustion concept was developed to control combustion via in-cylinder blending of two fuels with different reactivities via multiple injections. The RCCI method seeks to control combustion better, reduce NO_x and PM emissions, and improve fuel efficiency.

Although improved combustion efficiency is the goal of both HCCI and RCCI research, neither method is suitable for high-load operations. To improve the thermal efficiency of internal combustion engines at high loads, a different approach is required. The autoignition phenomenon that develops near the end-gas region often triggers knocking unless an appropriate combustion-controlling strategy is used. Knocking is the term used to describe unexpected/unwanted end-gas autoignition, and has been studied extensively [50–54]. Knocking is always unwanted because of its negative effects on engine components.

However, it was discovered that end-gas autoignition in the absence of pressure oscillations can improve engine operation at higher loads. This phenomenon has been termed premixed mixture ignition in the end-gas region (PREMIER) combustion [55]. We have studied such combustion using a dual-fuel gas engine operating under high loads. A second combustion that develops after the principal combustion of gaseous fuel and air is observed in the end-gas area in the absence of any pressure oscillation. Both the thermal efficiency and engine output are higher than those of normal combustion. Although several papers on PREMIER combustion have appeared, quantitative research data are not available. A parameter expressing the autoignition intensity is required when evaluating PREMIER combustion. Here, we evaluate the pressure, rate of heat release (ROHR), maximum pressure, ignition delay, engine performance, thermal efficiency, and end-gas autoignition characteristics of PREMIER combustion in great

detail. The end-gas autoignition characteristics include autoignition timing, autoignition delay, the duration of heat release after autoignition, the mass fraction burned (MFB) before autoignition commences, and the amount of heat released. Moreover, we propose a new parameter that we term PREMIER intensity (PI); this allows quantification of PREMIER combustion.

4.2. PREMIER combustion

The PREMIER combustion strategy was developed to improve the performance and exhaust emission profile of internal combustion engines [9, 55–63]. PREMIER combustion differs significantly from normal combustion and knocking combustion in its end-gas autoignition characteristics. After compression of gaseous fuel, some flame kernels are created via autoignition of the pilot fuel. Such autoignition triggers flame propagation within the gaseous fuel/air mixture. Combustion heat is released, and the in-cylinder pressure and temperature increase further. From this point onward, the characteristics of unburned gas play an important role in determining the mode of combustion. The timing of autoignition in the end-gas region and the heat release characteristics determine whether knocking or PREMIER combustion ensues. PREMIER combustion differs from knocking combustion; particularly, the pressure oscillation characteristic of knocking is absent. A higher thermal efficiency and improved engine output are achieved when the engine operates in the PREMIER mode. Figure 4.1 shows typical pressure histories and rates of heat release under normal, PREMIER, and knocking conditions [62]. When the injection timing is advanced from 3º before TDC (BTDC) to 6º BTDC, peaks in the pressure history and the ROHR are observed after a crank angle of 10º BTDC. These peaks indicate end-gas autoignition. High-frequency pressure oscillations are evident during knocking cycles; these are absent in the case of PREMIER combustion.

During PREMIER combustion, the rises in pressure and ROHR are not as steep as those during knocking combustion.

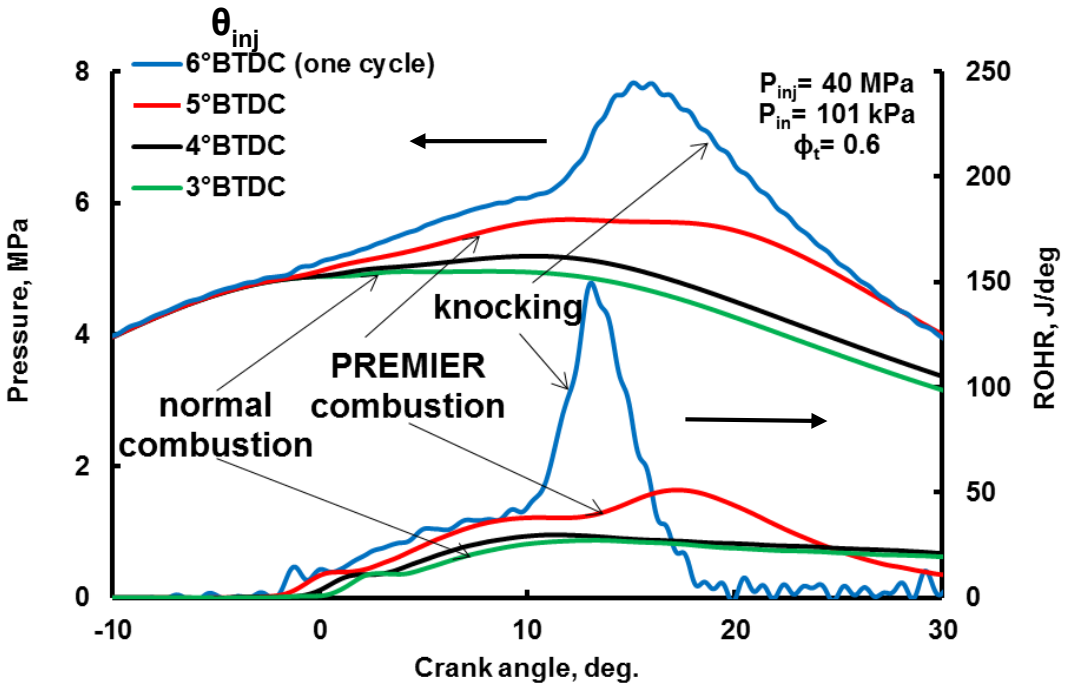

Figure 4.1: Pressure history and rate of heat release during normal combustion, PREmixed Mixture Ignition in the End-gas Region (PREMIER) combustion, and the knocking cycles (primary fuel: natural gas) [62].

In terms of exhaust emissions, our previous studies [9, 55, 56, 58–61] showed that CO and HC emissions decreased during PREMIER operation. These emissions are typically higher under dual-fuel operation but, in the PREMIER combustion mode, the levels decrease because of knock-free end-gas autoignition of the unburned mixture. Simultaneously, NO_x emissions increase because of the higher cylinder pressure and temperature attributable to autoignition in the end-gas region. Several strategies (such as EGR) have been introduced to decrease NO_x emissions, as have various treatment systems. However, NO_x reduction requires future study as PREMIER combustion strategies develop.

4.3. Experimental apparatus and data evaluation

We performed experiments using a single-cylinder, four-stroke, water-cooled, direct-injection, dual-fuel gas engine. A schematic diagram of the experimental setup is shown in Figure 4.2. The engine had a bore and stroke of 96 and 108 mm, respectively, a displacement volume of 781 cm^3, and a compression ratio of 17:1. A diesel fuel injector with a three-hole nozzle (ϕ 0.1 mm) operating on a common rail system was used to spray the pilot fuel, which was pressurized employing a high-pressure oil pump. We sought to inject as little diesel fuel as possible. The crank angle (CA) signal was formed by the saw blades and a photodiode; the resolution was 0.5° when identifying the piston location. Simulated biogas served as the primary fuel and diesel as the pilot fuel. The biogas consisted of CH_4, CO_2, and N_2 at 58, 35, and 7% by volume, respectively. The gaseous fuel was introduced through an intake port; the gas flow rates were controlled using mass flow controllers. In-cylinder pressure was measured by a Kistler 6052C pressure transducer. A Kistler 5011 charge amplifier was used to amplify the in-cylinder pressure signal. All tests were conducted at an engine speed of 1,000 rpm, and at three intake pressures (101, 150, or 200 kPa, established using a compressor). The pilot fuel was delivered at an injection pressure of 40 MPa at 0.8 mg/cycle. The overall equivalence ratio was set to 0.6 to achieve lean-burn combustion. Pilot fuel injection timing varied during the experiments. The engine details and experimental conditions are listed in Table 4.1. As noted above, the first indicator of knocking is pressure oscillation. The pressure history and ROHR were averaged over 80 cycles for each dataset. To explore pressure oscillation, a band-pass filter (4–20 kHz) was applied to all pressure history data. The maximum instantaneous pressure difference between consecutive signals passing

through the digital band-pass filter was defined as the KI. Any KI above a certain threshold (0.1 MPa) was defined as knocking.

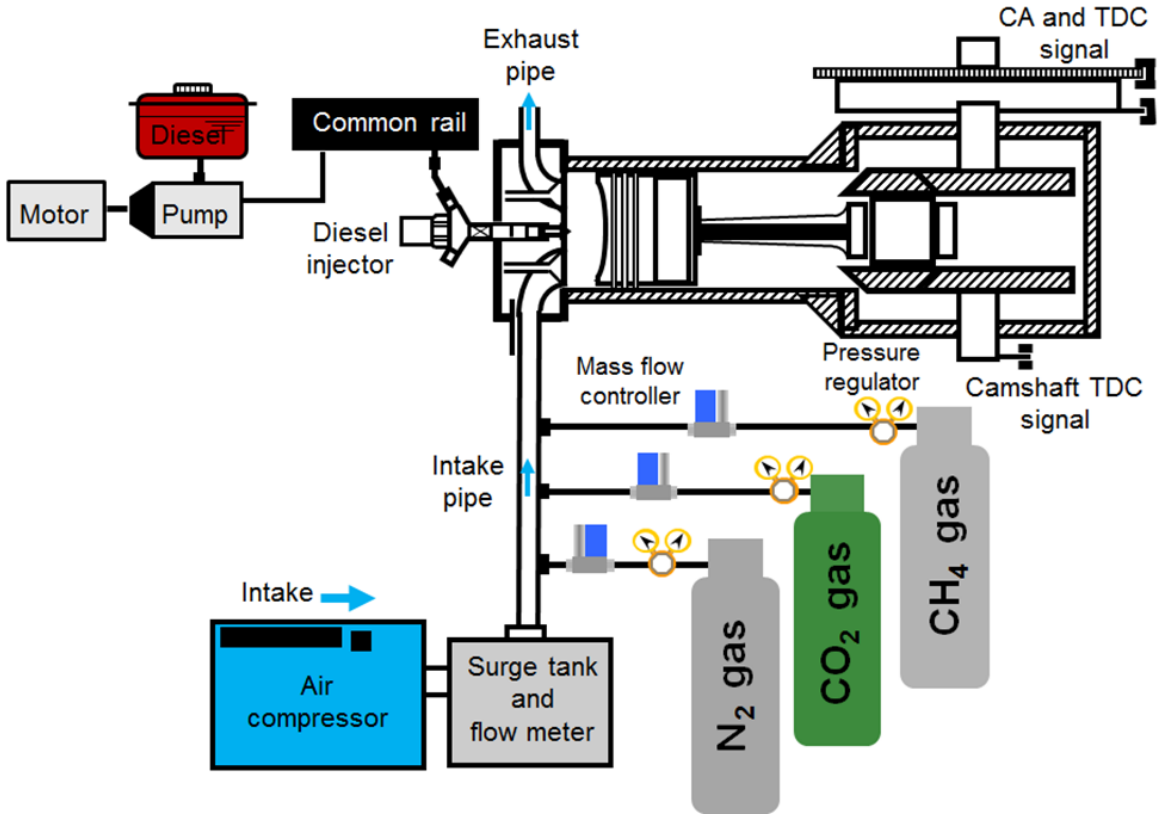

Figure 4.2: Schematic diagram of the experimental setup

Table 4.1 Test engine specification and experimental conditions

Engine type	Four stroke, single cylinder
Bore × stroke	96 mm ×108 mm
Displacement volume	781 cm^3
Equivalence ratio, ϕ_t	0.6
Compression ratio	17:1
Combustion system	Pilot ignited dual fuel combustion
Intake pressure, P_{in}	101, 150, 200 kPa
Intake charge temperature	40°C
Injection system	Common rail
Injection pressure	40 MPa
Injection quantity	0.8 mg/cycle
Nozzle hole×diameter	3 hole × ϕ 0.1mm
Engine speed	1000 rpm
Injection timing of pilot fuel	15, 17, 20°BTDC at P_{in}=101 kPa 10, 12, 14°BTDC at P_{in}=150 kPa 8, 9, 10°BTDC at P_{in}=200 kPa

If even 1 of the 80 cycles exhibited a KI > 0.1 MPa, we considered that knocking was present. In terms of PREMIER operation, we required that > 50% of cycles should exhibit end-gas autoignition without knocking (i.e., KI ≤ 0.1 MPa) [51]. Any cycle exhibiting < 50% end-gas autoignition was considered to correspond to normal combustion. Herein, we analyze the characteristics of PREMIER combustion in detail to confirm the presence of end-gas autoignition and a peak of heat release. The first ROHR peak corresponds to pilot fuel autoignition, the second to gaseous fuel-air combustion, and the third, which normally occurs after TDC, to end-gas autoignition. Figure 4.3 quantitatively explains PREMIER combustion and related parameters. All parameters relevant to end-gas autoignition were obtained from the heat release rates. During PREMIER combustion, we determined θ_{ea} values from the times of inflection shown in the ROHR curves; this is also how we identified the timing of first ignition (θ_{ign}). The time interval between θ_{ign} and θ_{ea} is τ_{ea}. $\Delta\theta_{ea}$ begins at θ_{ea} and continues until end-gas heat release is complete. We also determined the amount of heat released during end-gas autoignition (Q_{ea}). The PI value was determined using these parameters.

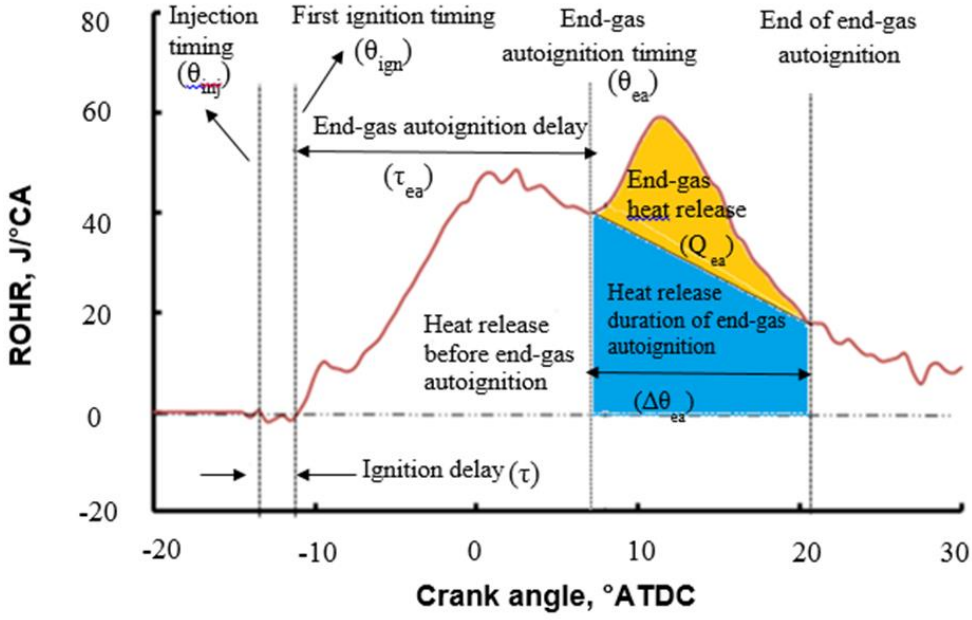

Figure 4.3: Graphical representation of parameters describing PREMIER combustion

4.4. Results and Discussion

4.4.1 Cylinder pressure, rate of heat release, ignition delay, and maximum cylinder pressure

Figure 4.4 shows the pressure history and ROHR at the three intake pressures of 101, 150, and 200 kPa. Both the maximum pressure and maximum ROHR increased when the pilot fuel injection timing, θ_{inj}, was advanced. Ignition delay (τ) is the time difference between commencement of injection and initiation of pilot fuel combustion and it is shown in Figure 4.5. Higher intake pressures showed a shorter delay, attributable to the higher molar fraction of oxygen associated with the higher pressure. In Figure 4.4(a), the first ROHR peak is that caused by pilot fuel autoignition can be observed clearly and it is 18.5 J/deg, however, when intake pressure is increased up to 150kPa, the ROHR peak became smaller as shown in Figure 4.4(b) and it is 16 J/deg. As shown in Figure 4.4(c), at P_{in}=200kPa, the ROHR peak caused by pilot fuel autoignition was almost disappeared because the ignition delay is reduced by higher intake pressure. However, the ROHR peak of 11 J/deg was obtained from small inflation point of ROHR data for P_{in}=200kPa.In the dual-fuel combustion mode, ignition commences after pilot fuel injection near the end of the compression stroke, and the flame propagates through the gaseous fuel-air mixture. Advancing the injection timing increases the in-cylinder pressure because the combustion phase is also advanced. This allows autoignition of regions of unburned mixture before they can be consumed by propagating flames. The end-gas autoignition phenomenon can also be observed in the ROHR traces. Figures 4.4(b) and (c) show that ROHR peaks were evident after TDC, attributable to autoignition of end-gas unburned mixture that had attained the required conditions after the injection timing was advanced. This was defined as PREMIER combustion. Under the conditions of Figures 4.4(b) and (c), knocking occurred when the injection timing was further advanced, although the data are not shown. Similar findings were noted in previous work using different gaseous fuels

(natural gas and hydrogen) [59]. Azimov et al. [59] reported that end-gas autoignition was affected by syngas composition. The cited authors used seven different gaseous fuels, all of which exhibited PREMIER combustion. The numbers of cycles exhibiting end-gas autoignition and KI are shown in Figures 4.6 and 4.7 respectively. Figure 4.6 shows that 77 cycles attained end-gas autoignition at θ_{inj} = 10° BTDC and P_{in} = 200 kPa, and that 60 cycles attained autoignition when θ_{inj} was 14° BTDC and P_{in} = 150 kPa. Both a higher intake pressure and advanced injection timing promoted PREMIER combustion. Figure 4.7 shows that all cycles exhibiting end-gas autoignition were associated with KI values < 0.1 MPa. Given our definitions of PREMIER and knocking operations, these were considered to be knock-free cycles. Only the combinations of θ_{inj} = 10 and 14° BTDC, for P_{in} = 200 and 150 kPa, respectively, allowed PREMIER combustion; all other combinations were associated with normal combustion. At P_{in} = 101 kPa (only), injection timing advancement did not trigger end-gas autoignition. The maximum in-cylinder pressures are shown in Figure 8 for all three intake pressures as injection timing changed. The maximum in-cylinder pressure was observed at θ_{inj} = 10° BTDC for P_{in} = 200 kPa, θ_{inj} = 14° BTDC for P_{in} = 150 kPa, and θ_{inj} = 20° BTDC for P_{in} = 101 kPa. A θ_{inj} = 10° BTDC for P_{in} = 200 kPa and a θ_{inj} = 14° BTDC for P_{in} = 150 kPa were defined as PREMIER conditions and are shown by open symbols. The higher maximum pressure of PREMIER combustion is attributable to end-gas autoignition of unburned mixture at a higher pressure and temperature.

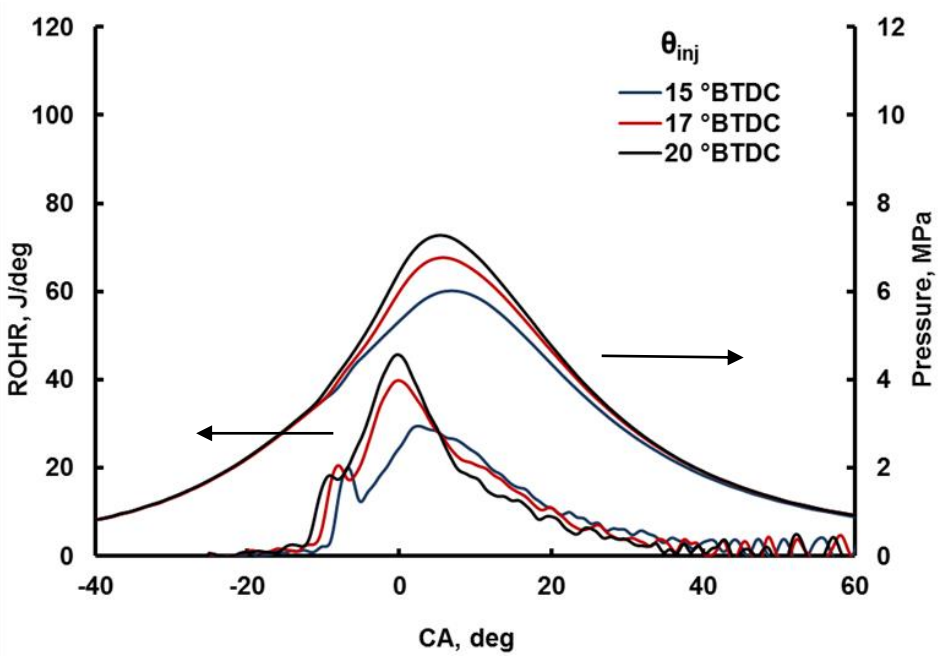

(a) P_{in} = 101 kPa

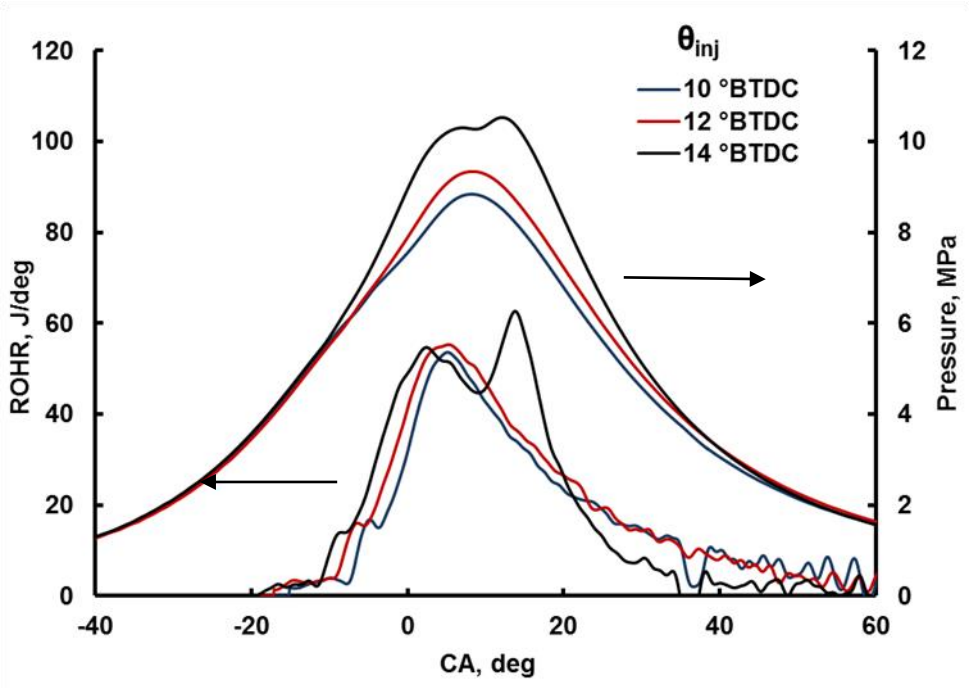

(b) P_{in} = 150 kPa

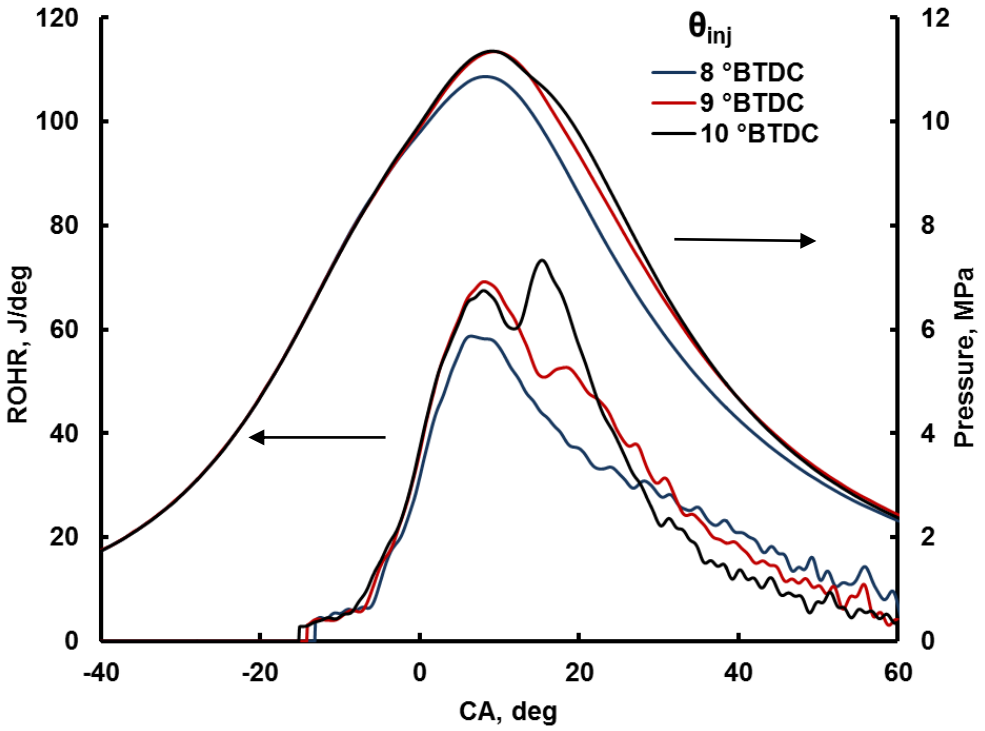

(c) P_{in} = 200 kPa

Figure 4.4: Pressure history and rate of heat release for P_{in} = 101, 150, and 200 kPa

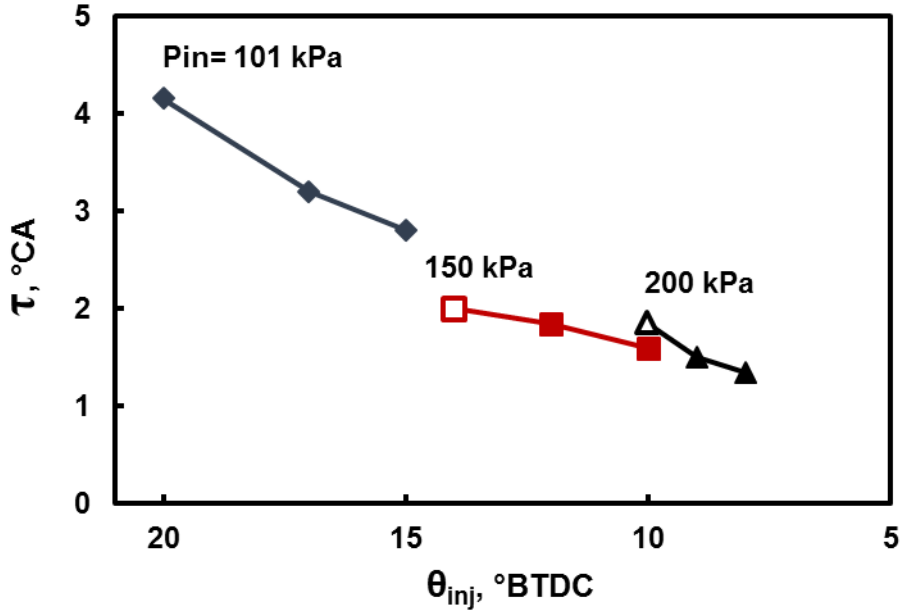

Figure 4.5: Ignition delays of initial combustion

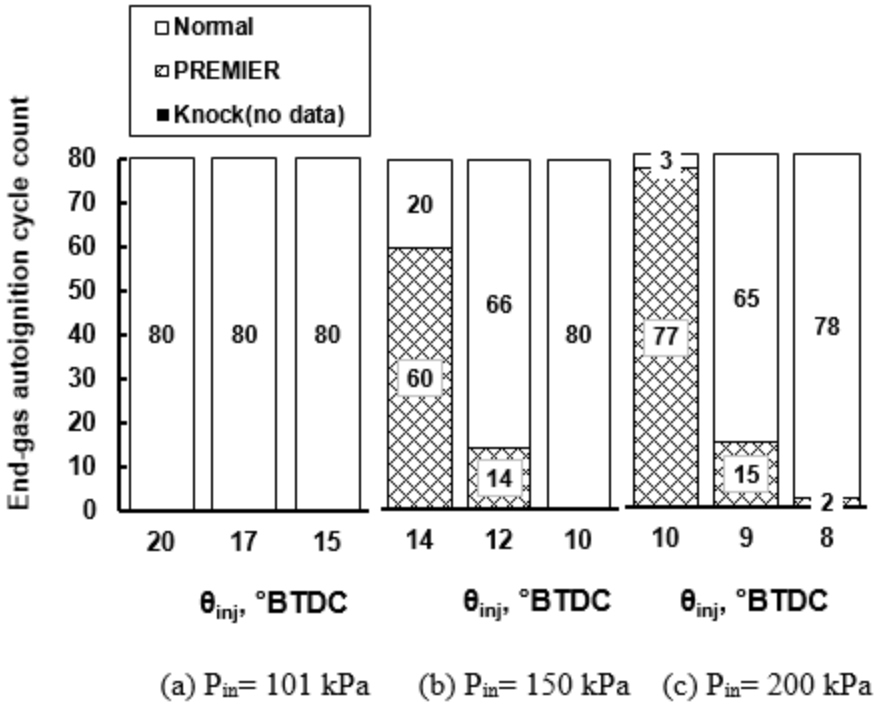

Figure 4.6: Number of cycles featuring end-gas autoignition at all intake pressures

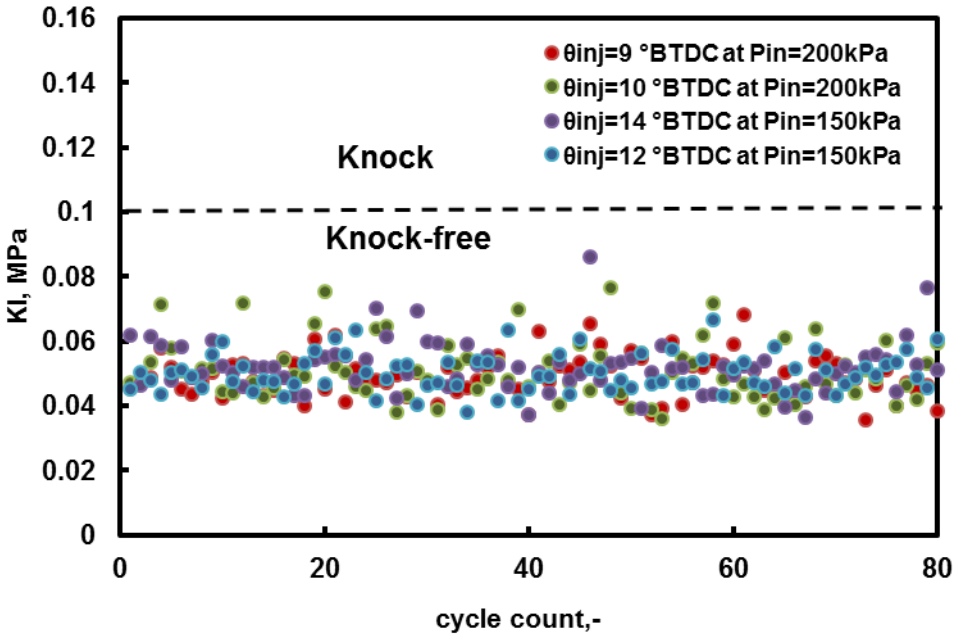

Figure 4.7: Knocking intensity at P_{in} =150 kPa and 200 kPa

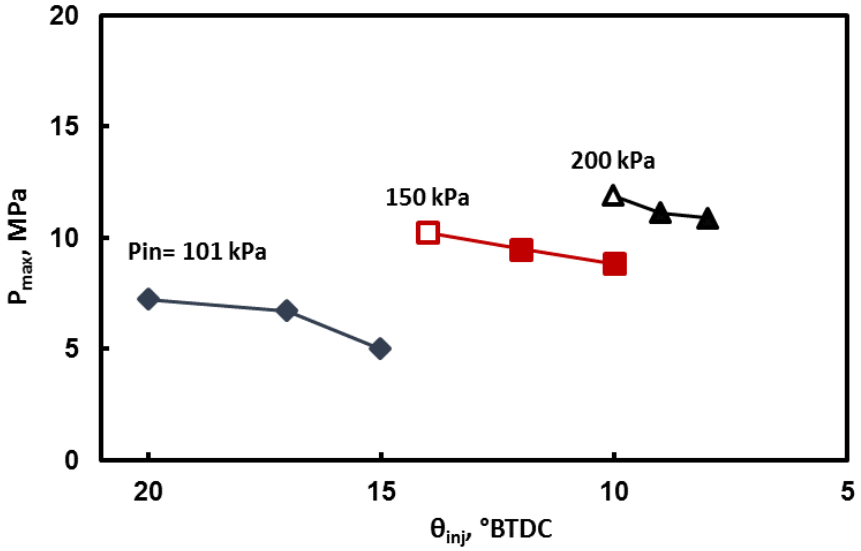

Figure 4.8: Maximum cylinder pressure versus injection timing

4.4.2 Engine performance

Figures 4.9(a), (b), and (c) show the IMEP, thermal efficiency, and coefficient of variation of the indicated mean effective pressure [$COV_{(IMEP)}$], respectively, as the pilot fuel injection timing changed. The performance data were determined from the pressure history. Figure 4.9(a) shows that the highest IMEP values were observed during the PREMIER operation mode at θ_{inj} = 10° BTDC for P_{in} = 200 kPa and θ_{inj} = 14° BTDC for P_{in} = 150 kPa. The IMEP values increased as the injection timing advanced. The highest indicated thermal efficiency was observed at θ_{inj} = 10° BTDC for P_{in} = 200 kPa and θ_{inj} = 14° BTDC for P_{in} = 150 kPa; both occurred when PREMIER combustion was in play. When the injection timing was advanced and PREMIER combustion achieved, the in-cylinder pressure increased because of the higher ROHR caused by end-gas autoignition of the unburned mixture. PREMIER combustion typically takes place during the expansion stroke; therefore, any pressure increase is followed by positive (volumetric) work and, consequently, enhanced IMEP and thermal efficiency. We earlier reported such

improvements afforded by end-gas autoignition (in the PREMIER combustion mode) using different gaseous fuels [55, 59–62]. Roy et al. [58] observed two-stage combustion as injection timing advanced; this afforded the highest IMEP and the best thermal efficiency. The stability of engine operation is indicated by the $COV_{(IMEP)}$; typically, better stability is associated with less output variation. The minimum $COV_{(IMEP)}$ was observed in the PREMIER operation mode. A lower $COV_{(IMEP)}$ reflects smoother engine operation. Roy et al. [58], Azimov et al. [59], and Aksu et al, [62] also reported stable combustion (< 4% variation) during PREMIER combustion of hydrogen and hydrogen-containing gaseous fuels, syngas, and natural gas in the dual-fuel mode. These facts are one of the features of PREMIER combustion. In consequence, improvement of engine performance under PREMIER combustion obtained from our previous experiments and this study shows the effectiveness of PREMIER combustion in dual-fuel combustion engines.

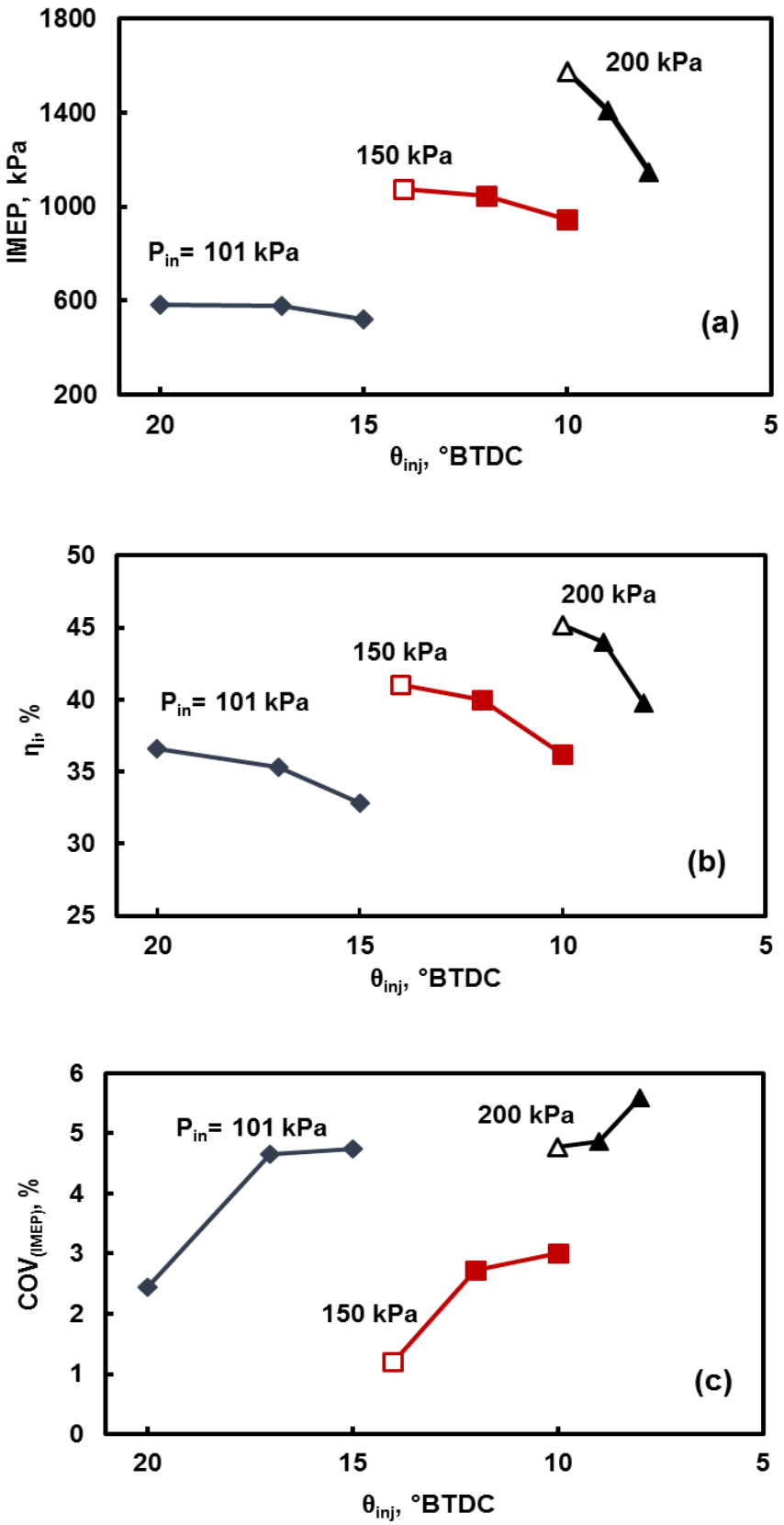

Figure 4.9: Engine performance: (a) indicated mean effective pressure (IMEP); (b) indicated thermal efficiency; (c) coefficient of variation of the IMEP for P_{in} = 101, 150 and 200 kPa.

4.4.3 Exhaust emissions

Exhaust emissions of NO_x, HC and CO are shown in Figure 4.10 (a), (b) and (c), respectively. NO_x is typically produced in high level when the in-cylinder temperature rises above 1600°C; therefore, production of NO_x emissions is more dependent on the combustion characteristics than the fuel type. As shown in Figure 4.10 (a), NO_x emissions were increased with advancing injection timing at all intake pressure conditions. However, NO_x emissions presented lower at P_{in} = 101 kPa compared to those in P_{in} = 150 kPa and 200 kPa. It is due to lower in-cylinder temperature of P_{in} = 101 kPa compared to other cases. Maximum NO_x emission were observed under PREMIER operation for θ_{inj} = 14° BTDC at P_{in} = 150 kPa and θ_{inj} = 10° BTDC at P_{in} = 200 kPa. It is due to higher cylinder temperature as a result of end-gas autoignition during PREMIER combustion.

Unburned hydrocarbons (HC) and carbon monoxide (CO) are produced as a result of incomplete combustion. Figure 4.10 (b) and (c) show that both CO and HC emission were decreased when injection timing advanced and intake pressure increased. Unlike NO_x emissions, higher combustion temperature causes lower CO and HC emissions due to complete combustion. When injection timing is advanced, combustion starts at earlier stage and there is a sufficient time for complete combustion. However, minimum CO and HC emissions were observed under PREMIER operation. In PREMIER combustion, unburned gas (mixture) undergoes another autoignition after main combustion and thus, remaining mixture is burned and this helps to reduce CO and HC emissions.

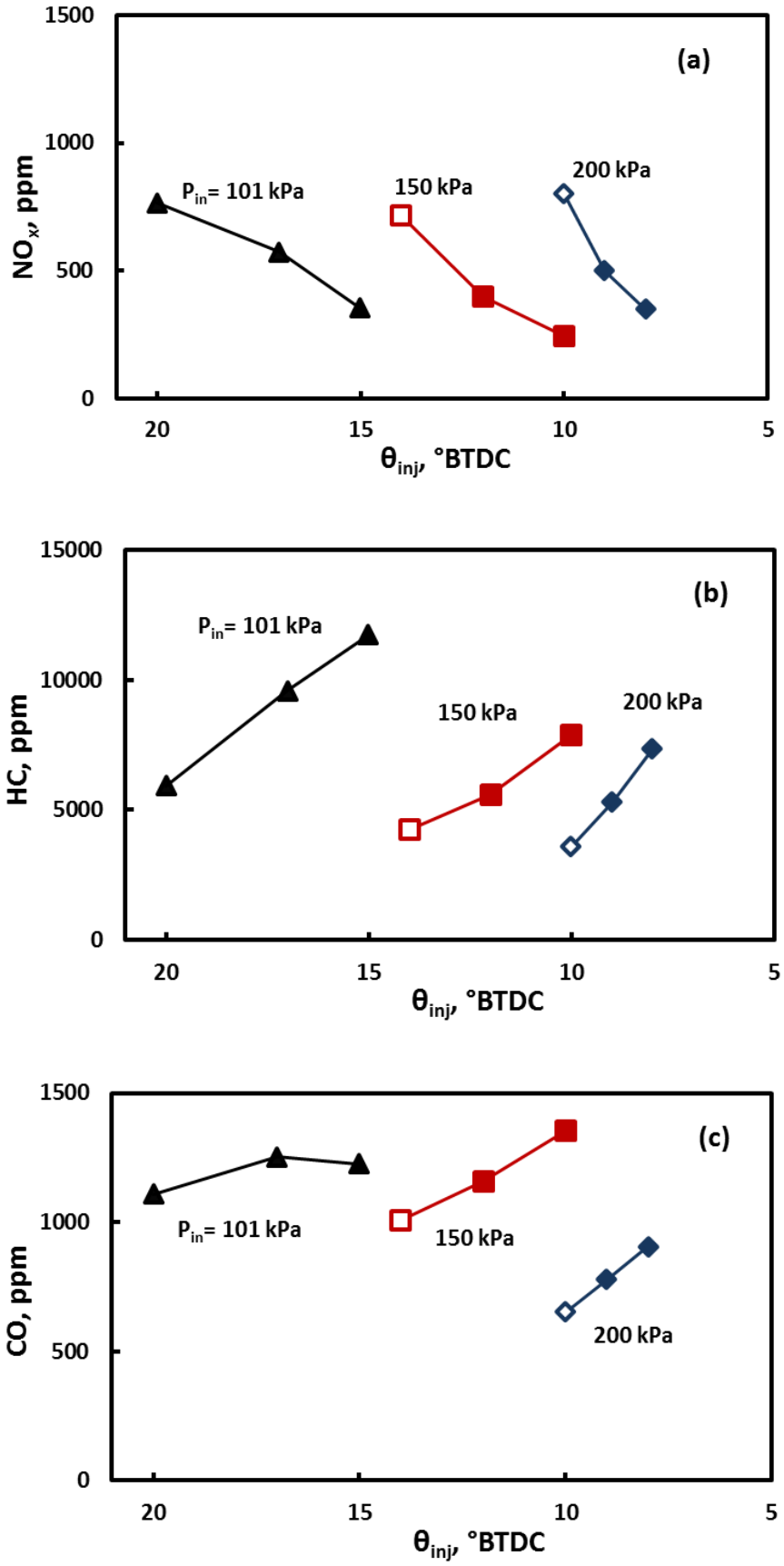

Figure 4.10: Exhaust emissions of (a) NO_x (b) unburned hydrocarbon (c) carbon monoxide

4.4.4 End-gas autoignition characteristics

4.4.4.1 End-gas autoignition timing and delay

The average θ_{ea} values of cycles exhibiting end-gas autoignition are shown in Figures 4.11 with the standard errors. The θ_{ea} for PREMIER combustion was 8.24° after TDC (ATDC) for θ_{inj} = 14° BTDC at P_{in} = 150 kPa; and 11.21°ATDC for θ_{inj} = 10° BTDC at P_{in} = 200 kPa. Also, end-gas autoignition was observed when θ_{inj} = 9° BTDC and P_{in} = 200 kPa, and when θ_{inj} = 12° BTDC and P_{in} = 150 kPa, at 14.21° and 12.45° ATDC respectively. θ_{ea} was earlier when injection timing was advanced. The commencement of end-gas autoignition relies on the ROHR of the initial and principal combustion. Advancing injection timing results in higher combustion activity owing to the higher pressure and temperature of the unburned mixture during flame propagation; consequently, end-gas autoignition commences earlier. Figures 4.12(a) and (b) illustrate unburned gas temperature from injection timing to end-gas autoignition timing at P_{in}=150kPa and P_{in}=200kPa, respectively. The process from intake valve close (IVC) time to injection timing was determined from polytropic change (equation 4.1) and the process from injection timing to end-gas autoignition was determined from adiabatic change (equation 4.2).

$$\frac{T_{inj}}{T_{IVC}} = \left(\frac{P_{inj}}{P_{IVC}}\right)^{\frac{n-1}{n}} \qquad n = polytropic\ index \qquad (4.1)$$

$$\frac{T_u}{T_{inj}} = \left(\frac{P}{P_{inj}}\right)^{\frac{k-1}{k}} \qquad k = ratio\ of\ specif\ heats \qquad (4.2)$$

Where T is the gas temperature, V is the volume of cylinder and P is the in-cylinder pressure. The subscripts u denotes unburned gas. The initial pressure at IVC time is known from in-cylinder pressure data and initial temperature was determined from equation of state and it is expressed in equation 4.3:

$$T_{IVC} = \frac{P_{IVC}\, V_{IVC}}{mR} \qquad R = \frac{R_o}{M} \quad (4.3)$$

Where R, R_o, M and m denote gas constant, universal gas constant, molecular weight and mass.

As shown in Figure 4.12(a), after injection timing, unburned gas temperature of θ_{inj}=14° BTDC is slightly higher than that in θ_{inj}=12° BTDC. Similarly, in Figure 4.12(b), unburned gas temperature of θ_{inj}=10° BTDC is slightly higher than that in θ_{inj}=9° BTDC. A noticeable differences of unburned gas temperature between θ_{inj}=14° BTDC and θ_{inj}=12° BTDC at P_{in}=150kPa compared to θ_{inj}=10° BTDC and θ_{inj}=9° BTDC at P_{in}=200kPa is because of differences between their in-cylinder pressure as shown in Figures 4.4 (b) and (c). In consequence, higher temperature of the unburned mixture during flame propagation, causes earlier end-gas autoignition commencement.

The average τ_{ea} values of cycles exhibiting end-gas autoignition are shown in Figures 4.13 with the standard errors. The lowest τ_{ea} of 19.4° CA was observed for θ_{inj} = 10° BTDC at P_{in} = 200 kPa. As shown in Figure 4.14, the lower τ_{ea} at P_{in} = 200 kPa compared to that at P_{in} = 150 kPa was attributable to the mass fraction burned (MFB) before end-gas autoignition commenced at θ_{ea}. When the intake pressure is higher, the unburned mixture is ignited more easily because of the shorter ignition delay. At P_{in} = 200 kPa, the MFB before autoignition in the end-gas region was smaller than that for P_{in} = 150 kPa. Less mixture was consumed during principal combustion (thus, during flame propagation). Autoignition develops in the end-gas region when the unburned mixture attains the required conditions. There are two possible outcomes after autoignition: flame development in the autoignition region or autoignition development. However, there is as yet no evidence that the phenomenon develops after end-gas autoignition commences.

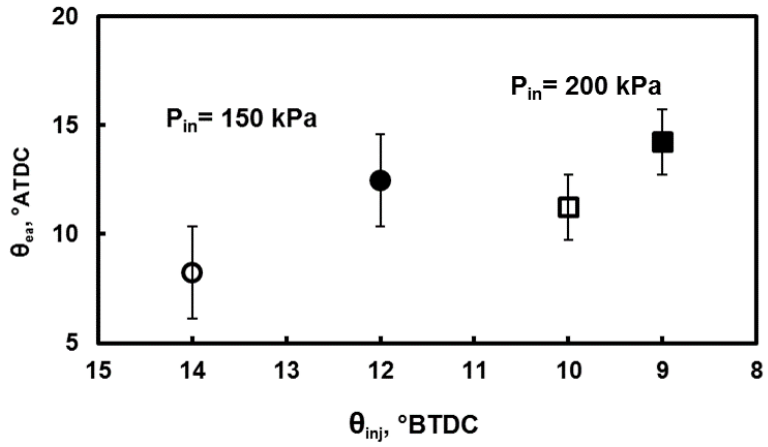

Figure 4.11: Average end-gas autoignition timing, with standard error

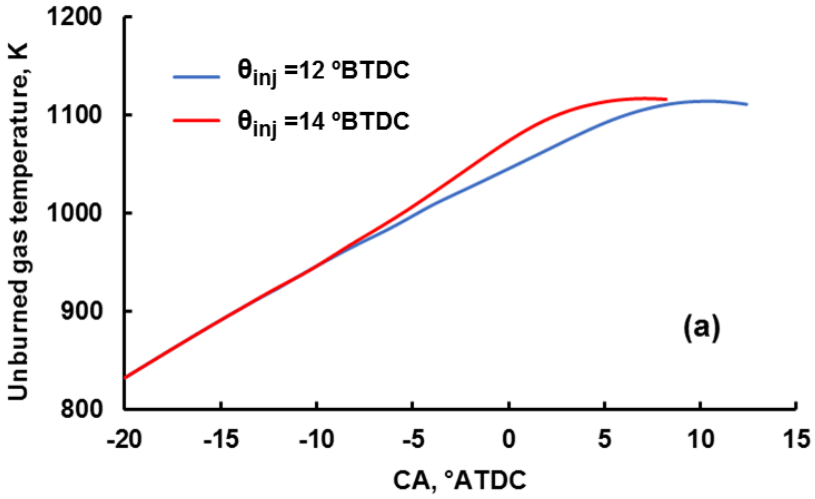

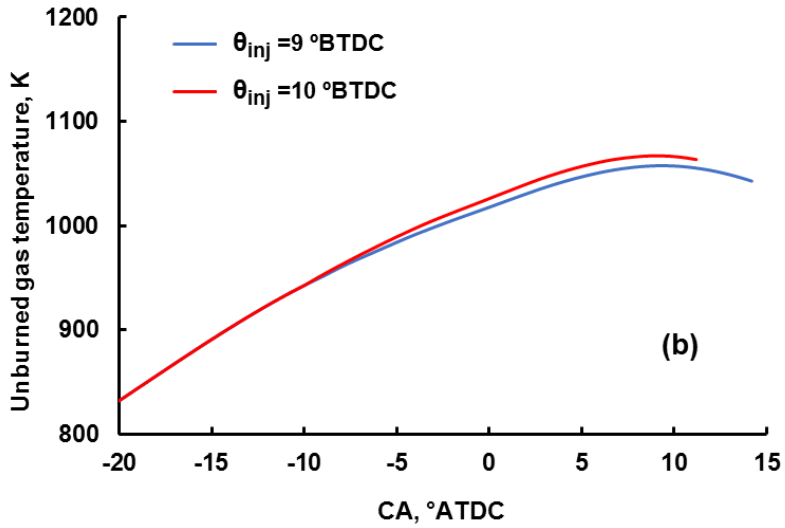

Figure 4.12: Unburned gas temperature from θ_{inj} to θ_{ea} at (a) P_{in}=150kPa and (b) P_{in}=200kPa

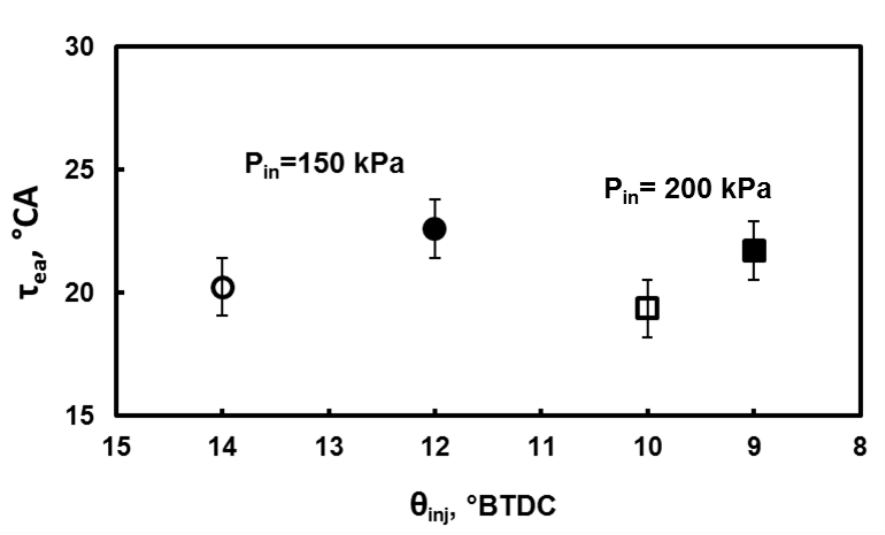

Figure 4.13: Average end-gas autoignition delay, with standard error

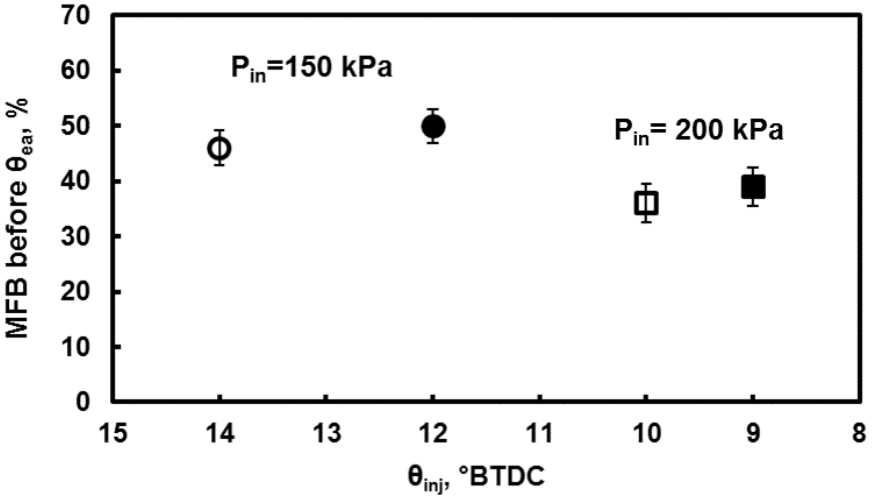

Figure 4.14: Average mass fraction burned before commencement of end-gas autoignition for P_{in} = 150 kPa and 200 kPa, with standard error.

4.4.4.2 The duration of heat release during end-gas autoignition

$\Delta\theta_{ea}$ is the time between the beginning and end of end-gas autoignition. The $\Delta\theta_{ea}$ values for cycles exhibiting end-gas autoignition are shown in Figure 4.15. When the pressure and temperature of the unburned mixture region increase as a result of advancing the injection timing, the end-gas autoignition delay is reduced; however, this does not greatly affect the duration of heat release after end-gas autoignition. The effect of injection timing

advancement was slightly greater at higher intake pressures. As shown in Figure 4.14, a smaller proportion of the gaseous mixture was consumed by the propagating flame at P_{in} = 200 kPa than at P_{in} = 150 kPa. A larger mass in the end-gas region can also prolong the $\Delta\theta_{ea}$ if the temperature and pressure in that region at end-gas autoignition timing, θ_{ea}, do not rise significantly. This means that more unburned mixture remains for later autoignition when the autoignition conditions are ultimately attained. A larger mass in the end-gas region increases the KI during knocking cycles but the KI was almost unchanged during PREMIER cycles [63]. However, even when the end- gas mass was large, the KI of the PREMIER combustion can be lower than the threshold, thus preventing knocking when the duration of end-gas autoignition is prolonged. Also, there is a possibility of shorter duration of end-gas autoignition when strong knocking is occurred. In this case, duration of end-gas autoignition is shorter, however, high amount of heat is released from end-gas region followed by extremely high in-cylinder pressure. The peak after TDC (as a result of end-gasautoignition) in pressure history and ROHR is very steep compared to that in PREMIER combustion. In case of weak PREMIER combustion, neither sudden pressure rise nor high amount of heat release would not be occurred. If the end-gas autoignition conditions are satisfied later, $\Delta\theta_{ea}$ would be shorter because lower amount of heat released due to end-gas autoignition. When knocking occurs, PI value is expected to become large. In the present stage, discussion may be done qualitatively due to no knocking data.

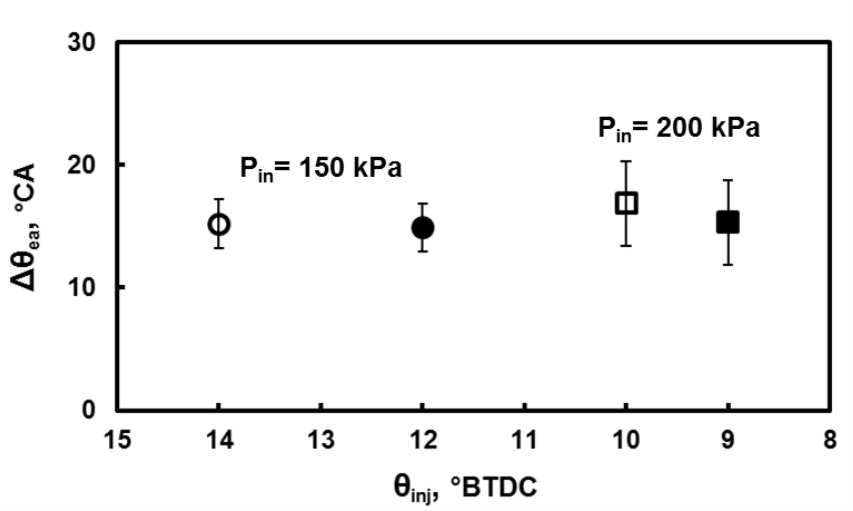

Figure 4.15: Average heat release duration of end-gas autoignition for P_{in} = 150 kPa and 200 kPa, with standard error.

4.4.4.3 Heat release after end-gas autoignition and PREMIER intensity

Quantification of PREMIER combustion was described above. A new parameter is needed to distinguish weak from strong end-gas autoignition. Therefore, we propose the PI, based on the end-gas autoignition data obtained from the heat release characteristics. The PI is defined as:

$$PI = \frac{100 * (Q_{ea}/Q_{total})}{\Delta\theta_{egai}} \quad (4.4)$$

where Q_{ea}, Q_{total}, and $\Delta\theta_{ea}$ are the amount of heat released during end-gas autoignition, the total energy inputs of all fuels based on their lowest heating values, and the duration of heat release following end-gas autoignition, respectively. We exploit the relationship between the proportion of heat released during end-gas autoignition and the duration of such release because this indicates the amount of heat released per unit time during such combustion. The yellow colored area in Figure 4.3 (delimited by the straight dashed line) is defined as the region of end-gas autoignition heat release, obtained by examining the rates of heat release at the start and end of this time. The heat released via flame

propagation is defined as the region below the straight line (blue colored area). The average Q_{ea} values of cycles exhibiting end-gas autoignition are shown in Figure 4.16. As expected, the amount of heat released without knocking was maximal for θ_{inj} = 10° BTDC at P_{in} = 200 kPa. The number of cycles featuring end-gas autoignition was highest under these conditions; more heat from the end-gas region was thus released. Consistent with Figure 4.15, the longest $\Delta\theta_{ea}$ was observed at the same injection timing. The amount of heat released increased from 180 to 432 kJ when the injection timing was advanced from 9 to 10° BTDC at P_{in} = 200 kPa. For P_{in} = 150 kPa, the amount of heat released increased from 150 to 275 kJ when the injection timing was advanced from 12 to 14° BTDC. The number of cycles featuring end-gas autoignition increased from 15 to 77 at P_{in} = 200 kPa, and from 14 to 60 at P_{in} = 150 kPa, as shown in Figures 4.6(b) and (c). The amount of heat released increased significantly as the number of end-gas autoignition cycles rose because of injection timing advancement. As shown in Figure 4.17, experiments exhibiting higher numbers of end-gas autoignition cycles had higher PI values. The largest PI value was observed for θ_{inj} = 10° BTDC at P_{in} = 200 kPa, followed by θ_{inj} = 14° BTDC at P_{in} = 150 kPa. The relationship between PI and the ratio of Q_{ea} to the total heat release, Q_{total}, and the relationship between PI and the heat release duration of end-gas autoignition (with standard errors), are shown in Figure 4.18. Below, we clarify the relationships between these parameters. We found a strong association between the PI value and Q_{ea}/Q_{total}. The PI value increased in a near-linear manner with increasing Q_{ea}/Q_{total}. Cycles featuring more instances of end-gas autoignition exhibited higher Q_{ea}/Q_{total} values. Both Q_{ea}/Q_{total} and the PI value increased as injection timing was advanced: at θ_{inj} = 10° BTDC and P_{in} = 200 kPa, 77 cycles exhibited end-gas autoignition, compared to 60 cycles at θ_{inj} = 14° BTDC and P_{in} = 150 kPa [Figures 6(b) and (c), respectively]. In Figure 4.18, the Q_{ea}/Q_{total} at θ_{inj} = 10° BTDC and P_{in} = 200 kPa lies slightly

above the linear trend line. The Q_{ea}/Q_{total} ratio rose during many cycles. Also, $\Delta\theta_{ea}$ increased at θ_{inj} = 10° BTDC and P_{in} = 200 kPa. According to equation (4.4), when $\Delta\theta_{ea}$ increases, the Q_{ea}/Q_{total} should rise to maintain the same PI value, but the PI value at θ_{inj} = 10° BTDC and P_{in} = 200 kPa in fact increased. This is because much more heat was released in the end-gas region. As shown in Figure 4.14, more unburned mixture remained in the end-gas region at θ_{inj} = 10° BTDC and P_{in} = 200 kPa.

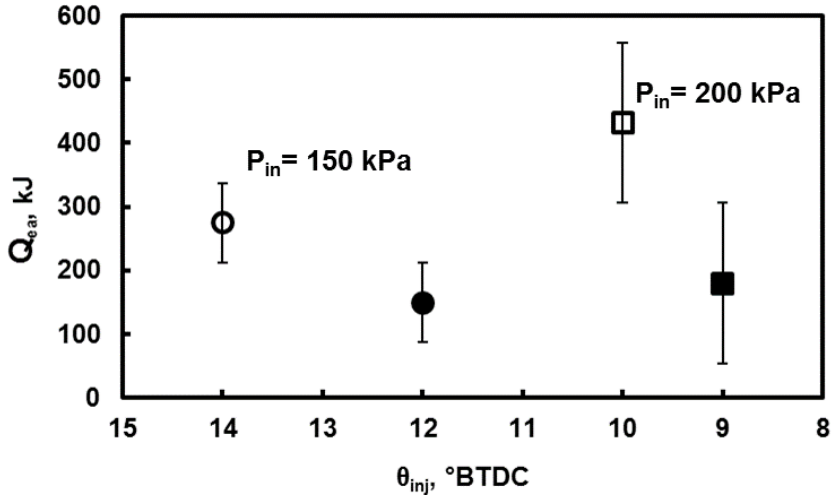

Figure 4.16: Average heat release due to end-gas autoignition for P_{in} = 150 kPa and 200 kPa, with standard error

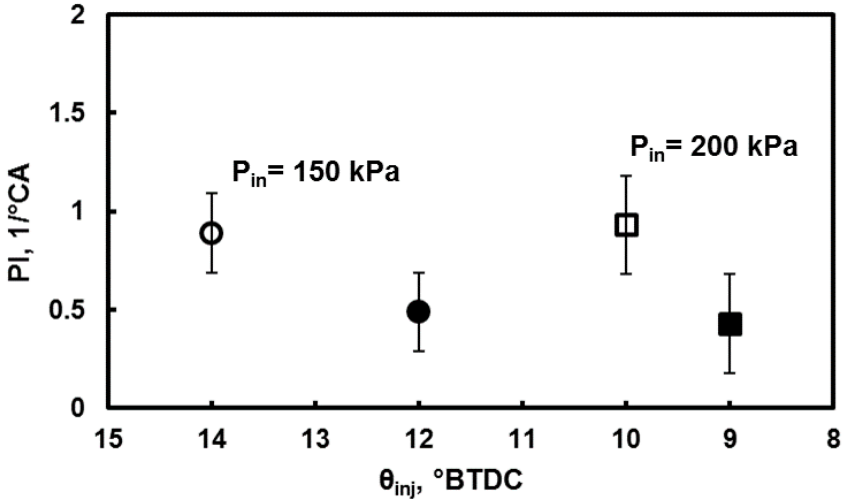

Figure 4.17: Average PREMIER intensity for P_{in} = 150 kPa and 200 kPa, with standard error

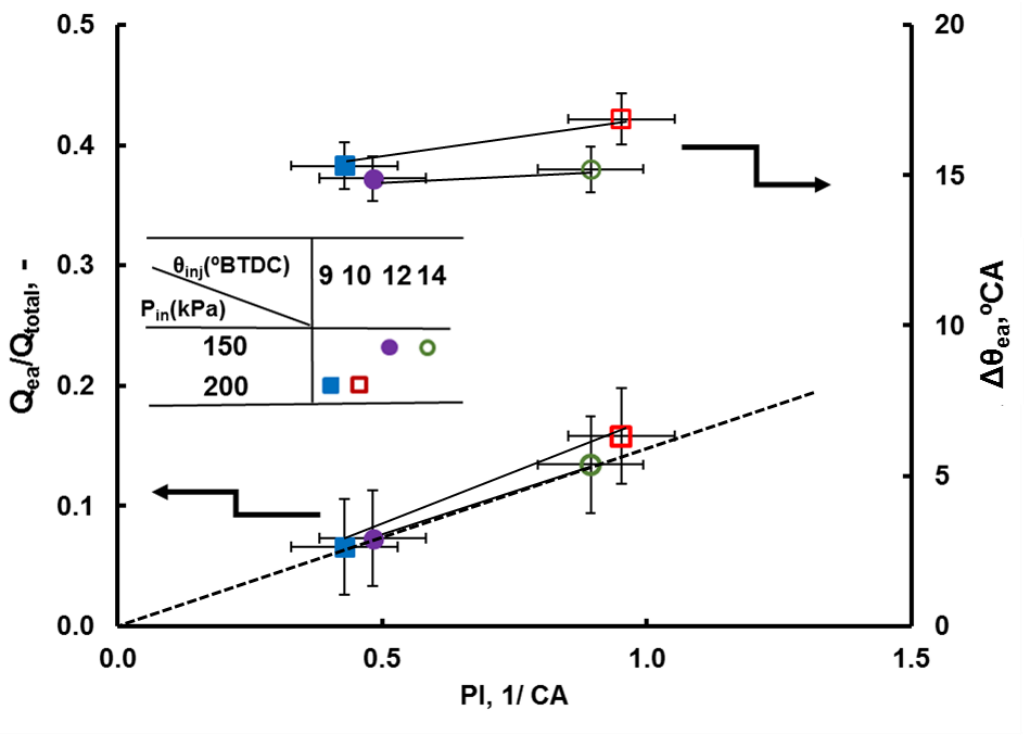

Figure 4.18: The ratio of heat released due to end-gas autoignition to total heat release and PREMIER intensity (PI), and the heat release duration of end-gas autoignition by PI, with standard error

4.5. Summary of observation

In this study, simulated biogas containing CH_4, CO_2, and N_2 was used as the primary fuel for a dual-fuel gas engine ignited using a pilot fuel (diesel). Experiments were performed at three intake pressures (101, 150, and 200 kPa), with the engine operating at a constant speed of 1,000 rpm and with various pilot fuel injection times. Engine performance and the detailed end-gas autoignition characteristics were evaluated as the average of 80 cycles. We measured end-gas autoignition timing and delay, heat release duration, heat release amount, mass fraction burned before commencement of end-gas autoignition; and PI. We also quantified PREMIER combustion based on the end-gas heat release characteristics, as revealed by cycle-to-cycle analysis of each dataset. Furthermore, we defined a new parameter, PI. The following results were obtained:

1. The parameter PI was proposed and used to evaluate the characteristics of PREMIER combustion. The PI value increased as the heat released by end-gas autoignition increased, and as the duration of heat release was extended. However, the Q_{ea}/Q_{total} ratio affected the PI more so than did the $\Delta\theta_{ea}$.

2. When PREMIER combustion was achieved, the heat released by end-gas autoignition and the PI increased as the injection timing was advanced. Under such circumstances, the number of cycles featuring end-gas autoignition increased and more heat was released in the end-gas region.

3. The ROHR values of both the initial and main combustion affected the occurrence of end-gas autoignition. When the pressure and temperature of a premixed fuel mixture rose as injection timing was advanced, end-gas autoignition commenced earlier. The end-gas autoignition delay became shorter as intake pressure was increased and injection timing advanced, because of the lower MFB before end-gas autoignition commenced. Under these conditions, less mixture was consumed during principal combustion, and more was burned in the end-gas region.

4. Advancing the injection timing and increasing the intake pressure improved both the IMEP and thermal efficiency because end-gas autoignition then occurred. The higher the number of cycles featuring end-gas autoignition, the greater the thermal efficiency, because of the larger amount of positive work performed during the expansion stroke.

5. In PREMIER combustion, exhaust emissions of CO and HC were decreased while NO_x emissions were increased.

References

[1] S. S. Nathan, J. M. Mallikarjuna and A. Ramesh, An experimental study of the biogas–diesel HCCI mode of engine operation, Energy Conversion and Management; 51 (2010); 1347–1353.

[2] A. Henham and M. K. Makkar. Combustion of simulated biogas in a dual-fuel diesel engine. Energy Conversion and Management; 39 (1998); 2001–2009.

[3] H. H. Jawurek, N. W. Lane and C. J. Rallis, Biogas/petrol dual fuelling of SI engine for rural third world use, Biomass 13 (1987); 87–103.

[4] P. Tewari, J. Subrahmanyam, M. Babu. Experimental investigations on the performance characteristics of a producer gas fuelled spark ignition engine. SAE Technical Paper 2001-01-1189, (2001).

[5] E. Porpatham, A. Ramesh, and A. Nagalingam. Investigation on the effect of concentration of methane in biogas when used as a fuel for a spark ignition engine. Fuel 87(8–9) (2007);1651–1659.

[6] G. A. Karim. A review of combustion processes in the dual-fuel engine – the gas diesel engine. Progress in Energy and Combustion Science, 6 (1980); 277–285.

[7] G. A. Karim. The dual-fuel engine of the compression ignition type - prospects, problems and solutions - a review. SAE Technical Paper 831073, 1983, https://doi.org/10.4271/831073.

[8] J. L. Walsh, C. C. Ross, M. S. Smith and S. R. Harper, Utilization of biogas, Biomass, 20 (1989); 277–290.

[9] E. Tomita, N. Kawahara, M. Kondo and Y. Sunada, Combustion and exhaust emissions characteristics of pilot-ignited engine fueled with digester gas; CIMAC congress, (2013), Shanghai, Paper No. 145.

[10] D. Barik, S. Murugan, Investigation on combustion performance and emission characteristics of a DI (direct injection) diesel engine fueled with biogas- diesel in dual fuel mode, Energy, 72 (2014); 760–771.

[11] M. Feroskhan and S. Ismail, Investigation of the effects of biogas composition on the performance of a biogas–diesel dual fuel CI engine, Biofuels, 7 (2016); 593–601.

[12] B. J. Bora and U. K. Saha. Optimization of injection timing and compression ratio of a raw biogas powered dual fuel diesel engine. Applied Thermal Engineering, 92 (2016); 111–121.

[13] X. Shan, Y. Qian, L. Zhu, X. Lu, Effects of EGR rate and hydrogen/carbon monoxide ratio on combustion and emission characteristics of biogas/diesel dual fuel combustion engine, Fuel, 181 (2016); 1050–1057.

[14] K. Cacua, A. Amell, F. Cadavid, Effects of oxygen enriched air on the operation and performance of a diesel-biogas dual-fuel engine, Biomass and Bioenergy, 45(2012); 159–167.

[15] V. Makareviciene, E. Sendzikiene, S. Pukalskas, A. Rimkusb and R. Vegneris. Performance and emission characteristics of biogas used in diesel engine operation. Energy Conversion and Management, 75 (2013); 224–233.

[16] D. Barik, A. K. Satapathy and S. Murugan, Combustion analysis of the diesel–biogas dual fuel direct injection diesel engine– the gas diesel engine, International Journal of Ambient Energy, 38 (2015), 259–266.

[17] H. Ambarita, Performance and emission characteristics of a small diesel engine run in dual-fuel (diesel-biogas) mode, Case Studies in Thermal Engineering, 10 (2017); 179–191.

[18] R. Chandra, V. K. Vijay, P. M. V. Subbarao, T. K. Khura, Performance evaluation of a constant speed IC engine on CNG, methane enriched biogas and biogas, Applied Energy, 88 (2011); 3969–3977.

[19] B. B. Sahoo, N. Sahoo, U. K. Saha, Effect of engine parameters and type of gaseous fuel on the performance of dual-fuel gas diesel engines—A critical review, Renewable and Sustainable Energy Reviews, 13 (2009); 1151–1184.

[20] B. J. Bora, UK Saha, S. Chatterjee and V. Veer. Effect of compression ratio on performance, combustion and emission characteristics of a dual fuel diesel engine run on raw biogas. Energy Conversion and Management, 87 (2014); 1000–1009.

[21] D. K. Ramesha, A. S. Bangari, C. P. Rathod and S. Chaitanya, Combustion, performance and emissions characteristics of a biogas fuelled diesel engine with fish biodiesel as pilot fuel, Biofuels, 6 (2015); 9–19.

[22] R. Uma, T. C. Kandpal and V. V. N. Kishore, Emission characteristics of an electricity generation system in diesel alone and dual fuel modes, Biomass & Bioenergy; 27 (2004), 195–203.

[23] N. Tippayawong, A. Promwungkwa and P. Rerkkriangkrai. Long-term operation of a small biogas/diesel dual-fuel engine for on-farm electricity generation, Biosystems Engineering, 98 (2007); 26–32.

[24] P. M. Duc, K. Wattanavichien, Study on biogas premixed charge diesel dual fuelled engine, Energy Conversion and Management, 48 (2007); 2286–2308.

[25] F. Z. Aklouche, K. Loubar, A. Bentebbiche, S. Awad, M. Tazerout, Experimental investigation of the equivalence ratio influence on combustion, performance and exhaust emissions of a dual fuel diesel engine operating on synthetic biogas fuel, Energy Conversion and Management, 152 (2017) 291–299.

[26] G. A. Karim. An examination of some measures for improving the performance of gas fuelled diesel engines at light load. SAE Technical Paper 912366, 1991.

[27] Z. Wang. Z. Zhao, D. Wang, M. Tan, Y. Han, Z. Liu and H. Dou. Impact of pilot diesel ignition mode on combustion and emissions characteristics of a diesel/natural gas dual fuel heavy-duty engine. Fuel, 167(2016); 248–256.

[28] J. Liu, X. Zhang, T. Wang, J. Zhang and H. Wang. Experimental and numerical study of the pollution formation in a diesel/CNG dual-fuel engine. Fuel, 159 (2015); 418–429.

[29] L. Tarabet, K. Loubar, M. S. Lounici, K. Khiari, T. Belmrabet and M. Tazerout. Experimental investigation of DI diesel engine operating with eucalyptus biodiesel/natural gas under dual fuel mode. Fuel, 133 (2014); 129–139.

[30] D. Dahl, I. Denbrat. HCCI/SCCI load limits and stoichiometric operation in a multicylinder naturally aspirated spark ignition engine operated on gasoline and E85, International Journal of Engine Research, 12 (2011), 58–68.

[31] A.P. Singh, A.K. Agarwal. Combustion characteristics of diesel HCCI engine: An experimental investigation using external mixture formation technique, Applied Energy, 99 (2012), 116–125.

[32] S. Jafarmadar, P. Nemati, R. Khodaie. Evaluation of Homogeneous Charge Compression Ignition (HCCI) autoignition development through chemiluminescence imaging and Proper Orthogonal Decomposition, Applied Energy, 210 (2018), 288–302.

[33] A. Gharehghani, Load limits of an HCCI engine fueled with natural gas, ethanol, and methanol, Fuel, 239 (2019), 1001–1014.

[34] D. S. Kim and C. S. Lee, Improved emission characteristics of HCCI engine by various premixed fuels and cooled EGR, Fuel, 85 (2006), 695–704.

[35] D Ganesh, G Nagarajan. Homogeneous charge compression ignition (HCCI) combustion of diesel fuel with external mixture formation. Energy; 35 (2010); 148–157.

[36] AP Singh, AK Agarwal. Combustion characteristics of diesel HCCI engine: An experimental investigation using external mixture formation technique. Applied Energy; 99 (2012): 116–125.

[37] M. Andreae, W. Cheng, T. Kenney, J. Yang. On HCCI engine knock. SAE Technical Paper 2007-01-1858, (2007).

[38] H. Ma, H Xu, J. Wang, C Tan. Investigation on the self-stabilization feature of HCCI combustion. SAE Technical Paper 2014-01-2663, (2014).

[39] L.K. Manofsky Olesky, R.J. Middleton, G.A. Lavoie, M.S. Wooldridge, J.B. Martz. On the sensitivity of low temperature combustion to spark assist near flame limit conditions. Fuel; 158 (2015), 11–22.

[40] H. Bendu, S. Murugan. Homogeneous charge compression ignition (HCCI) combustion: Mixture preparation and control strategies in diesel engines. Renewable and Sustainable Energy Reviews, 38 (2014), 732–746.

[41] T. Urushihara, K. Yamaguchi, K. Yoshizawa, T Itoh. A study of a gasoline-fueled compression ignition engine - expansion of HCCI operation range using SI combustion as a trigger of compression ignition, SAE Technical Paper 2005-01-0180, (2005).

[42] H. Xie, L. Li, T. Chen, W. Yu, X. Wang, H. Zhao, Study on spark assisted compression ignition (SACI) combustion with positive valve overlap at medium–high load, Applied Energy, 101 (2013), 622–633.

[43] G. Lavoie, J. Martz, M. Wooldridge, D. Assanis, A multi-mode combustion diagram for spark assisted compression ignition. Combustion and Flame. 157 (2010): 1106–1110.

[44] M. Chiodi, A. Kaechele, M. Bargende, D. Wichelhaus, Ch. Poetsch, Development of an innovative combustion process: Spark-assisted compression ignition, SAE Technical Paper 2017-24-0147, (2017).

[45] D. Koch, V. Berger, A. Bittel, M. Gschwandtner, G. Wachtmeister, M. Chiodi, A. Kaechele, M. Bargende, D. Wichelhaus, Investigation of an innovative combustion process for high-performance engines and its impact on emissions, SAE Technical Paper 2019-01-0039, (2019).

[46] Z. Wang, J. Wang, S. Shuai, G. Tian, X. An, Q. Ma, Study of the effect of spark ignition on gasoline HCCI combustion. Proceedings of the Institution of Mechanical Engineers, Journal of Automobile Engineering. 220 (2006); 817–825.

[47] D. Splitter, M. Wissink, D. DelVescovo, R.D. Reitz R. RCCI engine operation towards 60% thermal efficiency. SAE Technical Paper 2013-01-0279, (2013).

[48] Y. Li, M. Jia, Y. Chang, M. Xie, R.D. Reitz. Towards a comprehensive understanding of the influence of fuel properties on the combustion characteristics of a RCCI (reactivity controlled compression ignition) engine. Energy, 99 (2016), 69–82.

[49] F. Yang, C. Yao, J. Wang, M. Ouyang. Load expansion of a dieseline compression ignition engine with multi-mode combustion. Fuel, 171 (2016), 5-17.

[50] L. Bates, D. Bradley, I. Gorbatenko, A. S. Tomlin, Computation of methane/air ignition delay and excitation times, using comprehensive and reduced chemical mechanisms and their relevance in engine autoignition, Combustion and Flame, 185 (2017); 105–116.

[51] N. Kawahara, E. Tomita, Y. Sakata, Auto-ignited kernels during knocking combustion in a spark-ignition engine, Proceedings of the Combustion Institute, 31 (2007); 2999–3006.

[52] L. Bates, D. Bradley, G. Paczko, N. Peters, Engine hot spots: Modes of auto-ignition and reaction propagation, Combustion and Flame, 166 (2016); 80–85.

[53] Y. Qi, Z. Wang, J. Wang, X. He, Effects of thermodynamic conditions on the end gas combustion mode associated with engine knock, Combustion and Flame, 162 (2015) 4119–4128.

[54] D. Bradley, G.T. Kalghatgi, Influence of autoignition delay time characteristics of different fuels on pressure waves and knock in reciprocating engines, Combustion and Flame, 156 (2009), 2307–2318.

[55] U. Azimov, E. Tomita, N. Kawahara and Y. Harada, Premixed mixture ignition in the end-gas region (PREMIER) combustion in a natural gas dual-fuel engine: operating range and exhaust emissions, International Journal of Engine Research; 12 (2011); 484–497.

[56] E. Tomita, Y. Harada, N. Kawahara and A. Sakane, Effect of EGR on combustion and exhaust emissions in supercharged dual-fuel natural gas engine ignited with diesel fuel, SAE Technical Paper 2009-01-1832, (2009).

[57] E. Tomita, N. Kawahara and J. Zheng, Visualization of auto-ignition of end gas region without knock in a spark-ignition natural gas engine, Journal of KONES. Powertrain and Transport; 17 (2010), 521–527.

[58] M. M. Roy, E. Tomita, N. Kawahara, Y. Harada and A. Sakane, Comparison of performance and emissions of a supercharged dual-fuel engine fueled by hydrogen and hydrogen-containing gaseous fuels, International Journal of Hydrogen Energy; 36 (2011), 7339–7352.

[59] U. Azimov, E. Tomita, N. Kawahara and Y. Harada, Effect of syngas composition on combustion and exhaust emission characteristics in a pilot-ignited dual-fuel engine operated in PREMIER combustion mode, International Journal of Hydrogen Energy; 36 (2011), 11985–11996.

[60] U. Azimov, E. Tomita and N. Kawahara, Ignition, combustion and exhaust emission characteristics of micro-pilot ignited dual-fuel engine operated under PREMIER combustion mode, SAE Technical Paper; 2011-01-1764, (2011).

[61] C. Aksu, N. Kawahara, K. Tsuboi, S. Nanba, E. Tomita and M. Kondo, Effect of hydrogen concentration on engine performance, exhaust emissions and operation range of PREMIER combustion in a dual fuel gas engine using methane-hydrogen mixtures. SAE Technical Paper; 2015-01-1792, (2015).

[62] C. Aksu, N. Kawahara, K. Tsuboi, M. Kondo and E. Tomita, Extension of PREMIER combustion operation range using split micro pilot fuel injection in a dual fuel natural gas compression ignition engine: A performance-based and visual investigation, Fuel; 185 (2016), 243–253.

[63] N. Kawahara, Y. Kim, H. Wadahama, K. Tsuboi, E. Tomita, Differences between PREMIER combustion in a natural gas spark-ignition engine and knocking with pressure oscillations, Proceedings of the Combustion Institute; 37 (2019), 4983–4991.

5.1. Introduction

The excessive global carbon dioxide (CO_2) emissions and other greenhouse gas (GHG) emissions from the burning of fossil fuels causes the search for climate-friendly alternative fuels. Worldwide energy demand is increasing and therefore, fossil fuel consumption as a current main source of energy increases as a result. On the other hand, limitation and depletion of petroleum resources are of concern in the near future. Internal combustion (IC) engines are widely used for transportation, power generation and industrial application and therefore, the aforementioned problems are more critical for them. Biomass gas is considered as a most suitable renewable source of energy [1] and it is defined as biological matter obtained from animals or plants wastes. They can burn directly or can be converted to liquid biofuels such as bioethanol and biodiesel or gaseous biofuels such as biogas which can be used as a fuel for IC engines. Biogas is produced from biomass through decomposition of organic waste in an anaerobic environment, an environment absent of oxygen. Biogas consists of mainly methane (CH_4) and CO_2 and it is flammable due to high percentage of methane. The composition of CH_4 and CO_2 varies and depends on generation method as well as raw materials. The advantages of biogas can be listed as clean and environmental- friendly due to being carbon neutral, reduce landfill pollution, and quite cheap production technology. In regards to biogas application as a fuel in engine, it should be noticed that biogas has lower laminar burning velocity and narrow flammability limits and these characteristics influence engine performance. The energy density of biogas is low due to presence of CO_2. The lower heating value (LHV) of methane in the biogas is low but it has high autoignition temperature that causes biogas as knocking-resistance fuel.

Gas engine is used for electricity generation in small and big scale by using biogas as a fuel [2, 3]. Gas engine fueled with biogas can initiate combustion either by spark plug or diesel fuel. Biogas is widely used as a fuel in spark ignition (SI) engines [4- 6]. Jingdang and Crookes [4] studied the biogas fuel performance and exhaust emissions in SI engine. They reported that engine power and thermal efficiency were reduced when the fraction of CO_2 increased to 40%. The engine performance and thermal efficiency improved by increasing the compression ratio but emissions of nitrogen oxide (NO_x) and hydrocarbon (HC) increased [4]. Porpatham et al. investigated the CO_2 concentration effect namely 41%, 30% and 20%, in biogas in SI engine [6]. They reported that addition of CO_2 increased hydrocarbon emission but reduced CO and nitric oxide (NO) emissions and reduced the engine performance [6]. High autoignition temperature of biogas prevents it to be used directly in the compression ignition (CI) engine, hence an ignition source is needed. Dual-fuel is considered as most suitable strategy for using biogas in CI engines. Dual-fuel engines use typically gaseous fuel (biogas) as a main fuel and liquid fuel (diesel) as a pilot fuel. In this type of combustion system, biogas fuel is introduced at the intake port and mixed with the inlet air. Combustion does not occur by only compression of biogas-air mixture due to high autoignition temperature of biogas and therefore, liquid fuel which is typically diesel fuel is used as an ignition source by direct injection into cylinder at near the end of compression stroke. There are many works on the application of biogas in CI engines under dual-fuel mode [7-19]. Biogas dual-fuel engine causes reduction on thermal efficiency with increasing biogas flow rate [9, 16, 18], irregular combustion with 40% CO_2 in methane [19], increasing emission of CO and reduction in NO_x [9, 18]. Barik et. al. [9] reported reduction in thermal efficiency for dual-fuel operation with biogas compared to those in diesel operation. When biogas flow rate increased from 0.3 kg/h to 1.2 kg/h, thermal efficiency dropped from 2.1% to 9.2%

compared to diesel operation throughout the load range. Oxygen deficiency and lower flame propagation speed caused drop in thermal efficiency [9]. Cacua et al. [13] investigated the biogas with 60% CH_4-40% CO_2 in dual-fuel engine. The intake air was enriched by oxygen from 21% to 27%. Oxygen enriched air caused higher thermal efficiency and lower methane emissions. Biogas engines are also studied with different pilot fuel such as dimethyl ether (DME) [20] and biodiesel [17, 18, 21, 22]. Advancing injection timing improved indicated mean effective pressure (IMEP) [20] and increased cylinder peak pressure [22].

Although gaseous fuels and in particular biogas are suitable in dual-fuel operation, the amount of these fuels are limited due to knocking [23, 24]. Biogas is also studied in homogeneous charged compression ignition (HCCI) mode [25-27] and reactivity controlled compression ignition (RCCI) [28]. In HCCI mode, knocking and misfiring are reported by using low and higher amount of biogas, respectively [26]. Knocking is an unexpected end-gas autoignition that accompanied by pressure oscillation and therefore, it should be suppressed due to its negative effects on damage of engine components [29-31]. Dual-fuel operation at high load, high compression ratio and advanced injection timing increase thermal efficiency [10, 12] but it may increase the risk of knocking [19]. However, end-gas autoignition without any pressure oscillation was found in Ref. [32]. This could help to improve the engine performance as well as thermal efficiency and could help to reduce the emissions of CO and HC which are typically higher under dual-fuel mode. This phenomenon has been named premixed mixture ignition in the end-gas region (PREMIER) combustion. PREMIER combustion differs significantly from normal combustion and knocking combustion in its end-gas autoignition characteristics. Similar to dual-fuel combustion system, gaseous fuel-air mixture is compressed and then pilot fuel is injected near top dead center (TDC). Autoignition of pilot fuel creates some flame

kernels and the combustion is initiated. Pilot fuel autoignition triggers flame propagation of gaseous fuel-air mixture and combustion heat is released as a result. From these points onward, the characteristics of unburned gas play an important role in determining the mode of combustion. If propagating flame consume the gaseous fuel-air mixture completely, normal combustion achieves, otherwise, unburned mixture will be autoignited in the end- gas region and yields either knocking or PREMIER combustion. The end-gas autoignition commencement and the volume of unburned mixture are important to determine combustion mode and it can be controlled mainly by means of injection timing of pilot fuel. PREMIER combustion aimed to improve engine performance as well as thermal efficiency of IC engines [32- 39]. Except studies of [34] and [39] which confirm PREMIER combustion in SI engines, the rest of our works are done in dual-fuel gas engine at high load operation. A split injection of pilot fuel is tested to suppress knocking to PREMIER or promote normal dual-fuel combustion to PREMIER combustion [38]. Quantification of PREMIER combustion has been done by means of PREMIER intensity (PI), as an indicator of strength of PREMIER combustion in chapter 4. Our previous works show that the engine performance and thermal efficiency improved and emissions of CO and HC reduced owing to knock-free end-gas autoignition of unburned mixture with slightly increase of emission of NO_x. The purpose of this section was to investigate the effect of CO_2 on the biogas engine performance, emissions and end-gas autoignition characteristics of PREMIER combustion. One of the challenges in this study was to extend the PREMIER operation range by increasing CO_2 to the methane and increase number of cycles featuring end-gas autoignition without pressure oscillation.

5.2. Experimental setup and data evaluation

The experiments are carried out using a single-cylinder, four-stroke, water-cooled, direct-injection, dual-fuel gas engine. The engine had a bore and stroke of 96 and 108 mm, respectively, with a displacement volume of 781 cm^3 and compression ratio of 16.4:1. A shallow dish piston is used during experiments. In this study, a solenoid valve controlled injector with a three-hole nozzle (ϕ 0.11 mm) was used with a common rail system to spray the pilot fuel. The purpose of this nozzle was to inject as little diesel fuel as possible. The pilot fuel was delivered at an injection pressure of 40 MPa at 1.6 mg/cycle. A schematic diagram of the experimental setup is shown in Figure 5.1 and the engine details and experimental conditions are listed in Table 5.1. In order to detect camshaft top dead center position, an optical sensor (photo interrupter) was used. A crank angle signal of every 0.5 °CA was detected with a photo interrupter. In-cylinder pressure was measured with a Kistler type 6052A pressure transducer. A Kistler type 5011 charge amplifier was used to amplify the in-cylinder pressure signal. The gaseous fuel was introduced from intake port and gas flow rate was controlled with mass flow controllers. The gas flow rates were automatically determined by using a programmable logic controller (PLC) in order to obtain an accurate gas composition and equivalence ratio. The simulated biogas consisted of CH_4 and CO_2 was used as a primary fuel and diesel was used as a pilot fuel. The ratio of CO_2 was varied from 0 to 50% by volume, in order to investigate the effect of CO_2 ratio to CH_4 on the engine performance, exhaust emissions and end-gas autoignition characteristics. All tests were conducted at an engine speed of 1,000 rpm, and at intake pressure of 200 kPa. The overall equivalence ratio was set to 0.56 to achieve lean-burn combustion. Pilot fuel injection timing was varied during the experiments and it was advanced until occurrence of knocking. In this study, CO_2 was added in the intake pipe.

The ratio of CO_2 to CH_4 was varied from 0 to 50% by volume. The gaseous fuel flow rate is continuously adjusted based on the air flow rate readings obtained from the flowmeter while intake pressure was kept constant of 200kPa. This strategy was applied to keep the equivalence ratio constant throughout the experiments. Figures 5.2 (a) and (b) show the fuel supply strategies and heat value per cycle for all fueling cases, respectively. As shown in Figure 5.2(b), the heat value was changed from 2624J/cycle to 2510J/cycle in changing the ratio of CO_2 to CH_4 from 0 to 50%. Table 5.2 shows gas composition and injection timing of pilot fuel. In Table 5.2, red colored numbers denote injection timings of PREMIER combustion. The main indicator of knocking is pressure oscillation. The pressure history and rate of heat release (ROHR) were averaged over 80 cycles for each dataset. To explore pressure oscillation, a band-pass-filter (4–20 kHz) was applied to all pressure history data. The maximum instantaneous pressure difference between consecutive signals passing through the digital band-pass-filter was defined as the knocking intensity (KI) as shown in Figure 5.3. Any KI above a certain threshold (0.1 MPa) was defined as knocking. If even 1 of the 80 cycles exhibited a KI > 0.1 MPa, this experimental condition is judged as knocking. In terms of PREMIER operation, it is required that over 50% of cycles should exhibit end-gas autoignition without knocking (i.e., KI ≤ 0.1 MPa) [38]. Any cycle exhibiting less than 50% end-gas autoignition was considered to correspond to normal combustion. Herein, we analyze the characteristics of PREMIER combustion in detail.

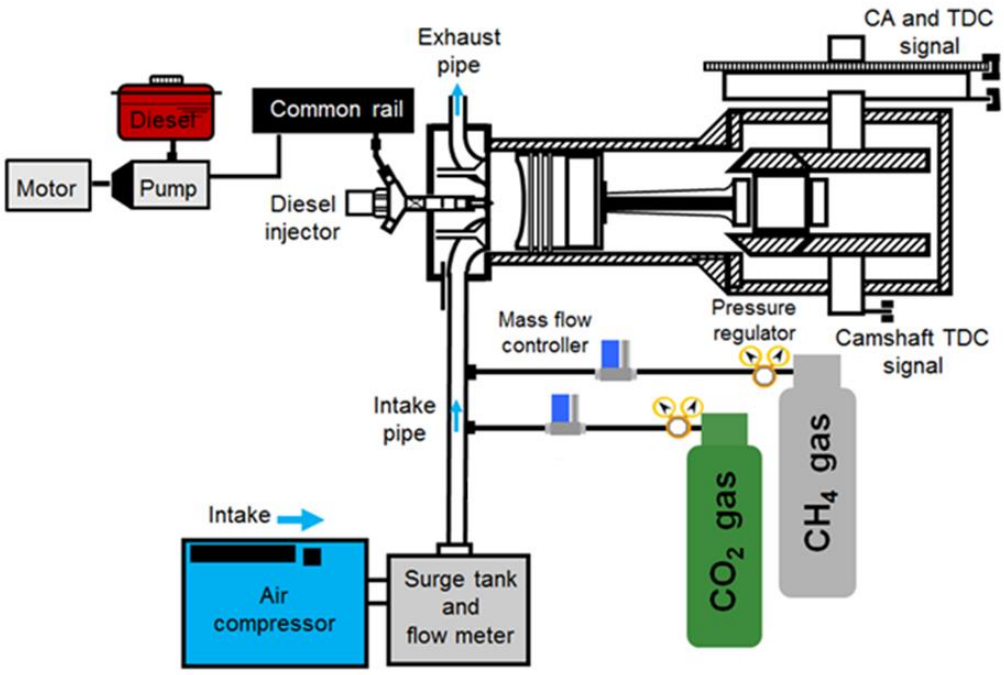

Figure 5.1: Schematic diagram of the experimental setup

Table 5.1. Test engine specification and experimental conditions

Engine type	Four stroke, single cylinder
Bore * stroke	96 mm * 108 mm
Displacement volume	781 cm^3
Equivalence ratio, ϕ_t	0.56
Compression ratio	16:4
Combustion system	Pilot ignited dual fuel combustion
Intake pressure, P_{in}	200 kPa
Injection system	Common rail direct injection
Injection pressure	40 MPa
Injection quantity	1.6 mg/cycle
Injection timing	Varying
Fuel delivery	3 hole, ϕ 0.11
Engine speed	1000 rpm
Gaseous fuel supply	Premixed charged through intake port
Air intake	Supercharged condition
Intake valve open/close	340°ATDC/135°BTDC
Exhaust valve open/close	130°ATDC/345°BTDC

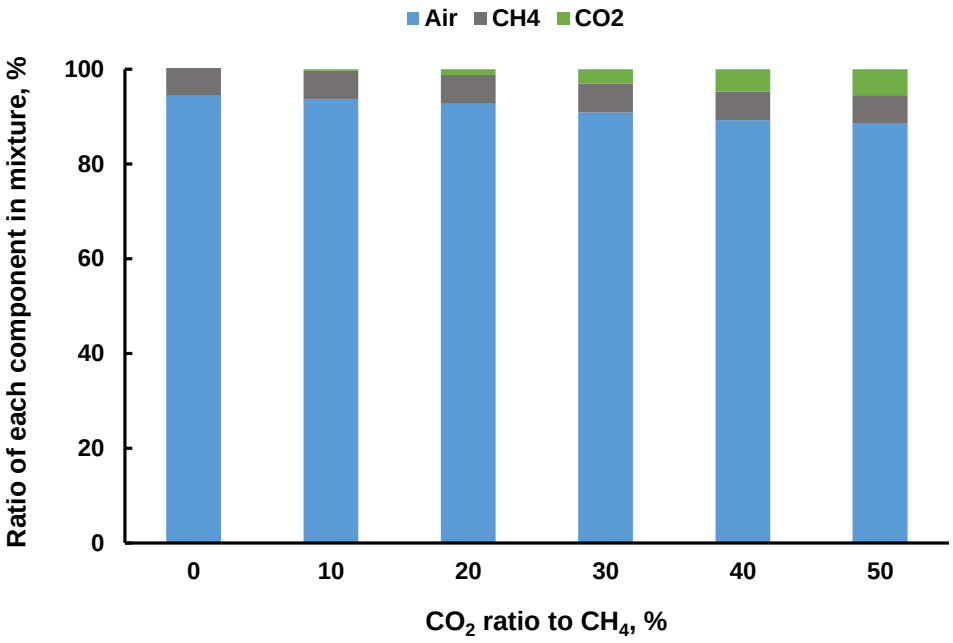

(a)

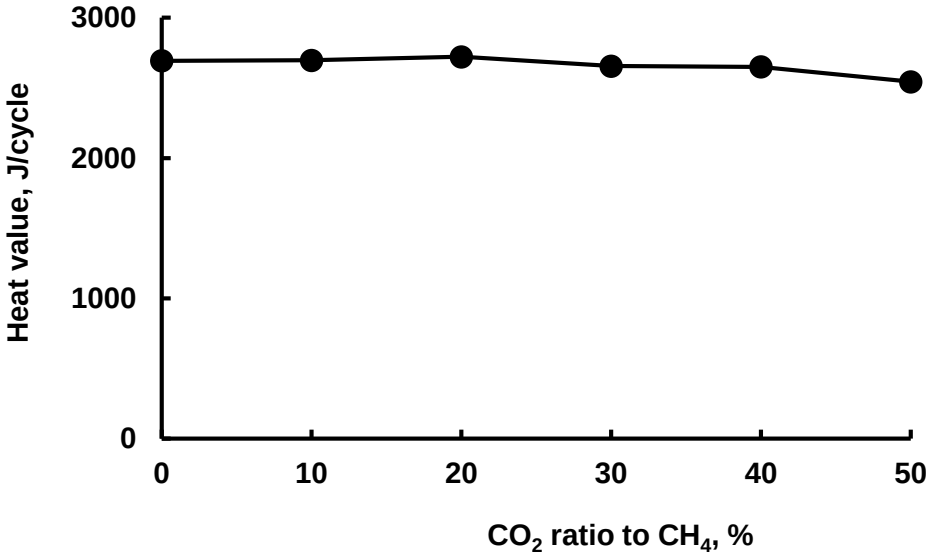

(b)

Figure 5.2: (a) Gaseous fuel supply strategy (b) heat value per cycle for all fuelling cases

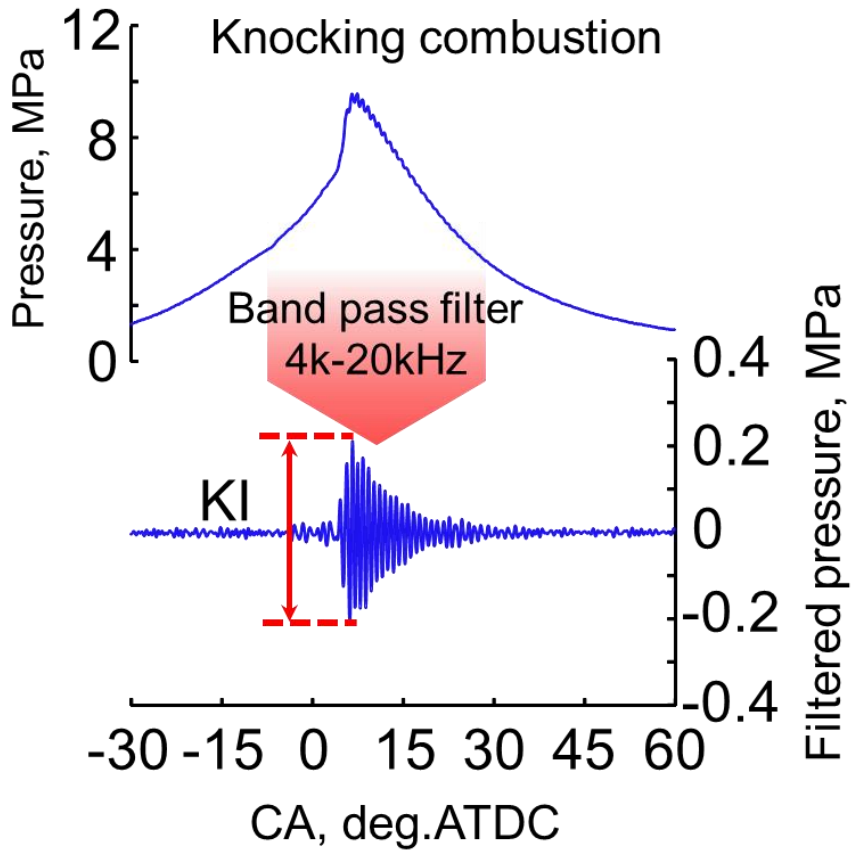

Figure 5.3: Example of band pass filter

Table 5.2. Gas composition and diesel fuel injection timing

Fuel mixture	CH_4 (Vol.%)	CO_2 (Vol.%)	Injection timing (°CA)
50% CO_2	50	50	12, 14, 15, 16, 17, 18, **19**, **20**
40% CO_2	60	40	12, 14, 15, 16, **17**, 18
30% CO_2	70	30	10, 11, 12, 13,14, **15**, **16**, 17
20% CO_2	80	20	10, 11, 12, **13**, 14
10% CO_2	90	10	10, 11, **12**, 13
Pure Methane	100	0	10, 11, **12**, 13

5.3. Results and discussion

5.3.1 Cylinder pressure, rate of heat release, ignition delay

Figure 5.4 (a) and (b) show the pressure history and ROHR for pure methane and 10, 20, 30, 40 and 50% CO_2 ratio by volume, at the most beneficial injection timings, as an average of 80 cycles. Additionally, pressure histories and rate of heat release characteristics of wide ranges of injection timings at each fueling case are given in Figure 5.5 and Figure 5.6, respectively. Throughout the CO_2 fraction range, addition of CO_2 helped to advance the injection timing more, which is an expected scenario due to low reactivity of CO_2. Generally, increasing CO_2 to the methane tends to reduce the peak pressure [7, 16, 20] when the injection timing is not varied but advancing injection timing causes higher in-cylinder peak pressure [9, 18]. Cylinder pressure increases and becomes closer to TDC by increasing CO_2 at advanced injection timing. On the other hand, ROHR characteristics at the most beneficial injection timing show that when higher amount of CO_2 added in the mixture ROHR is slightly decreased. The CO_2 actually acts as an inert gas because of non-combustible gas. As shown in the Figure 5.4 (b), after main combustion of gaseous fuel-air mixture, another peak around crank angle of 15 °ATDC can be seen. It is due to autoignition of unburned mixture in the end-gas region. In the all conditions of Figure 5.4, the end-gas autoignition did not associated with pressure oscillation or any sign of knocking. These are PREMIER combustion which simply consider as knock-free end-gas autoignition.

Figure 5.5 and Figure 5.6 show that when injection timing is advanced, both cylinder pressure and ROHR increased. Furthermore, as shown in the Figure 5.7, the duration from the start of combustion to the heat release peak of flame propagation ($\Delta\theta_{fp}$) became gradually longer as the higher amount of CO_2 added in the mixture. Similarly, the duration

from the start of combustion to the heat release peak of end-gas autoignition ($\Delta\theta_{egai}$) became gradually longer as the higher amount of CO_2 added in the mixture (Figure 5.7). It means when higher amount of CO_2 added in the mixture, heat released due to propagating flames is slower. In addition, the end-gas autoignition timings that can be obtained from heat release characteristics was within a range of 8°ATDC to 14°ATDC.

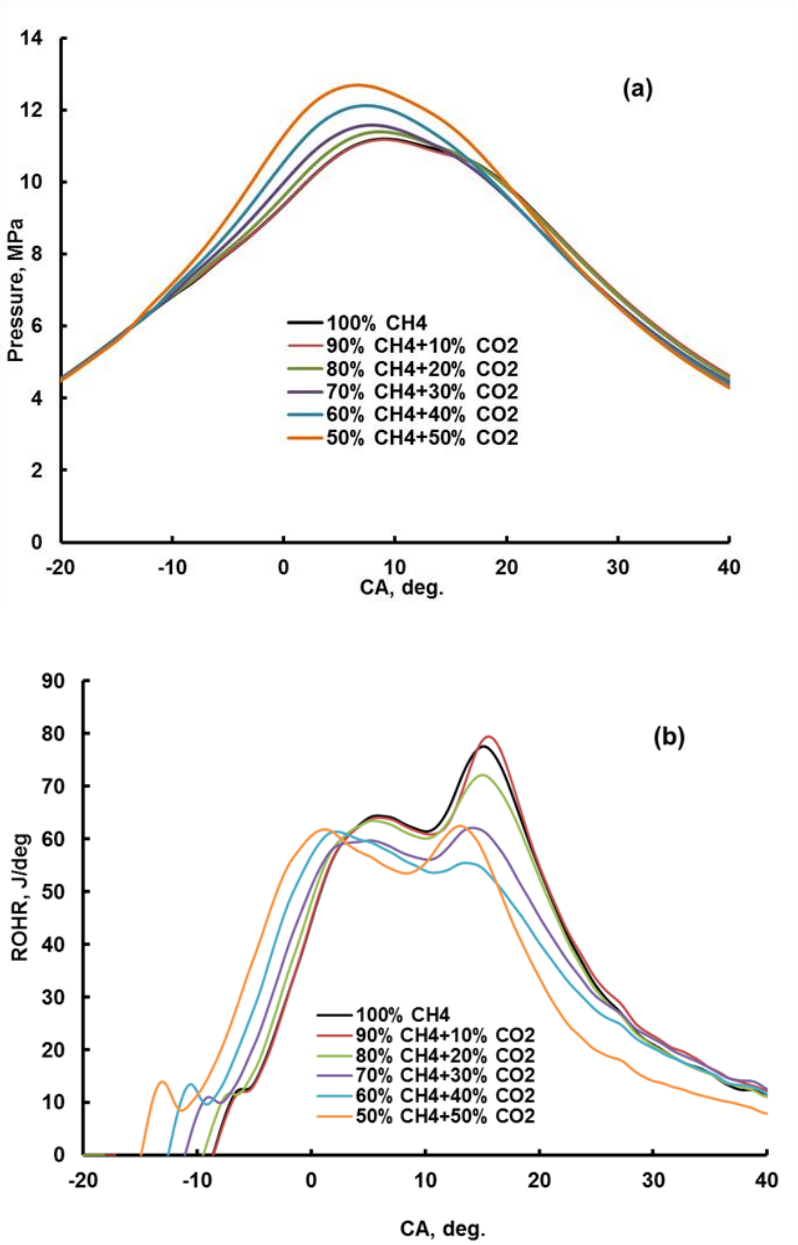

Figure 5.4: (a) Pressure history and (b) rate of heat release of CH_4-CO_2 mixtures at the most beneficial injection timings of all fueling cases

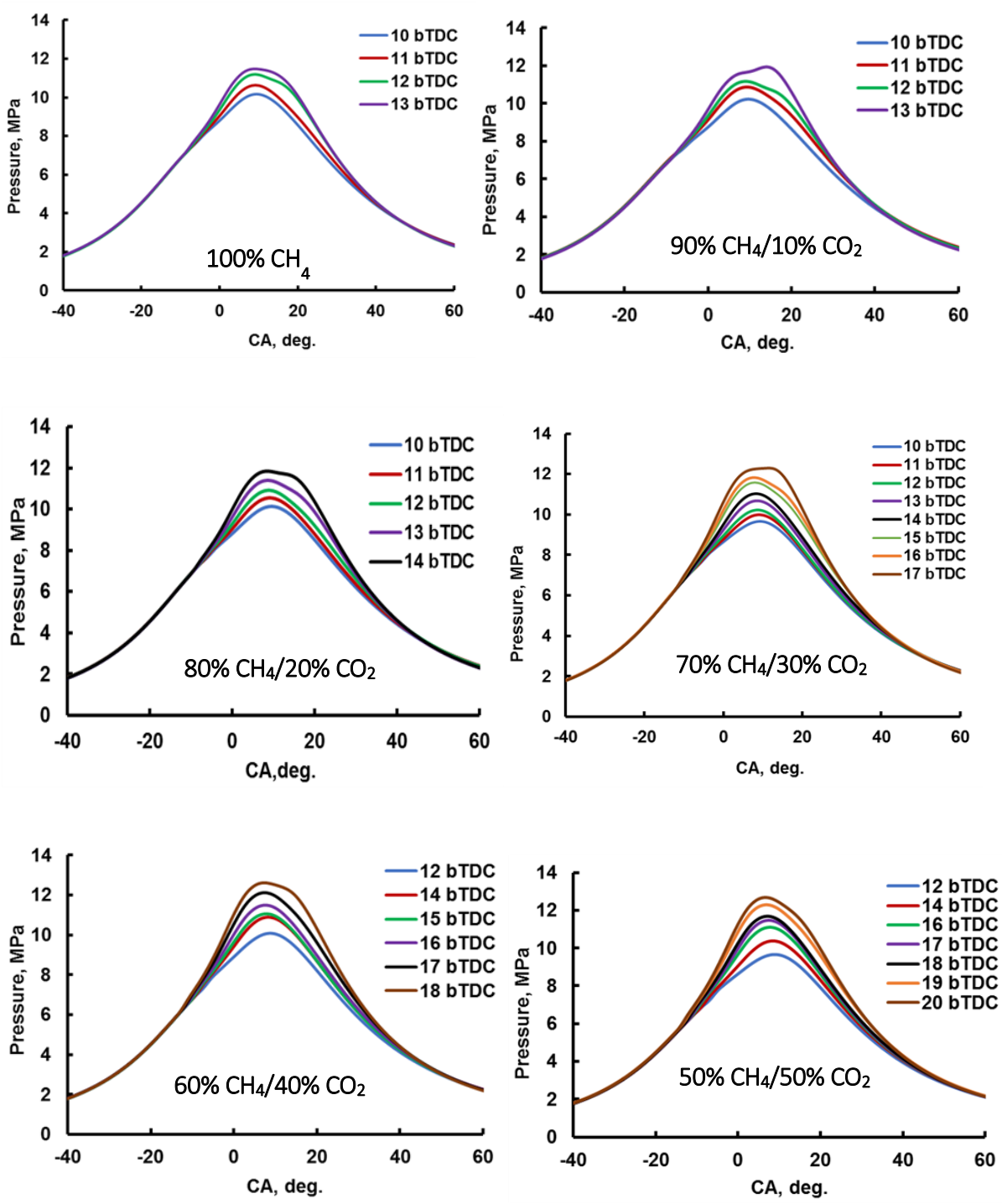

Figure 5.5: Pressure histories of CH_4-CO_2 mixtures of all fueling cases

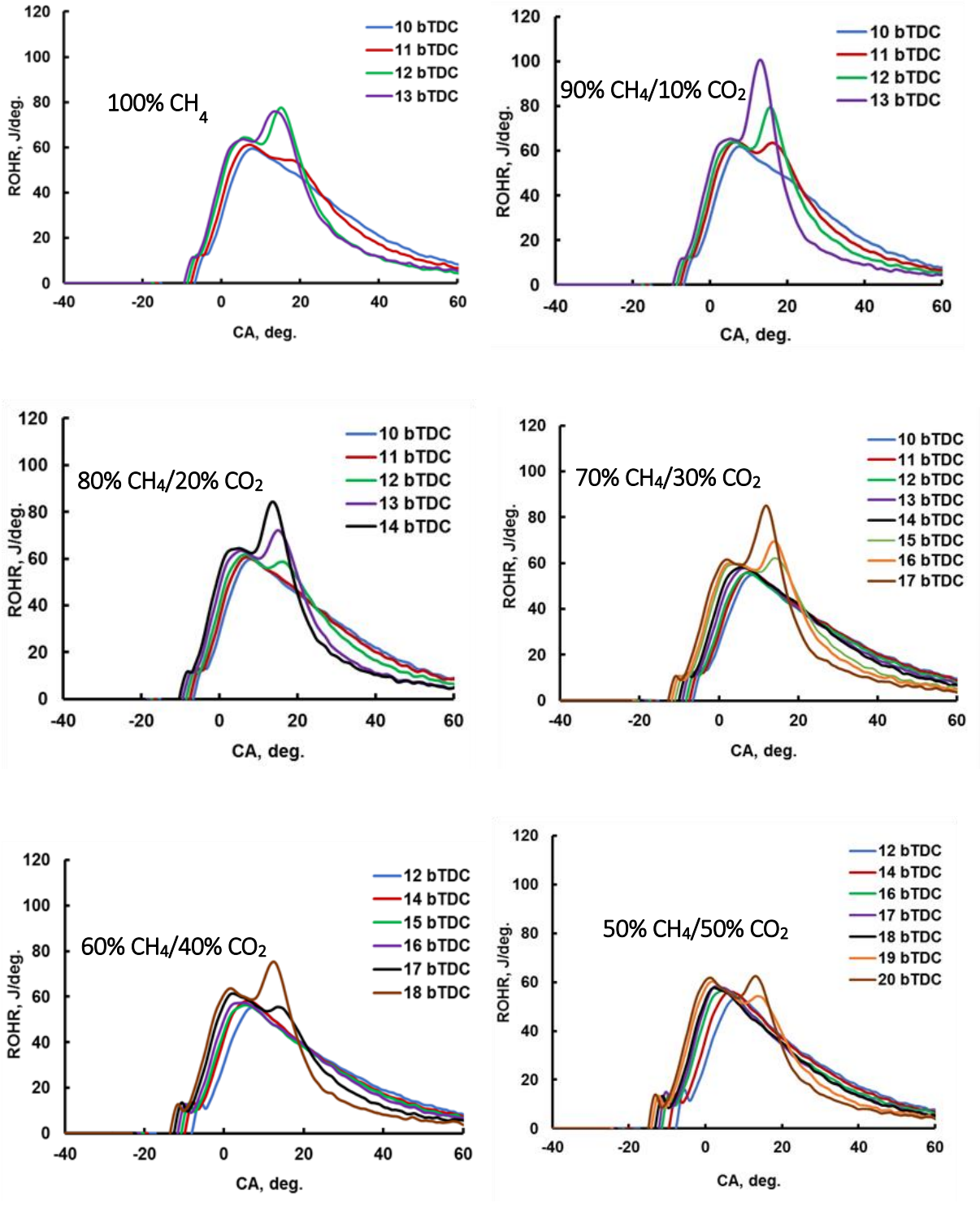

Figure 5.6: Rate of heat release of CH_4-CO_2 mixtures of all fueling cases

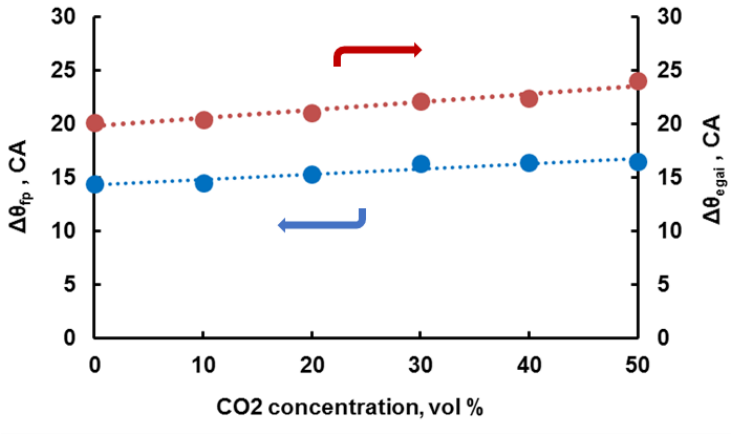

Figure 5.7: (blue) Duration from the start of combustion to the heat release peak of flame propagation **(red)** duration from the start of combustion to the heat release peak of end-gas autoignition

As shown in Figure 5.3(b), the first peak of ROHR caused by pilot fuel autoignition was increased when CO_2 ratio to CH_4 is increased to 50% and it is attributed to longer ignition delay of mixture with higher CO_2 as shown in Figure 5.8. It can be seen that either increasing of CO_2 or advancing injection timing resulted longer ignition delay. When pilot fuel injection timing is advanced and CO_2 in the mixture is increased, the in-cylinder mixture temperature is lower at the timing of fuel injection beginning, therefore, it takes longer time to be auto-ignited and results longer ignition delay. Also, ignition delay became longer when CO_2 ratio to CH_4 increased owing to lower specific heat ratio of mixture with higher CO_2. The same result was observed in other works [7, 9, 18, 20].

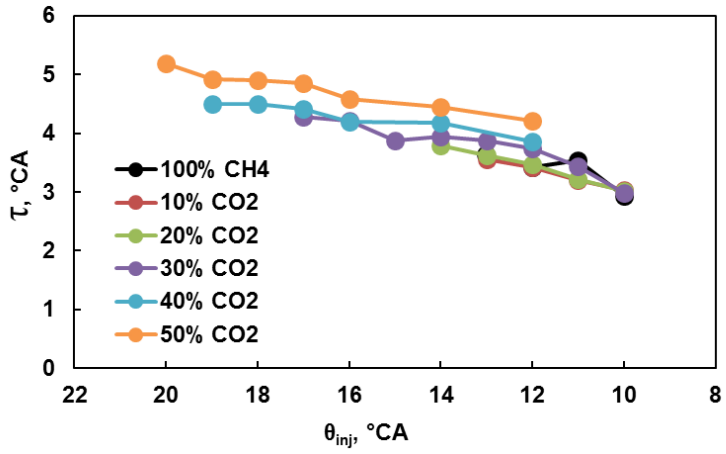

Figure 5.8: Ignition delays of initial combustion

The percentage and number of cycles featuring end-gas autoignition are shown in Figure 5.9(a) and (b). It should be pointed out here that from Figure 5.9(a) onwards, filled symbols, open symbols and cross marks represent normal combustion, PREMIER combustion and knocking combustion, respectively. Based on the results in Figure 5.9, the distinction among normal, PREMIER and knocking combustion has been done. The symbols above each bar in Figure 5.9 (b), K, P and N denote knocking, PREMIER and normal combustion. Figure 5.9(a) shows that percentage of cycles with end-gas autoignition is higher when injection timing is advanced. When the ratio of CO_2 to CH_4 increases, ratio of PREMIER combustion increases as well. Mixtures with higher CO_2 ratio to CH_4, namely 40% and 50%, have one and zero knocking cycles, respectively as shown in Figure 5.9(b). It means addition of CO_2 could help to reduce the possibility of knocking cycles. Mixture with 50% CO_2, underwent knock-free end-gas autoignition up to θ_{inj} = 20°BTDC. If injection timing is advanced more, knocking may take place.

Figure 5.9 (b) shows that the maximum number of cycles featuring knock-free end-gas autoignition belongs to 20% CO_2 mixture (55 cycles) at θ_{inj} = 13°BTDC followed by 50% CO_2 mixture (53 cycles) at θ_{inj} = 20°BTDC. Mixture with 50% of CO_2, underwent knock-free end-gas autoignition up to θ_{inj} = 20°BTDC. It can be inferred that addition of CO_2 in the mixture can reduce the risk of knocking. By looking at the timing of commencement of PREMIER combustion, it is observed that injection timing could advance from 12°BTDC for pure methane to 20°BTDC for 50% CO_2 mixture without sign of knocking.

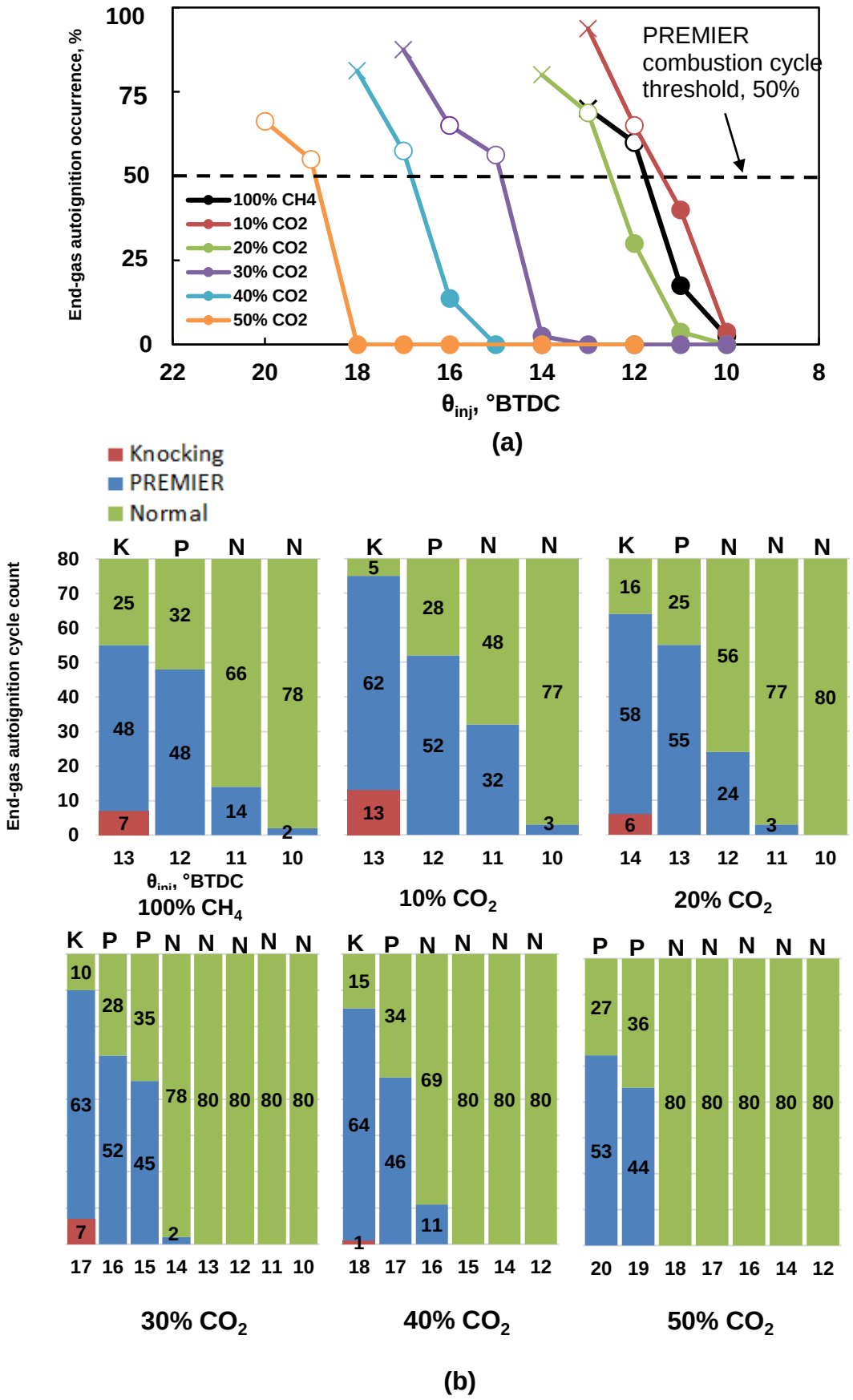

Figure 5.9: (a) Percentages of end-gas autoignition occurrence (b) number of cycles featuring end-gas autoignition

In terms of end-gas autoignition characteristics as shown in Figure 5.3(b), the first ROHR peak corresponds to pilot fuel autoignition, the second to gaseous fuel-air combustion, and the third, which normally occurs after TDC, to end-gas autoignition. After main combustion of gaseous fuel-air mixture, third peak around crank angle of 15°ATDC can be seen. It is due to autoignition of unburned mixture in the end-gas region. In the all conditions of Figure 5.3(b), the end-gas autoignitions did not associate with pressure oscillation These are PREMIER combustion which is simply considered as knock-free end-gas autoignition. As we mentioned earlier, all results in Figure 5.3(b) are the average of 80 cycles. For better understanding of differences between PREMIER combustion with both normal and knocking combustion, Figure 5.10 is presented. It shows three cycles out of 80 cycles for the condition of 20% CO_2 addition at θ_{inj} = 14°BTDC. Pressure oscillation and sudden rise of ROHR can be observed for knocking cycle. However, in PREMIER condition, no pressure oscillation is observed although end-gas autoignition occurred. The end-gas autoignition occurred later for PREMIER combustion compared to knocking and the maximum value of ROHR is smaller. The cylinder pressure and ROHR is higher than normal combustion but without any characteristics of knocking combustion. PREMIER combustion is differentiated from knocking combustion by KI value. When in-cylinder pressure passed through band-pass-filter in the range of 4-20 kHz, knocking cycles exhibited KI> 0.1 MPa; 0.1 was selected based on noise level of pressure signal. Any cycles below the threshold is considered as knock-free cycle. We therefore concluded that knock-free autoignition can be considered as a positive phenomenon to improve gaseous-fuel combustion at higher load without knocking and associated with better engine performance.

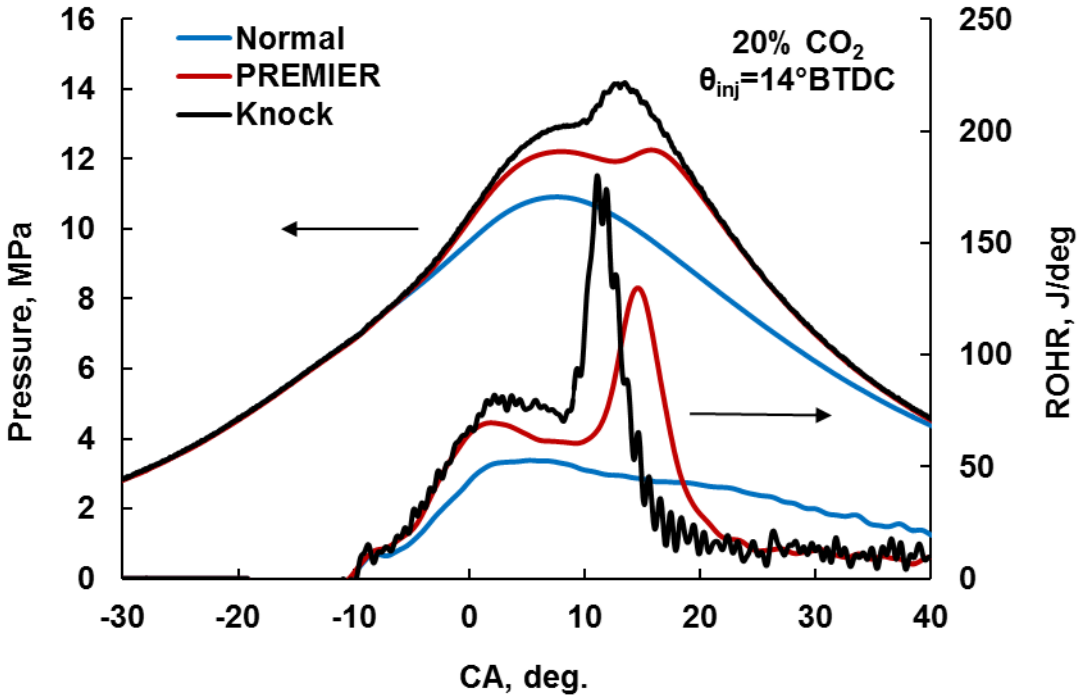

Figure 5.10: Pressure history and rate of heat release during normal combustion, PREmixed Mixture Ignition in the End-gas Region (PREMIER) combustion, and the knocking cycles

5.3.2 Engine performance

Figures 5.11(a), (b) and (c) show indicated mean effective pressure (IMEP), indicated thermal efficiency, and coefficient of variation of the IMEP, [$COV_{(IMEP)}$], respectively, as a function of injection timing for CO_2-CH_4 mixture. A highest IMEP achieved by 10% CO_2 mixture followed by pure methane. However, slightly lower IMEP of pure methane than 10% CO_2 mixture is due to lower air flow rate of pure methane than mixture with 10% CO_2 during the experiment with same equivalence ratio. Experiments were done in different days and due to different weather conditions, in particular air density and humidity, amount of inlet air and gaseous fuel are changed slightly. Also, it can be due to slightly lower heating value of pure methane (2624 J/cycle) than that of 10% CO_2 mixture (2627 J/cycle) due to same reason. When injection timing was advanced and PREMIER

combustion achieved, IMEP increased as a result. When injection timing is advanced, combustion is triggered earlier and therefore, larger amount of heat is released in early stage and this yields higher in-cylinder pressure as well as increasing work, thus, increasing IMEP.

Addition of CO_2 slightly reduced the IMEP for less than 20% CO_2 addition but larger drop in IMEP was observed for the mixture with more than 30% CO_2 in the mixture. It is due to lower heating value of mixture with higher CO_2 in the mixture. Increasing CO_2 in the mixture causes longer duration of main combustion owing to slower rate of flame propagation. When flame propagation speed is lower, amount of mixture consumed before TDC is larger when engine is in compression stroke, therefore, negative work is increases which means the produced energy is wasted while the engine did compression work, thus, less work can be obtained and this yields drop in IMEP. The maximum IMEP was obtained under PREMIER combustion for all fueling conditions as a result of end-gas autoignition. Autoignition typically occurs during expansion stroke and pressure rise as a result of autoignition increases the useful work However, IMEP under PREMIER combustion gradually decreased when CO_2 increased in the mixture.

In regards to thermal efficiency, the trend shows almost the same to IMEP, in which advancing injection timing resulted higher thermal efficiency. However, maximum thermal efficiency was obtained under PREMIER combustion operation. It is observed that when CO_2 increased in the mixture, thermal efficiency gradually became lower. Investigating thermal efficiency, it is apparent that the scenario seen in IMEP applies to thermal efficiency as well. However, maximum thermal efficiency under PREMIER combustion was almost similar although CO_2 in the mixture increased. It is due to lower heating value of the mixture with higher CO_2 in the mixture. Reduction of thermal

efficiency caused by increasing CO_2 in the mixture have been reported [9, 16, 18]. However, if PREMIER combustion could be achieved in these studies, thermal efficiency becomes higher.

The operation stability is indicated by $COV_{(IMEP)}$. When injection timing was advanced, $COV_{(IMEP)}$ was reduced for all fueling conditions. The operation stability was improved under PREMIER combustion regardless of CO_2 fraction in the mixture. The $COV_{(IMEP)}$ of PREMIER operation mode for all fueling conditions is less than 5%. The lowest $COV_{(IMEP)}$ of PREMIER combustion was observed for the 50% CO_2 fraction in the mixture at θ_{inj} = 20°BTDC ($COV_{(IMEP)}$ =2.9%).

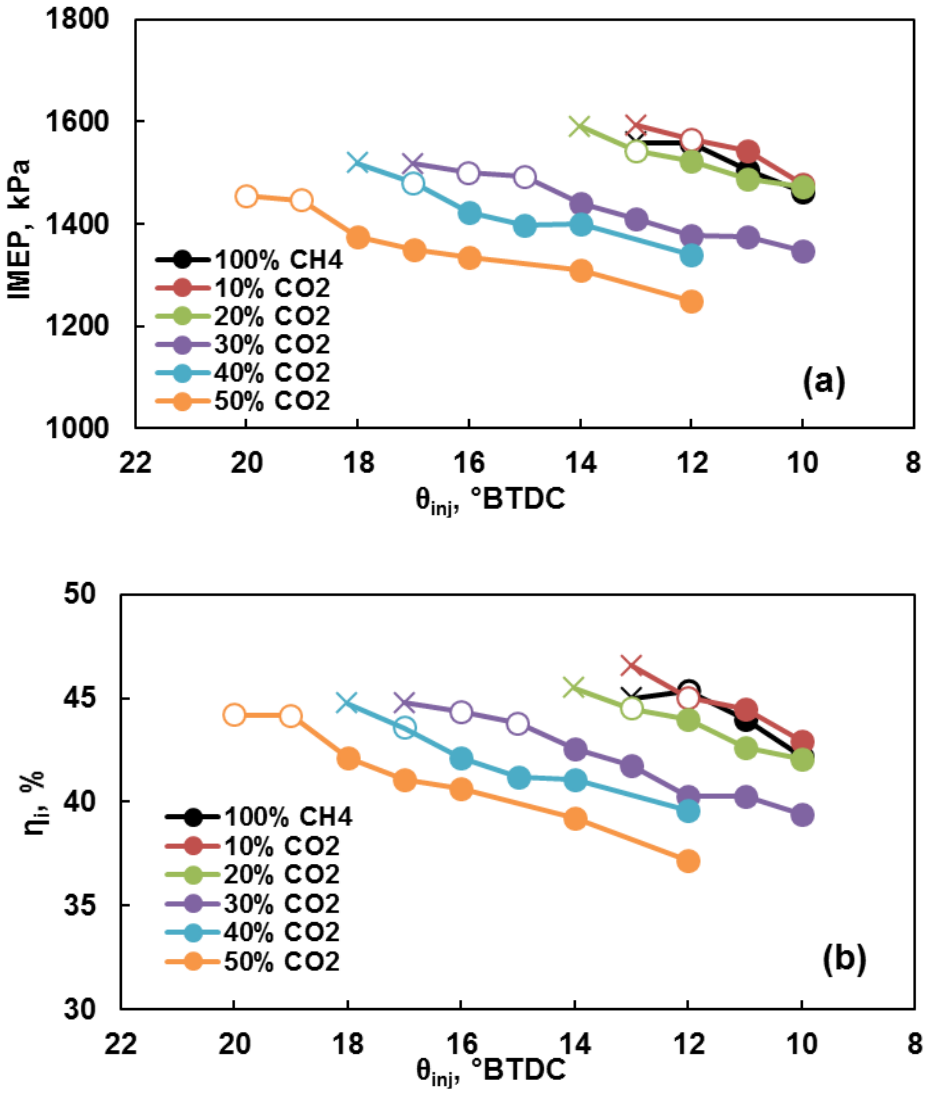

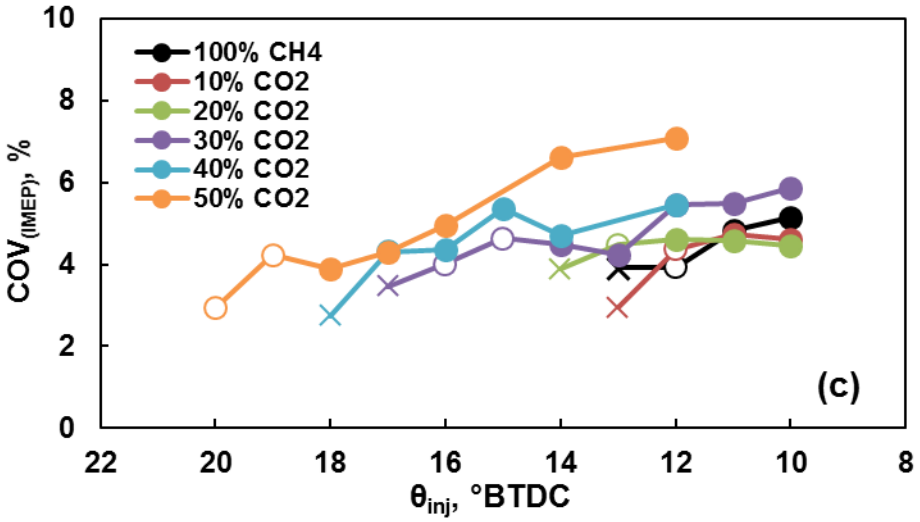

Figure 5.11: Engine performance: (a) indicated mean effective pressure (IMEP); (b) indicated thermal efficiency; (c) coefficient of variation of the IMEP

5.3.3 Maximum cylinder pressure and maximum pressure rise rate

Figure 5.12 depicts the maximum cylinder pressure as a function of CO_2 in the mixture. All data shown here are the average value of 80 cycles. The maximum obtainable cylinder pressure increases with higher CO_2 in the mixture. Dashed line in the Figure 5.12 shows that maximum cylinder pressure increases with increases of CO_2 in the mixture. Maximum cylinder pressure of PREMIER combustion is 11.8 MPa for mixture from 0 to 30% CO_2, 12.1 MPa for 40% CO_2 and 12.7 MPa for 50% CO_2 in the mixture. Above these pressure levels, it is observed that the cylinder pressure after passing through the band-pass-filter shows a KI larger than 0.1 MPa. Figure 5.13 shows the maximum rate of pressure rise as a function of CO_2 in the mixture. The maximum rate of pressure rise of 483 kPa/°CA was obtained for 50% CO_2 mixture and lowest pressure rise rate was observed for pure methane as a 342 kPa/°CA. The increase of pressure rise is noticeable between 20% CO_2 mixture and 50% CO_2 mixture and it can be seen by steep dashed line in Figure 5.13. The fuel mixture from 0% to 30% CO_2 shows maximum rate of pressure rise below 400 kPa/°CA. In the study of [40] and [41], it is observed that pressure rise

rate higher than 400 kPa/°CA yielded knocking by using natural gas-hydrogen blends as a gaseous fuel and diesel as a pilot fuel. Aksu et al. [37] reported maximum pressure rise of 400 kPa/°CA for 0 to 60% hydrogen ratio in the methane. However, the critical pressure rise rate depends on operation condition and mixture. In this study, it is inferred that for higher CO_2 ratio in the mixture namely 40 and 50%, pressure rise rate of 428 kPa/°CA and 483 kPa/°CA could be a safe limit. However, knocking cycles have both high maximum in-cylinder pressures and maximum rate of pressure rise.

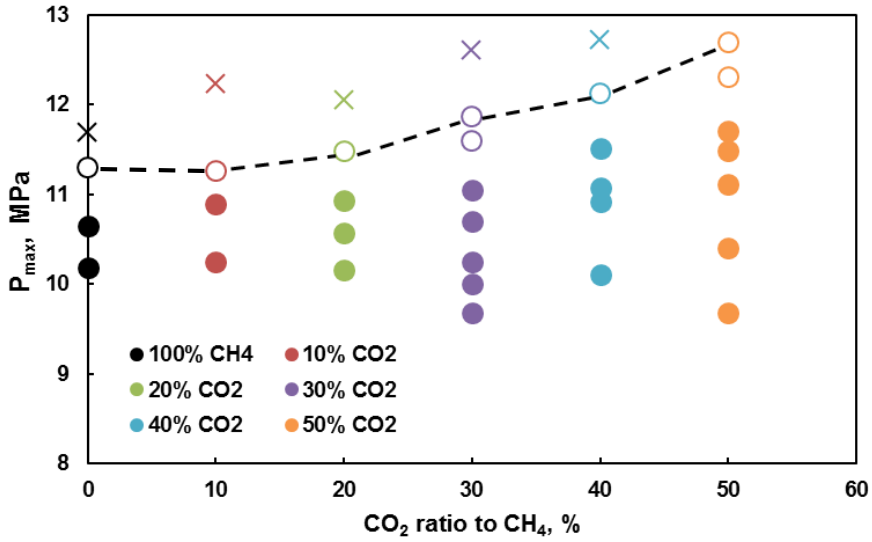

Figure 5.12: Maximum cylinder pressure versus CO_2 concentration

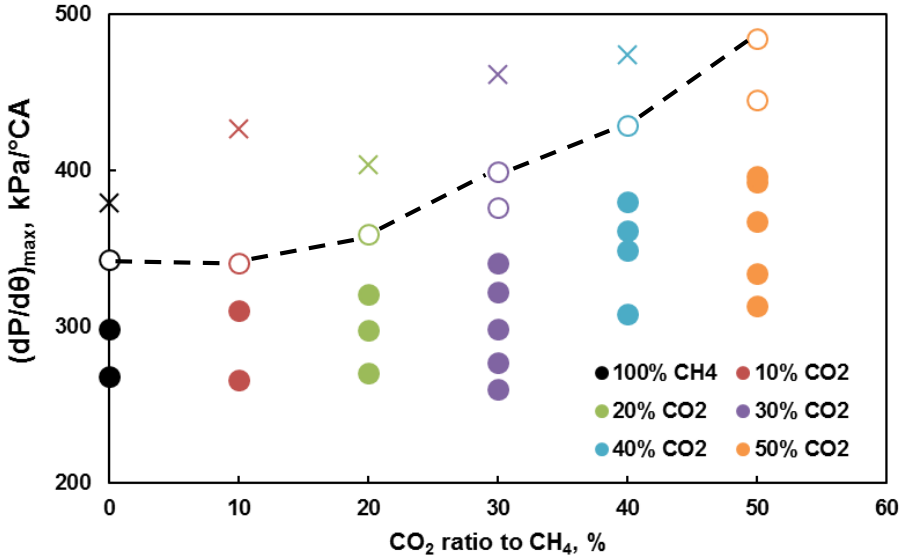

Figure 5.13: Maximum of pressure rise rate versus CO_2 concentration

5.3.4 Exhaust emissions

Exhaust emissions of NO_x, HC and CO are shown in Figures 5.14(a), (b) and (c), respectively. Similar to section 5.3.2, due to experiment condition, pure methane showed lower NO_x emission than 10% CO_2 mixture. However, NO_x emissions were decreased with increasing CO_2 in the mixture. It is due to presence of non-reactive CO_2 which results lower combustion temperature. It is known that NO_x emissions are highly temperature dependent and therefore, by increasing CO_2 in the mixture, lower NO_x emission is emitted [18]. On the other hand, advancement of injection timing promoted NO_x emissions. It is reported that when injection timing is advanced, ignition start in an earlier stage (earlier CA), thus almost all injected fuels are burned before TDC during compression stroke, hence, in-cylinder temperature as well as unburned gas temperature increase and consequently increases NOx emissions [19]. NOx emissions were maximum under PREMIER operation except knocking. It may be due to higher cylinder temperature as a result of end-gas autoignition that caused the higher NOx emissions. Dashed line in Figure 5.14(a) indicates that maximum NO_x emissions were gradually decreased when CO_2 increased in the mixture. In regards to HC and CO emissions, both of these emissions were increased by increasing the CO_2 in the mixture. Lower combustion temperature causes higher CO and HC emissions as a result of incomplete combustion [18, 19]. When injection timing was advanced, both HC and CO emissions decreased. However, the influence of injection timing is noticeable for 50% CO_2, 40% CO_2 and 30% CO_2 mixtures but for the rest of cases, it is little effect and the results are almost similar. The minimum HC and CO emissions are observed under PREMIER combustion for each fueling cases owing to end-gas autoignition. Under PREMIER operation, unburned mixture undergoes autoignition after main combustion of gaseous fuel-air mixture and therefore, the amount of HC and CO decrease. However, dashed line in Figure 5.14(b) and (c) indicates that values of HC

emission under PREMIER combustion are very close among all fueling cases while in case of CO emission, slightly increase under PREMIER combustion was observed.

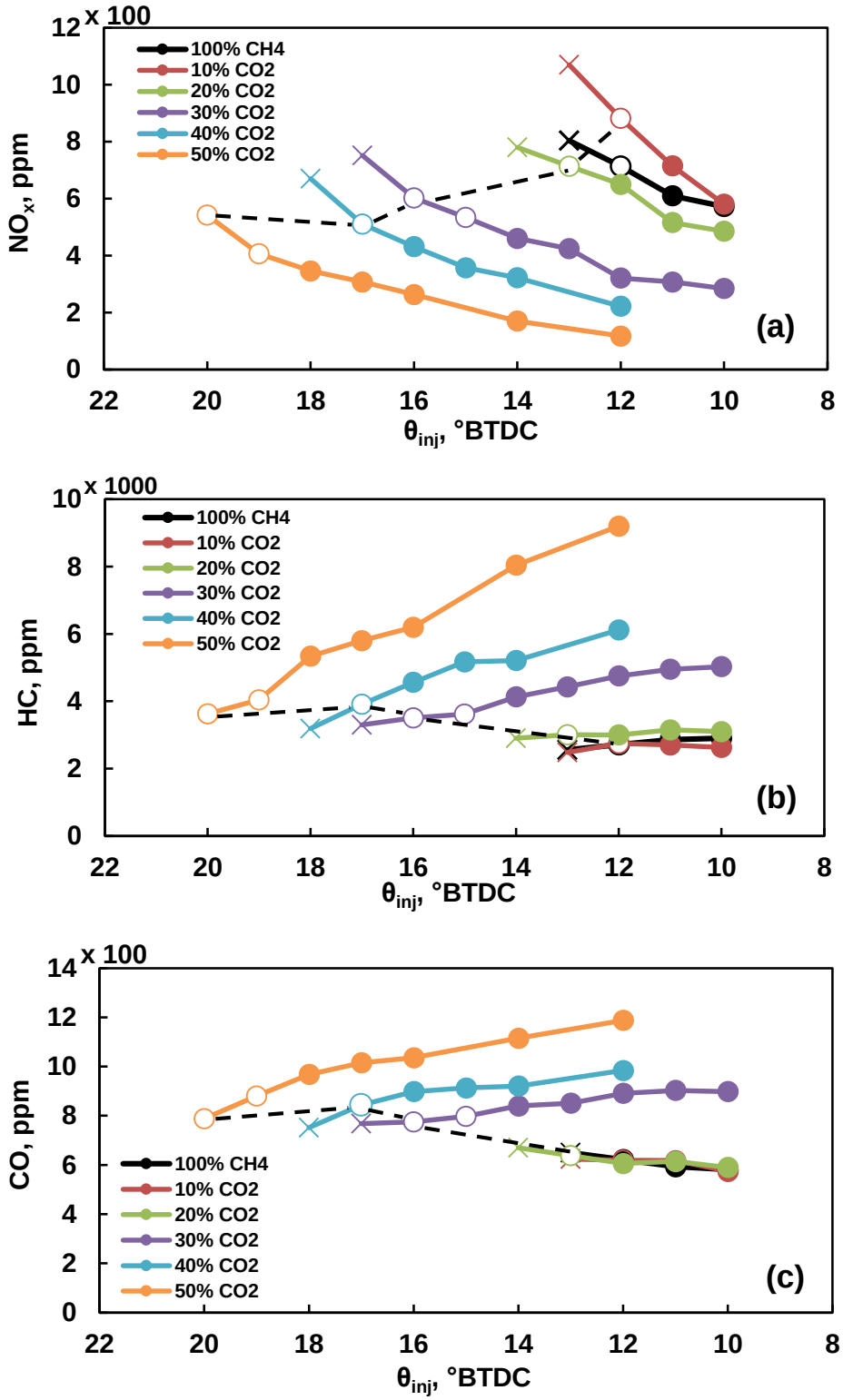

Figure 5.14: Exhaust emissions of: (a) NO_x (b) unburned hydrocarbon (c) carbon monoxide

5.3.5 End-gas autoignition characteristics

Figure 5.15 explains PREMIER combustion and related parameters that can be obtained from rate of heat release. The pilot fuel ignition timing, θ_{ign}, is identified from inflection point in the ROHR curves. Similarly, a parameter of θ_{ea}, end-gas autoignition timing, is determined from the times of inflection shown in the ROHR curves. Ignition delay of end-gas autoignition, τ_{ea}, is defined as time interval between θ_{ign} and θ_{ea}. The duration of heat release during end-gas autoignition, $\Delta\theta_{ea}$, begins at θ_{ea} and continues until end-gas heat release is complete. The amount of heat released during flame propagation and during end-gas autoignition, Q_{ea}, are shown in Figure 5.15, too. The yellow colored area delimited by the straight dashed line in Figure 5.15 is the region of end-gas autoignition heat release, obtained by examining the rate of heat release at the start and end of this time. The heat released due to flame propagation is defined as the region below the straight line (blue colored area). The PREMIER intensity, PI, is further determined by using these parameters based on the end-gas autoignition data and is defined as:

$$\mathrm{PI} = \frac{100 * (Q_{ea}/Q_{total})}{\Delta\theta_{egai}} \qquad (5.1)$$

where Q_{ea}, Q_{total}, and $\Delta\theta_{ea}$ are the amount of heat released during end-gas autoignition, the total energy inputs of all fuels, and the duration of heat release following end-gas autoignition, respectively. We exploit the relationship between the proportion of heat released during end-gas autoignition and the duration of such release because this indicates the amount of heat released per unit time during such combustion.

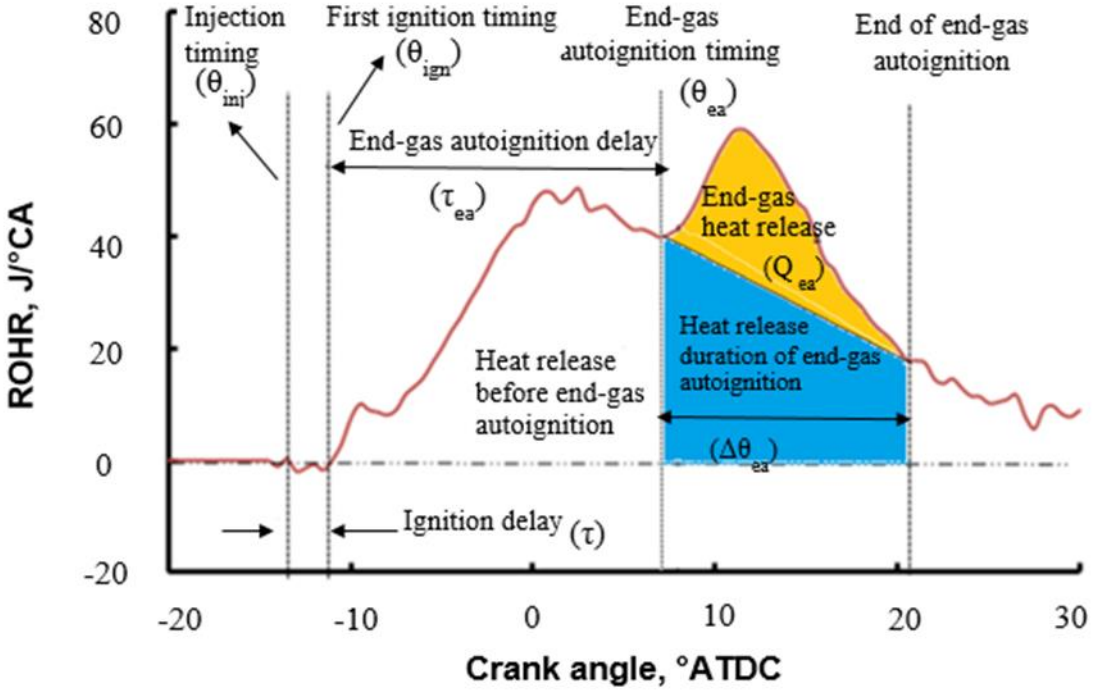

Figure 5.15: Graphical representation of parameters describing PREMIER combustion

5.3.5.1 End-gas autoignition timing and delay

Figure 5.16 shows the average end-gas autoignition timing of PREMIER cycles as a function of pilot fuel injection timing. It is determined as a duration in degree of crank angle of commencement of end-gas autoignition after TDC. Figure 5.16 shows that when pilot fuel injection timing was advanced, end-gas autoignition was commenced earlier. Advancing injection timing causes higher pressure and temperature of unburned mixture as a result of longer ignition delay of initial combustion. Increasing CO_2 in the mixture causes slightly earlier commencement of the end-gas autoignition. It is known that specific heat ratio of CH_4 is higher than CO_2, thus, mixture with higher CO_2 has a lower specific heat ratio. Combustion of lower specific heat ratio mixture results higher in-cylinder pressure and temperature and thus, earlier commencement of end-gas autoignition. When CO_2 in the mixture is increased, it was possible to advance injection timing earlier, so combustion is triggered earlier and rate of heat released during main

combustion was larger before TDC as shown in Figure 5.3(b). An earliest end-gas autoignition commencement of PREMEIR combustion was observed for 50% CO_2 mixture which was 9.18 °ATDC.

Figures 5.17 represents the end-gas autoignition delay and it is determined as a duration in degree of crank angle between ignition timing of pilot fuel and commencement of end-gas autoignition. Advancing the injection timing did not affect on end-gas autoignition delay noticeably. However, by increasing CO_2 in the mixture, end-gas autoignition delay was slightly longer. The delay of end-gas autoignition strongly depends on ROHR of initial and main combustion. Increasing CO_2 in the mixture causes lower flame propagation speed, thus, it takes longer time for mixture to be autoignited. Also, heating value of the mixture with higher CO_2 is lower and it reduces combustion activity of in-cylinder mixture and therefore, delay of end-gas autoignition becomes longer. In fact, longer end-gas autoignition delay helps to avoid sudden pressure rise due to less fraction of mixture undergoing autoignition and thus, knocking is avoided. However, end-gas autoignition delays of PREMIER combustion are almost similar for all fuelling cases with minor increase for the mixture with larger CO_2 in the mixture.

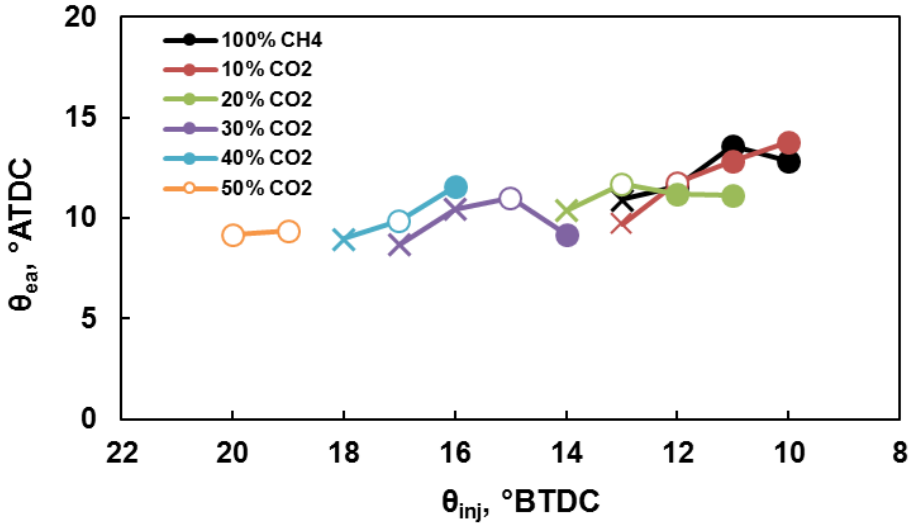

Figure 5.16: Average end-gas autoignition timing of all fueling conditions

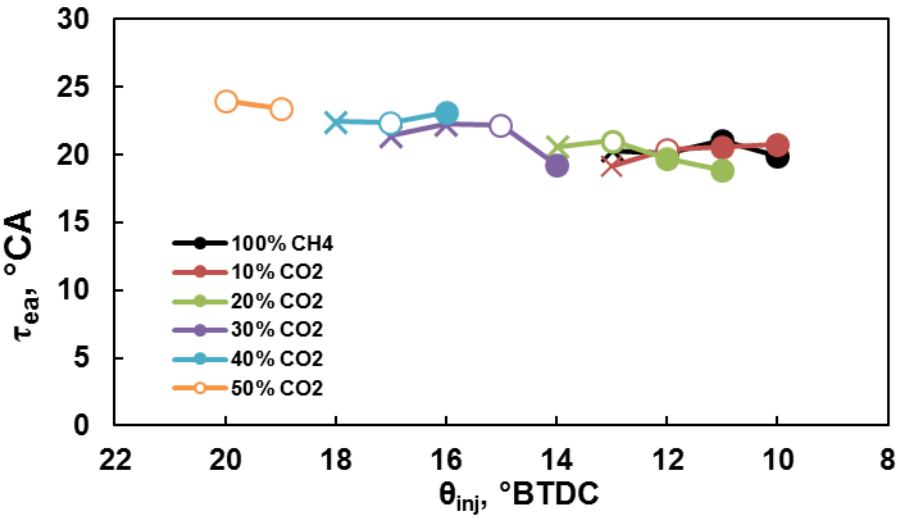

Figure 5.17: Average end-gas autoignition delay of all fueling conditions

5.3.5.2 Heat release after end-gas autoignition, the duration of heat release during end-gas autoignition and PREMIER intensity

The average heat release after end-gas autoignition (Q_{ea}) values of cycles exhibiting end-gas autoignition are shown in Figure 5.18. The Q_{ea} value increased when injection timing was advanced at the same fueling condition because number of cycles featuring end-gas autoignition became larger as a result of advancing injection timing as shown in Figure 5.9(b). Mixture with higher CO_2 in the mixture sustained lower Q_{ea} value. In previous chapter, in simulated biogas experiment, it was found that when number of cycles featuring end-gas autoignition is the largest, the value of Q_{ea} is also the largest in the same injection timing. Also, fuel mixture component affects the value of Q_{ea} as well as injection timing. Addition of larger CO_2 in the mixture slightly dropped the heating value and it can be seen from Figure 5.3(b) that the third peak as a result of end-gas autoignition (PREMIER combustion) is fallen. Same scenario was observed in Figure 5.18 as well and the value of Q_{ea} gradually decreased under PREMIER combustion for all fuelling cases. Figure 5.19 shows the duration of heat release due to end-gas autoignition ($\Delta\theta_{ea}$). The value of $\Delta\theta_{ea}$ is determined by the duration from beginning to the end of end-gas

autoignition. Both injection timing and fuel mixture did not have so much effect on $\Delta\theta_{ea}$ value when PREMIER combustion cases are selected. The value of $\Delta\theta_{ea}$ is mainly influenced by the end-gas volume. In the previous study of simulated biogas, it is observed that larger mass of end-gas region prolonged $\Delta\theta_{ea}$. When end-gas autoignition occurs later, majority of the premixed mixture will be consumed by propagating flames, leaving a smaller portion to be autoignited. Smaller end-gas volume needs shorter time to be autoignited if the temperature as well as pressure do not rise significantly in that region. When temperature and pressure are not very high, sudden pressure rise as a result of high intensity autoignition does not occur and thus, PREMIER combustion may be achieved with longer duration of end-gas autoignition. However, in this study, $\Delta\theta_{ea}$ did not change because end-gas autoignition timing of all fuelling cases shown in Figure 5.16 did not change much. Also, number of cycles featuring end-gas autoignition are very close to each other for all fuelling cases as shown in Figure 5.9(b). These two scenarios cause $\Delta\theta_{ea}$ unchanged.

Figure 5.20 shows the PI value as a function of injection timing of pilot fuel. The trend is similar to Figure 5.18. It can be seen from equation (5.1) that parameters of Q_{ea} and $\Delta\theta_{ea}$ are used in determining PI value. As shown in Figure 5.18, Q_{ea} is decreased when CO_2 increased in the mixture and on the other hand, $\Delta\theta_{ea}$ value did not change in all fuelling cases, thus, PI value was much influenced by amount of Q_{ea} and consequently followed similar trend to the Q_{ea}. When injection timing of pilot fuel was advanced, PI value increased because number of cycles with end-gas autoignition was larger and larger amount of heat from end-gas region was released. Cycles with smaller number of end-gas autoignition displayed the lower PI values in their respective groups. Knocking cycles allocate the peak values in their respective data set except 50% CO_2 mixture that there is not any knocking data.

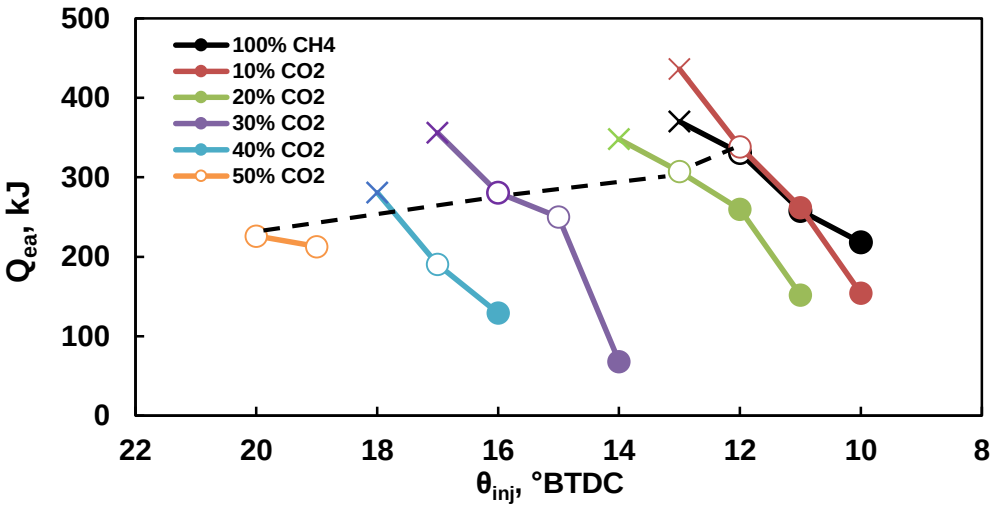

Figure 5.18: Average heat release via end-gas autoignition

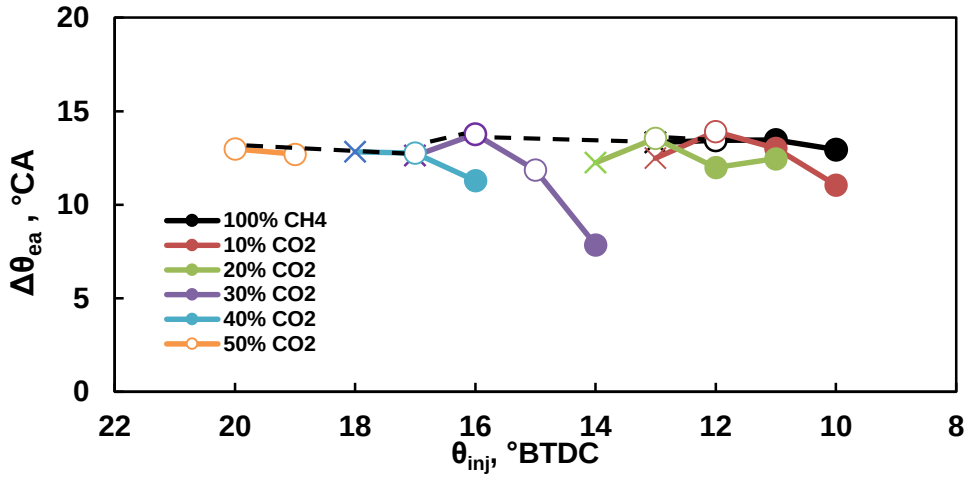

Figure 5.19: Average heat release duration of end-gas autoignition

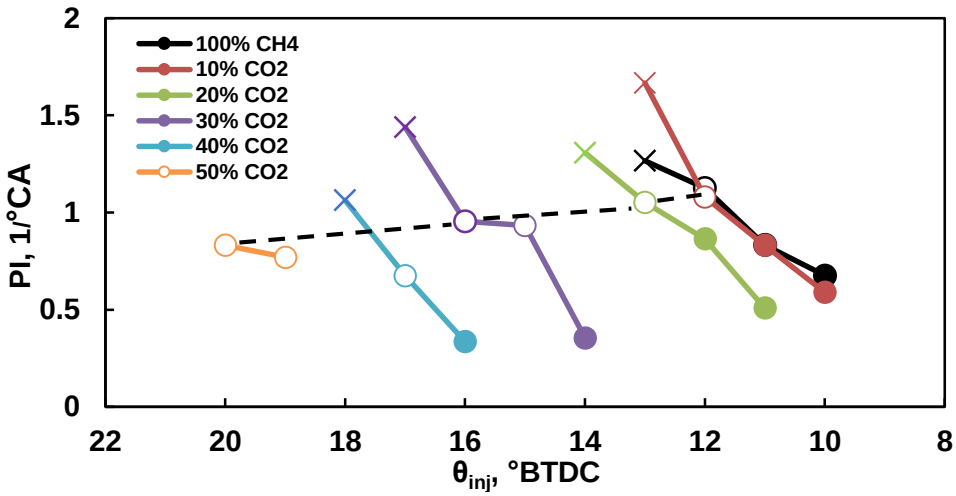

Figure 5.20: Average PREMIER intensity

5.3.5.3 Relationship between PI and thermal efficiency

Figure 5.21 and 5.22 show a relationship between PI and thermal efficiency and relationship between PI and IMEP for all fueling conditions. Here we tried to clarify the relationship between these parameters and data shown here are all cycles' data. Knocking cycles are indicated by cross mark symbols. The strong relationship between PI value and those of thermal efficiency and IMEP was found. Thermal efficiency increased when PI increased. It means that PREMIER combustion could help to improve the engine thermal efficiency by means of knock-free end-gas autoignition. Data shown on PI= 0 column represent normal combustion cycles without any end-gas autoignition. It is observed that knocking cycles occurrence started at PI value larger than 1.4 deg.$^{-1}$, thus, this is indicated as a knocking criteria. There are cycles that featuring end-gas autoignition in the area which mostly knocking cycles are shown (PI> 1.4 deg.$^{-1}$) but they are not knocking. These cycles exhibit higher intensity of end-gas autoignition and they expected to yield knocking. However, we think that these cycles underwent autoignition in later stage when the engine is already in expansion stroke. Therefore, autoignited mixture could help for faster expansion rate and thus suppress the pressure rise due to end-gas autoignition and consequently, yields PREMIER combustion. The same scenario was observed for IMEP.

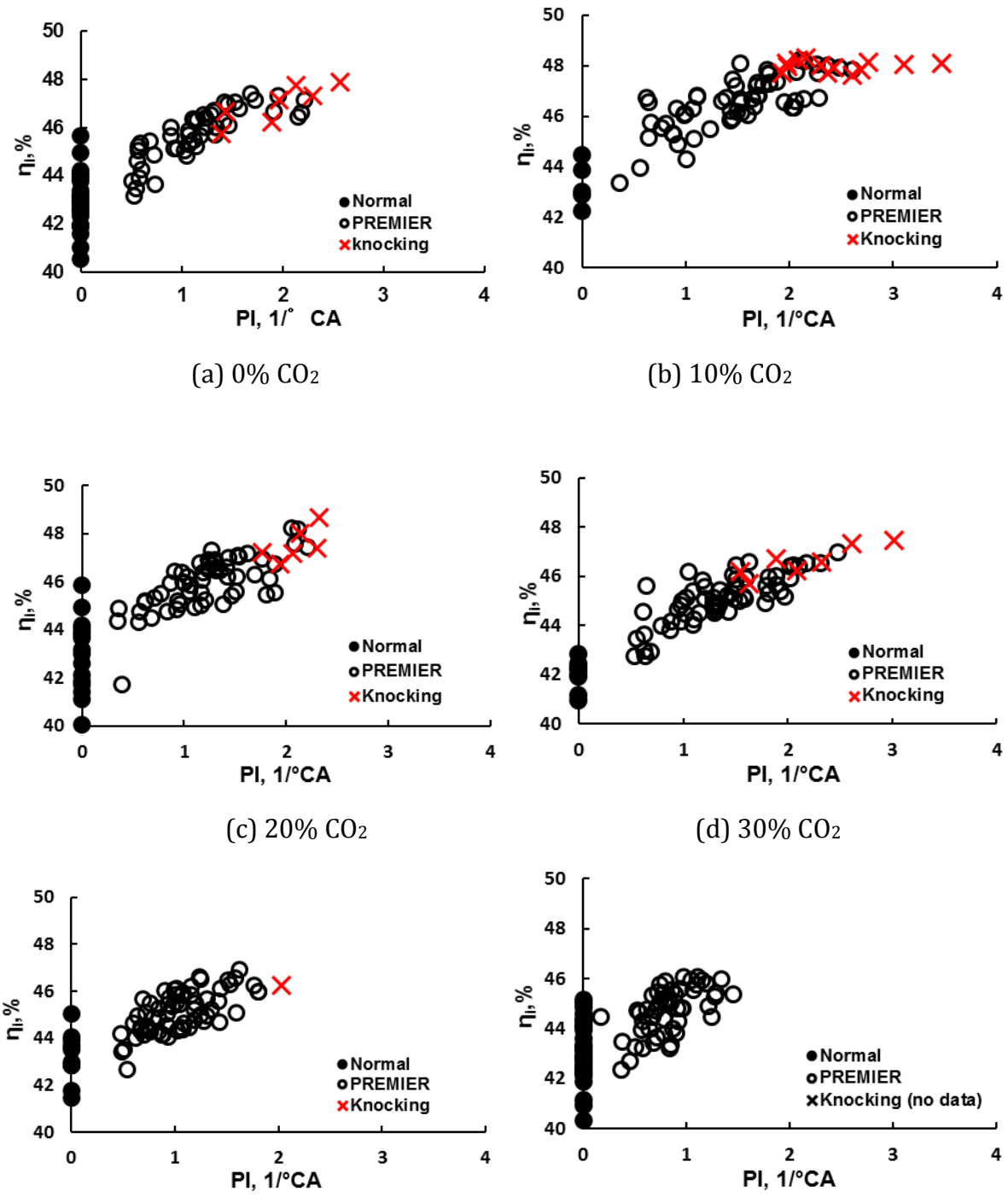

(a) 0% CO_2 (b) 10% CO_2

(c) 20% CO_2 (d) 30% CO_2

(e) 40% CO_2 (f) 50% CO_2

Figure 5.21: Relationship between PI and thermal efficiency for all fueling conditions

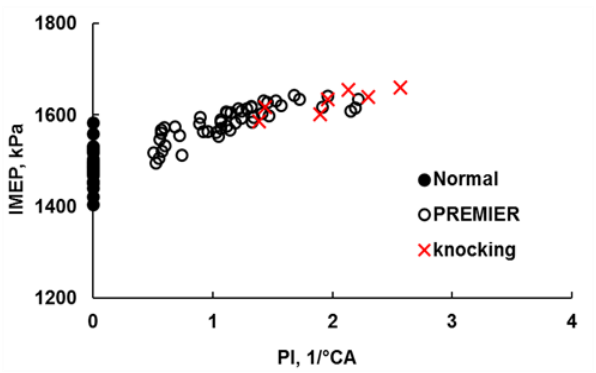

(a) 0% CO_2

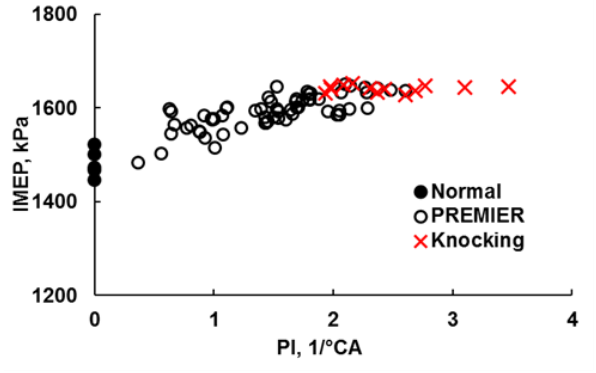

(b) 10% CO_2

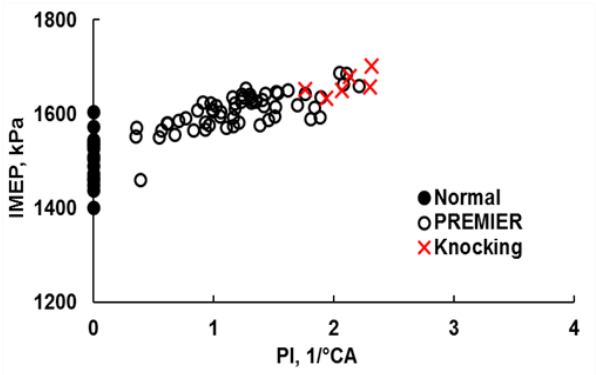

(c) 20% CO_2

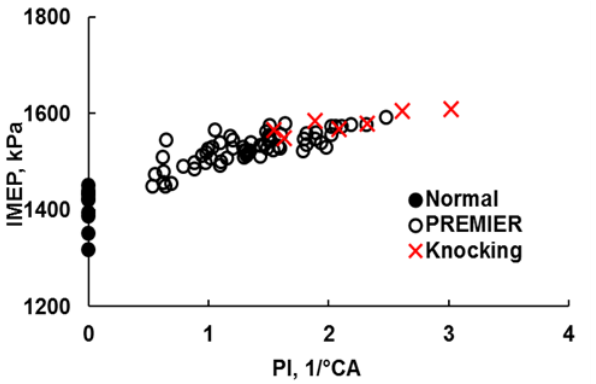

(d) 30% CO_2

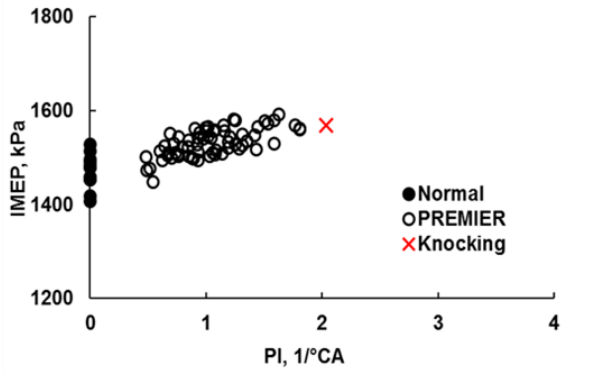

(e) 40% CO_2

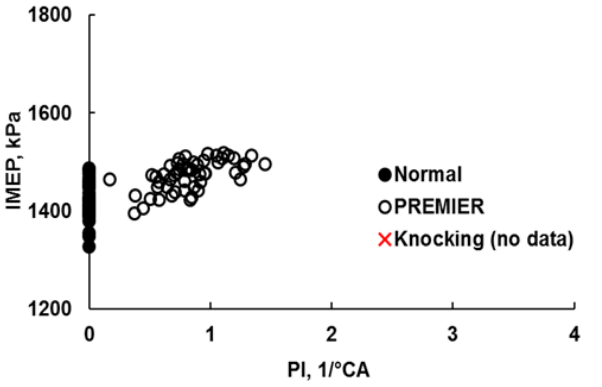

(f) 50% CO_2

Figure 5.22: Relationship between PI and IMEP for all fueling conditions

5.4. Summary of observations

In this study, experiments were carried out in the dual-fuel gas engine at constant speed of 1,000 rpm with different pilot fuel injection timing at supercharged condition with intake pressure of 200kPa. Simulated biogas containing CH_4 and CO_2 was used. The CO_2 in the mixture was changed from 0 to 50% by volume. Engine performance, emissions and end-gas autoignition characteristics were evaluated. Relationship between PREMIER intensity and engine performance were clarified by cycle-to-cycle analysis of all data. The following results were obtained:

1. A relationship between PI and thermal efficiency and PI and IMEP are evaluated. It is inferred that better engine performance can be achieved by higher PREMIER intensity.

2. IMEP and thermal efficiency were increased when injection timing was advanced, However, IMEP and thermal efficiency of PREMIER combustion slightly decreased by addition of CO_2 in the mixture.

3. The PI value of 1.4 $deg.^{-1}$ was observed as commencement of knocking combustion in pure methane case. However, there were cycles of end-gas autoignition without pressure oscillation with the PI value larger than 1.4 $deg.^{-1}$.

4. The maximum value of attainable in-cylinder pressure and pressure rise rate increased with increase in CO_2 in the mixture.

5. End-gas autoignition timing became shorter when CO_2 increased in the mixture and injection timing was advanced. However, end-gas autoignition delay of mixture with higher CO_2 was slightly longer.

6. Advancing injection timing caused increase of Q_{ea} value and PI. In selecting PREMIER combustion, addition of CO_2 in the mixture decreased the Q_{ea} value and PI because of higher non-combustible CO_2 gas, however, $\Delta\theta_{ea}$ value did not change significantly.

7. When injection timing was advanced and PREMIER combustion was achieved, emissions of HC and CO decreased although NO_x increased. However, under PREMEIR operation, NO_x emission could reduce by increasing CO_2 in the mixture with slightly penalty of CO and HC emissions.

References

[1] A. Henham and M. K. Makkar, Combustion of simulated biogas in a dual-fuel diesel engine, Energy Conversion and Management; 39(1998); 2001–2009.

[2] Y. Kim, N. Kawahara, K. Tsuboi, E. Tomita, Combustion characteristics and NO_X emissions of biogas fuels with various CO_2 contents in a micro co-generation spark-ignition engine, Applied energy; 182(2016); 539-547.

[3] N. Tippayawong, A. Promwungkwa, P. Rerkkriangkrai, Long-term operation of a small biogas/diesel dual-fuel engine for on-farm electricity generation, Biosystem Engineering; 98(2007); 26–32.

[4] H. Jingdang, R.J. Crookes, Assessment of simulated biogas as a fuel for the spark ignition engine, Fuel; 77(1998); 1793-1801.

[5] S.O. Bade Shrestha and G. Narayanan, Landfill gas with hydrogen addition – A fuel for SI engines, Fuel; 87(2008); 3616–3626.

[6] E. Porpatham, A. Ramesh, and B. Nagalingam, Investigation on the effect of concentration of methane in biogas when used as a fuel for a spark ignition engine, Fuel; 87(2008); 1651–1659.

[7] S. Verma, L. Das, S. Kaushik, Effects of varying composition of biogas on performance and emission characteristics of compression ignition engine using exergy analysis, Energy Conversion and Management; 138 (2017); 346-359.

[8] F. Z. Aklouche, K. Loubar, A. Bentebbiche, S. Awad, M. Tazerout, Experimental investigation of the equivalence ratio influence on combustion, performance and exhaust emissions of a dual fuel diesel engine operating on synthetic biogas fuel, Energy Conversion and Management; 152 (2017); 291–299.

[9] D. Barik, S. Murugan, Investigation on combustion performance and emission characteristics of a DI (direct injection) diesel engine fueled with biogas- diesel in dual fuel mode, Energy; 72 (2014); 760–771.

[10] B. J. Bora and U. K. Saha, Optimization of injection timing and compression ratio of a raw biogas powered dual fuel diesel engine, Applied Thermal Engineering; 92 (2016); 111–121.

[11] V. Makareviciene, E. Sendzikiene, S. Pukalskas, A. Rimkusb and R. Vegneris, Performance and emission characteristics of biogas used in diesel engine operation, Energy Conversion and Management; 75 (2013); 224–233.

[12] B. J. Bora, UK Saha, S. Chatterjee and V. Veer, Effect of compression ratio on performance, combustion and emission characteristics of a dual fuel diesel engine run on raw biogas, Energy Conversion and Management; 87 (2014); 1000–1009.

[13] K. Cacua, A. Amell, F. Cadavid, Effects of oxygen enriched air on the operation and performance of a diesel-biogas dual-fuel engine, Biomass and Bioenergy; 45(2012); 159–167.

[14] D. Barik, A. K. Satapathy and S. Murugan, Combustion analysis of the diesel–biogas dual fuel direct injection diesel engine– the gas diesel engine, International Journal of Ambient Energy; 38 (2015); 259–266.

[15] H. Ambarita, Performance and emission characteristics of a small diesel engine run in dual-fuel (diesel-biogas) mode, Case Studies in Thermal Engineering; 10 (2017); 179–191.

[16] M. Feroskhan and S. Ismail, Investigation of the effects of biogas composition on the performance of a biogas–diesel dual fuel CI engine, Biofuels; 7 (2016); 593–601.

[17] SS. Kalsi, K. Subramanian, Effect of simulated biogas on performance, combustion and emissions characteristics of a bio-diesel fueled diesel engine, Renewable Energy; 106(2017); 78-90.

[18] SH. Yoon, CS. Lee, Experimental investigation on the combustion and exhaust emission characteristics of biogas–biodiesel dual-fuel combustion in a CI engine, Fuel Processing Technology; 92(2011); 992-1000.

[19] B. Sahoo, N. Sahoo, U. Saha, Effect of engine parameters and type of gaseous fuel on the performance of dual-fuel gas diesel engines—A critical review, Renewable and Sustainable Energy Reviews; 13(2009); 1151-1184.

[20] SH. Park, SH. Yoon, J. Cha, CS. Lee, Mixing effects of biogas and dimethyl ether (DME) on combustion and emission characteristics of DME fueled high-speed diesel engine, Energy; 66(2014); 413-422.

[21] D. Barik, S. Murugan, N. Sivaram, E. Baburaj, PS. Sundaram, Experimental investigation on the behavior of a direct injection diesel engine fueled with Karanja methyl ester-biogas dual fuel at different injection timings, Energy; 118(2017); 127-138.

[22] BJ. Bora, UK. Saha, Experimental evaluation of a rice bran biodiesel–biogas run dual fuel diesel engine at varying compression ratios, Renewable Energy; 87(2016); 782-790.

[23] G. A. Karim. An examination of some measures for improving the performance of gas fuelled diesel engines at light load, SAE Technical Paper; 912366, (1991).

[24] Z. Wang. Z. Zhao, D. Wang, M. Tan, Y. Han, Z. Liu and H. Dou, Impact of pilot diesel ignition mode on combustion and emissions characteristics of a diesel/natural gas dual fuel heavy-duty engine, Fuel; 167(2016); 248–256.

[25] ID. Bedoya, S. Saxena, FJ. Cadavid, RW. Dibble, M. Wissink, Experimental study of biogas combustion in an HCCI engine for power generation with high indicated efficiency and ultra-low NOx emissions, Energy Conversion and Management; 53(2012); 154-162.

[26] S. Swami Nathan, JM. Mallikarjuna, A. Ramesh, An experimental study of the biogas–diesel HCCI mode of engine operation, Energy Conversion and Management; 51(2010); 1347–1353.

[27] ID. Bedoya, S. Saxena, FJ. Cadavid, RW. Dibble, M. Wissink, Experimental evaluation of strategies to increase the operating range of a biogas-fueled HCCI engine for power generation, Applied Energy; 97(2012); 618-629.

[28] SH. Park, SH. Yoon, Effect of dual-fuel combustion strategies on combustion and emission characteristics in reactivity controlled compression ignition (RCCI) engine, Fuel; 181(2016); 310-318.

[29] L. Bates, D. Bradley, I. Gorbatenko, A. S. Tomlin, Computation of methane/air ignition delay and excitation times, using comprehensive and reduced chemical mechanisms and their relevance in engine autoignition, Combustion and Flame; 185 (2017); 105–116.

[30] N. Kawahara, E. Tomita, Y. Sakata, Auto-ignited kernels during knocking combustion in a spark-ignition engine, Proceedings of the Combustion Institute; 31 (2007); 2999–3006.

[31] L. Bates, D. Bradley, G. Paczko, N. Peters, Engine hot spots: Modes of auto-ignition and reaction propagation, Combustion and Flame; 166 (2016); 80–85.

[32] U. Azimov , E. Tomita , N. Kawahara and Y. Harada, Premixed mixture ignition in the end-gas region (PREMIER) combustion in a natural gas dual-fuel engine: operating range and exhaust emissions, International Journal of Engine Research; 12 (2011); 484–497.

[33] E. Tomita, Y. Harada, N. Kawahara and A. Sakane, Effect of EGR on combustion and exhaust emissions in supercharged dual-fuel natural gas engine ignited with diesel fuel, SAE Technical Paper; 2009-01-1832, (2009).

[34] E. Tomita, N. Kawahara and J. Zheng, Visualization of auto-ignition of end gas region without knock in a spark-ignition natural gas engine, Journal of KONES. Powertrain and Transport; 17 (2010), 521–527.

[35] U. Azimov, E. Tomita, N. Kawahara and Y. Harada, Effect of syngas composition on combustion and exhaust emission characteristics in a pilot-ignited dual-fuel engine operated in PREMIER combustion mode, International Journal of Hydrogen Energy; 36 (2011), 11985–11996.

[36] U. Azimov, E. Tomita and N. Kawahara, Ignition, combustion and exhaust emission characteristics of micro-pilot ignited dual-fuel engine operated under PREMIER combustion mode, SAE Technical Paper; 2011-01-1764, (2011).

[37] C. Aksu, N. Kawahara, K. Tsuboi, S. Nanba, E. Tomita and M. Kondo, Effect of hydrogen concentration on engine performance, exhaust emissions and operation range of PREMIER combustion in a dual fuel gas engine using methane-hydrogen mixtures, SAE Technical Paper; 2015-01-1792, (2015).

[38] C. Aksu, N. Kawahara, K. Tsuboi, M. Kondo and E. Tomita, Extension of PREMIER combustion operation range using split micro pilot fuel injection in a dual fuel natural gas compression ignition engine: A performance-based and visual investigation, Fuel; 185 (2016), 243–253.

[39] N. Kawahara, Y. Kim, H. Wadahama, K. Tsuboi, E. Tomita, Differences between PREMIER combustion in a natural gas spark-ignition engine and knocking with pressure oscillations, Proceedings of the Combustion Institute; 37 (2019), 4983–4991.

[40] J. Kubash, D. Brehob, Analysis of knock in a dual- fuel engine, SAE Technical Paper; 922367 (1992-10-01). doi: 10.4271/922367.

[41] PV. Puzinauskas, Examination of methods used to characterize engine knock, SAE Technical Paper; 920808 (1992-02-01). Doi: 10.4271/920808.

6. Conclusions

In this study, experiment is carried out in a single cylinder, direct injection, dual-fuel gas engine under constant speed of 1000rpm. Simulated biogas consisted of CH_4, CO_2 and N_2 at 58, 35 and 7% by volume, respectively is used as a primary fuel in the first part of this study. Experiments were performed at three intake pressures (101, 150, and 200 kPa), with various pilot fuel injection times. The second part of this study aimed to investigate the effect of CO_2 ratio to CH_4 with the same engine and operating conditions. Engine performance, exhaust emissions and combustion characteristics are evaluated. PREMIER combustion, as a promising strategy for improvement of engine performance and thermal efficiency, is studied in details. The following results are obtained:

- **Simulated biogas (CH_4-CO_2-N_2) experiment:**

1. The parameter PI is proposed and used to evaluate the characteristics of PREMIER combustion. The PI value increased as the heat released by end-gas autoignition increased, and as the duration of heat release is extended. However, the Q_{ea}/Q_{total} ratio affected the PI more so than did the $\Delta\theta_{ea}$.

2. When PREMIER combustion is achieved, the heat released by end-gas autoignition and the PI increased as the injection timing is advanced. Under such circumstances, the number of cycles featuring end-gas autoignition increased and more heat is released in the end-gas region.

3. The ROHR values of both the initial and main combustion affected the occurrence of end-gas autoignition. When the pressure and temperature of a premixed fuel mixture rose as injection timing is advanced, end-gas autoignition commenced earlier. The end-gas autoignition delay became shorter as intake pressure is increased and injection

timing advanced, because of the lower MFB before end-gas autoignition commenced. Under these conditions, less mixture is consumed during principal combustion, and more is burned in the end-gas region.

4. Advancing the injection timing and increasing the intake pressure improved both the IMEP and thermal efficiency because end-gas autoignition then occurred. The higher the number of cycles featuring end-gas autoignition, the greater the thermal efficiency, because of the larger amount of positive work performed during the expansion stroke.

- **Simulated biogas (CH_4-CO_2) experiment:**

1. A relationship between PI and thermal efficiency and PI and IMEP are evaluated. It is inferred that better engine performance can be achieved by higher PREMIER intensity.

2. IMEP and thermal efficiency are increased when injection timing is advanced, However, IMEP and thermal efficiency of PREMIER combustion slightly decreased by addition of CO_2 in the mixture.

3. The PI value of 1.4 deg.$^{-1}$ was observed as commencement of knocking combustion in pure methane case. However, there were cycles of end-gas autoignition without pressure oscillation with the PI value larger than 1.4 deg.$^{-1}$.

4. The maximum value of attainable in-cylinder pressure and pressure rise rate increased with increase in CO_2 in the mixture.

5. End-gas autoignition timing became shorter when CO_2 increased in the mixture and injection timing is advanced. However, end-gas autoignition delay of mixture with higher CO_2 was slightly longer.

6. Advancing injection timing caused increase of Q_{ea} value and PI. In selecting PREMIER combustion, addition of CO_2 in the mixture decreased the Q_{ea} value and PI because of higher non-combustible CO_2 gas, however, $\Delta\theta_{ea}$ value did not change significantly.

7. When injection timing is advanced and PREMIER combustion is achieved, emissions of HC and CO decreased although NO_x increased. However, under PREMEIR operation, NO_x emission could reduce by increasing CO_2 in the mixture with slightly penalty of CO and HC emissions.